

Internal Report  
DESY F41-78/03  
August 1978

INSTRUMENTATION FOR SPECTROSCOPY AND OTHER APPLICATIONS

**DESY-Bibliothek**  
20. OKT. 1978

W. Gudat

Institut für Festkörperforschung  
Kernforschungsanlage Jülich GmbH  
Postfach 1913, D-5170 Jülich 1

and

C. Kunz

Deutsches Elektronen-Synchrotron DESY  
Notkestraße 85, D-2000 Hamburg 52

Chapter 3 for "Synchrotron Radiation" edited by C. Kunz Topics in Current Physics  
Springer Verlag, Heidelberg 1978



Internal Report  
DESY F41-78/03  
August 1978

INSTRUMENTATION FOR SPECTROSCOPY AND OTHER APPLICATIONS

W. Gudat

Institut für Festkörperforschung  
Kernforschungsanlage Jülich GmbH  
Postfach 1913, D-5170 Jülich 1

and

C. Kunz

Deutsches Elektronen-Synchrotron DESY  
Notkestraße 85, D-2000 Hamburg 52

Chapter 3 for "Synchrotron Radiation" edited by. C. Kunz Topics in Current Physics  
Springer Verlag, Heidelberg 1978



3. Instrumentation for Spectroscopy and other Applications

by W. Gudat and C. Kunz

3.1 Layout and Operation of Laboratories

3.1.1 VUV Laboratory at a Small Storage Ring

3.1.2 VUV and X-Ray Laboratory at a Large Storage Ring

3.1.3 Beam Line Optics

3.2 Optical Components

3.2.1 Mirrors and Reflective Coatings

3.2.2 Dispersive Elements

3.2.3 Filters and Polarizers

3.3 VUV Monochromators

3.3.1 General Considerations

3.3.2 Normal Incidence Monochromators

3.3.3 Grazing Incidence Monochromators

3.3.4 New Concepts

3.4 X-Ray Monochromators

3.4.1 Plane Crystal Instruments

3.4.2 Higher Order Rejection

3.4.3 Bent Crystal Monochromators

3.5 Photon Detectors

3.5.1 VUV Detectors

3.5.2 X-Ray Detectors

3.6 Typical Experimental Arrangements

3.6.1 Experiments in the VUV Range

3.6.2 Experiments in the X-Ray Range

Acknowledgements

References



W. Gudat and C. Kunz

The peculiar nature of a synchrotron radiation (SR) source has given rise to a quite special instrumentation (3.1-3.9) which differs in many respects from that used with ordinary light sources (3.10-3.16). In addition to new monochromator designs there are other new interesting instrumental developments which are due to the fact that with synchrotron radiation a strong light source became available in large spectral regions for the first time.

Those properties of a synchrotron radiation source (see also Chapter 1) which have an important influence on the instruments (especially on monochromator design) are: 1. The immobility of the source, 2. the good vertical collimation of the SR emission, 3. the continuous white spectrum, 4. the polarization with a predominantly horizontal electric vector of polarization, 5. the fact that the source (namely the electron beam) is usually by far wider horizontally than vertically, 6. the large distance between the source and the experimental equipment, which is either determined by radiation safety considerations or at least by the finite size of the bending magnets and other installations near the source.

A first attempt to review the instrumentation for SR was made in 1973 at the first international users meeting (3.2) at which one of the present authors also gave a contribution (3.17). Even in these early days it was barely possible to give a complete survey on the activities in this field. Nowadays, with the rapid development of SR technologies, it has become even more difficult. We have therefore to apologize if recent published or unpublished developments have escaped our attention. New developments, which in many cases are still unpublished, are coming up with reflecting coatings, reduction of straylight, holographic gratings, zone plates, filters, soft x-ray lithography and microscopy, new monochromator designs, UHV monochromators, new x-ray monochromator designs and many other applications

of the x-ray part of the spectrum. We refer those readers who are eager to learn more about details of the instrumentation than we could include in this chapter to the handbooks (3.7,8,18-20) and the preprint series which are issued at SRC (Daresbury), DESY (Hamburg), LURE (Orsay), SSRP (Stanford). There is also a survey on the present and future European (3.21) activities and those planned in the USA (3.22) available.

In accordance with the much longer development of instrumentation in the vacuum ultraviolet region (namely the region of grating monochromators) this type of instrumentation will occupy a large fraction of this chapter. The x-ray field is in a process of rapid expansion but the number of instruments uniquely designed for SR sources is still limited. Already the lay-out of the beam lines determine to a large extent the type of instruments which can be used efficiently for monochromatization. Of course, small (up to 1 GeV) and large (typically 3 GeV) SR sources require completely different types of laboratories. Examples of such laboratories are described in Section 3.1. The necessary optical components and crystals are described in Section 3.2. Sections 3.3 and 3.4 are concerned with the vacuum ultraviolet and x-ray monochromators respectively. These are the most important units of instrumentation, since only a few experiments can do without them. Although there are probably no detectors and filters in use which could not be operated also with other light sources they deserve a special section (3.5) in this chapter. Synchrotron radiation covers a spectral range by far larger than any other source. Selective detectors and filters are therefore needed in addition to monochromators in order to avoid excessive stray-light and higher order radiation. In section 3.6, finally, we describe several typical experimental arrangements which exemplify the way experiments in the different subfields using SR are carried out. Several important techniques in a SR laboratory, like e.g. vacuum technology and computerization, had to be omitted almost completely since there are not so many aspects of these techniques which would differ from their applications elsewhere.

### 3.1 Lay-out and Operation of Laboratories

#### 3.1.1 VUV Laboratory at a Small Storage Ring

A small storage ring for the VUV is usually a machine with a beam energy in the range 200 - 800 MeV and of a typical size of up to 10 m in diameter (see Chapter 2). Storage rings of such a size can be located in the center of a single hall and many experiments can be grouped around the machine. Usually each experiment can have its own beam line and more than ten beam lines can be installed quite easily. We take as a typical installation at a small storage ring the TANTALUS I laboratory (3.20, 3.23-3.29) in Stoughton, Wisconsin, which is shown in Figs. 3.1 a) and b). This is a 240 MeV storage ring with an average diameter of about 3 m (see also Tables 1.1 and 1.2).

From the point of view of space for installing experiments this size is already a minimum. It would be possible with present day superconducting magnets to miniaturize such a storage ring further. Ideas of this nature were around in the early days of SR work (e.g. building of a storage ring with 50 cm diameter) but have not been followed up any further since it became evident that the installation of many different experiments at small distances from the source point would not be possible with such a mini-storage ring. Machines, twice as large as TANTALUS I are probably of the optimum size for offering sufficient space for the installation of equipment. Unless very small storage rings become so simple that it will be affordable to use them as a kind of laboratory source for only one or two experiments, this idea appears to have no future prospectives.

One important aspect of experimental installations at a small storage ring is the short distance between the source and the first optical element. While in principle an unlimited use of optical lenses (focusing mirrors) renders such geometrical considerations irrelevant, practical considerations are usually in favor of short optical paths. There are several reasons why this holds:

1. The only useful optical element with imaging properties in the VUV are reflecting mirrors, and optical gratings. Usually the beam line optics consists of one or several mirrors. The efficiency of such mirrors, however, is fairly low and even at grazing incidence a loss of intensity of at least 50 % due to limited reflectivity and stray light has to be tolerated. This limits the number of optical elements and consequently the flexibility of design.
2. A focusing mirror may need a complicated shape, which causes its price to increase considerably with its size. A mirror intercepting a beam of the same angular width at a shorter distance is cheaper and easier available.
3. Beams of a certain angular spread are blowing up to considerable dimensions over large distances. This requires wide and expensive UHV beam lines, large valves and mirror boxes etc. A further disadvantage of such wide beam-lines is their large conductivity and therefore the necessity for large vacuum pumps in cases where a pressure difference between an experiment and the storage ring has to be maintained along the beam line by differential pumping.

At TANTALUS I, which is the first dedicated storage ring used extensively in the VUV region, the vacuum system is not extremely sophisticated. Fairly small mirrors (about 4 cm wide and 10 cm long) intercept about 10 mrad horizontally. They fit into small mirror boxes. Beam lines are mostly made of 35 mm inner diameter tubes sealed with 2 3/4 inch outer diameter conflat flanges.<sup>\*)</sup> Hand operated valves allow for the vacuum isolation between beam lines and the storage ring. A vacuum isolation chamber with a fairly large volume and a high speed ion getter pump is located between the experiment and the storage ring. It serves, together with the narrow beam lines as a differential pumping system and would reduce the effect of a slow increase of pressure in the experimental arrangement to the storage ring. It is not of much help in the event of a catastrophic vacuum break down. The short distances between experiment and storage ring are adverse to installation

<sup>\*)</sup> Trade name of Varian all-metal flange connections

of fast closing valves. This is one of the big problems and dangers at the TANTALUS storage ring. Vacuum break-down at one of the experiments could ruin detectors and other equipment not only in the storage ring itself, but also in all the experiments which are connected to it.

Quite some effort probably has to go into vacuum safety considerations at future small storage rings. There is a tendency to operate many experiments in the future with more complicated detectors and other sensitive and expensive equipment simultaneously. One has just to imagine the damage which would result from a vacuum failure in one experiment to all the others if several of them have one or more of the very expensive channel plate arrays (see Sect. 3.5) in operation. For protection acoustic delay lines [3.19, 3.30, 3.31] were developed at the ACO storage ring and are introduced into the beam lines there (see below).

Alignment of instruments at TANTALUS I is done quite easily by making use of the visible part of the spectrum. Since free access is possible all around the storage ring after a beam is stored, optical elements can be adjusted in the same way as it would be done with a laboratory source. If vacuum lines are temporarily closed off with windows in order to obtain the visible beam out in the air care has to be taken to use windows with zero wedge angle in order to avoid beam deflections. The vertical center of the beam can be found by using a polarizer foil set at 90 degrees to the horizontal polarization direction of synchrotron radiation. Extinction will occur in the plane of the orbit according to Fig. 1.4.

While these small storage rings can be built in a way that radioactive radiation due to particle loss during operation causes no danger (the lost particles are buried under appropriate conditions in the yokes of the magnets) the experimental area has to be cleared from people during injection into the storage ring. As a consequence also those experiments which are in the process of installing equipment have to interrupt their work at periodic intervals.

### 3.1.2 VUV and X-Ray Laboratory at a Large Storage Ring

Storage rings operating at beam energies in the region of 3 GeV have average diameters of 50 m or more (see Chapter 2 and Tables 1.1 and 1.2). Further, radiation safety is an important factor with such machines, because of their emission of hard x-rays and also because of potential hazards due to particle losses. Accordingly, there is usually heavy shielding set up between the experimental area and the storage ring. It is customary to make the shielding so effective that the experimental area with the exception of small regions around the direct beam lines does not need to be cleared from people during the experiment. In this respect synchrotrons are more dangerous sources of radiative radiation due to the continuous refilling of particles. They need a much heavier shielding all the time. One of the unwanted consequences of this radiation shielding is a larger distance between the source point and the experiment than it would be necessary already from the size of the magnets and other installations. It is proposed [3.32] to insert scrapers at two points along the orbit after storage of a beam is accomplished. Any particles getting out of step would be lost there. Consequently, all the other parts are accessible when a stored beam is in orbit if only care is taken for the much lighter x-ray shielding. This concept which is proposed for the SRS storage ring under construction at Daresbury [3.33] however, demands evacuation of people from all the experimental area during the injection process.

Figures 3.2 a) and b) show the arrangement of the laboratory at the DORIS storage rings [3.8, 3.34]. This is quite typical also for the laboratory at the SPEAR storage ring at Stanford [3.7] although the distances and specific arrangements of beams differ. At DORIS a water cooled copper absorber, which is incorporated in the vacuum chambers within the magnets, absorbs most of the emitted radiation. A narrow fan of SR penetrates a hole in the absorber and enters the beam line. A water cooled removable beam stop protects closed valves from overheating by SR.

A beam shutter, BS, protects the experimental area during injection into DORIS and, when closed, allows access to experiments in the direct beam D. This direct beam is collimated to a very narrow region at the experimental area by several shielding blocks. Access to this region is blocked while the the beam is on, mainly because of the potential danger of a loss of the stored beam into the direction of the laboratory. A permanent magnet M serves to deflect any charged particles in such a beam while the  $\gamma$  quanta would continue along the beam line. In the radiation safety considerations this magnet serves to reduce the total dosis in the laboratory by one order of magnitude. At the SPEAR laboratory individual beam shutters are available for each x-ray beam. At this laboratory, due to special conditions of the injection into the storage ring, beam shutters may be open during injection provided that a very narrow region around the direct beam is inaccessible. This is achieved by a so-called "hutch system". The shielding is so close to the beam that only small lead covered doors are necessary to provide sufficient access to the experiment. Beam shutters can only be opened if electrical switches confirm that all openings of the hutch are closed. The hutches are sufficiently small to prevent accidental enclosure of any person inside the hutch.

At DORIS an automatic fast closing valve with all-metal seals is located in the beam line near the storage ring (FCV). It is activated by vacuum sensors at the experimental area located 18 m upstream from it. The closing time of  $\sim 30$  msec is sufficiently short for stopping a shock wave from entering DORIS. This valve (FCV), however, is not completely tight. Another slowly closing UHV valve nearer to DORIS has to be activated simultaneously in order to prevent a slow venting of the machine. Such a system might not be effective anymore if the distance between the experimental area and the source is reduced to less than 15 m which is geometrically possible in principle. For such reduced beam line lengths at the ACO storage ring at Orsay an acoustic delay line [3.19, 3.30, 3.31] was constructed which would increase the transit time of a shock wave by 190 msec. Such a device, however, is quite clumsy.

At the DORIS laboratory a beam of 3.8 mrad horizontal aperture is available. Grazing incidence mirrors split off secondary beams so that altogether four simultaneously operational beams are formed (Fig. 3.3). At SPEAR the first mirrors are located much nearer to the source point. Figure 3.4 [3.7] shows a beam arrangement in which altogether 18 mrad are utilized for four different beams. Similar arrangements are also planned for a new laboratory at DORIS [3.8] and other storage rings of similar sizes. The beam splitting and arrangement of the optical elements of the different monochromators and experiments in the DORIS laboratory are illustrated in Fig. 3.3. Only one station is reserved for x-ray experiments. In a second special x-ray laboratory devoted to molecular biology and administered by the European Molecular Biology Laboratory (EMBL) the x-ray radiation is used from 1978 on. In this laboratory [3.34] four x-ray beams are split off by very grazing incidence mirrors and by crystals in an arrangement quite similar to that at the SPEAR laboratory (see Fig. 3.4).

The determination and continuous monitoring of the vertical beam position is of considerable importance for these very long beams especially in the x-ray region where, according to Chapter 1, the vertical angular spread of intensity is very narrow. If the beam at 10 keV is misaligned at a distance of 40 m from the source by only 10 mm, this could mean a loss in intensity of one to two orders of magnitude depending on the aperture of the experimental arrangement. This becomes even more serious, if the experiment needs a well defined degree of polarization. Misalignments then will not only affect the result quantitatively but also qualitatively.

There are several methods in use to determine the position of the beam. The center of the beam can be determined visually with a polarizer foil oriented perpendicular to the main direction of polarization (see Section 3.1.1). At high powers it may, however, not be wise to extract the visible light through a window directly exposed to the beam (even if the observer is protected by lead glass) because the glass may break. If x-rays are involved a TV camera imaging a fluorescence screen can be used. Another method is exposure of a ZnS covered screen behind a Be-window. The beam shutter can be closed after an exposure of about 1 minute and the ZnS screen, if kept in the dark, will fluoresce for about 5 minutes with good visibility. Additional absorbers serve to isolate the hard radiation which gives a good indication of the center of the beam. At 40 m distance at DESY for instance a bright band of less than 5 mm vertical width will allow for a determination of the beam level with an accuracy of 0.5 mm. The same procedure could be carried out with microscope slides. After exposure a blackening due to radiation induced defects marks the beam position. In this case several of these glass monitors could be placed along the beam and if these glass pieces have no appreciable wedge angle a laser beam can be easily brought into position afterwards to simulate the beam for making adjustments. There is also a special type of x-ray paper in usage which shows different colors depending on beam intensity (Kodak, linagraph-paper).

After having determined the beam position the next problem is long term stability of this position. Two possible effects have to be expected: displacement of the electron beam at the source point and changes of the direction of the beam. The second effect is the dominating one with long beam lines. These parameters can be influenced by the activation of correction magnets. This requires a more or less continuous monitoring of the beam position. Figure 3.5 shows two monitor systems which have been realized. Figure 3.5 a) shows a

system of 3 metal strips mounted in the DORIS Lab (3.8) at the front end of the beam shutter BS in Fig. 3.2. The photoemission current is measured. A similar system is used at SPEAR. Maximum current from the central strip and equal currents from the upper and lower strips are required. This system is operative only when the beam shutter is closed. With DORIS, however, beam positions are very reproducible for one setting of energy and beam optics. Only when these parameters are changed drastic deviations occur (by as much as 1.5 mrad) which need to be corrected for before experiments are resumed. Figure 3.5 b) shows the SPEAR monitor (3.7) consisting of a graded screen cut out for the part of the beam used by the experiments. This allows for a continuous supervision.

There is one point which can become important with an extensive usage of synchrotron radiation from one storage ring at several points. The electron beam in a storage ring cannot be displaced easily by correction coils in such a way that it meets externally determined conditions in a series of several magnets. Even if these conditions are met at one energy and with one beam optics they might not be fulfillable with other parameters. This might necessitate a complicated mechanical realignment procedure of the storage ring magnets or a frequent realignment of experimental equipment.

With synchrotrons, e.g. like DESY, motion and deformation of the beam during the acceleration period (10 msec) can take place (3.34'). These can be especially large at the end of the acceleration cycle when electrons are extracted by exciting orbit deformations. Experiments can use gate signals to eliminate such time intervals. It is also of great importance with synchrotrons to monitor the beam intensity which is available at the sample. Figure 3.6 shows as an example three curves which were measured simultaneously (3.35). Figure 3.6 a displays

a spectrum without any monitoring exhibiting all the fluctuations of the source. For obtaining curve b) the signal was divided by the signal from a monitor which was located in front of the experiment. Curve c) shows a normalization of the spectrum to a reference signal which monitors exactly the same light beam which is hitting the sample. Obviously the last method is the best for suppressing fluctuations.

Although synchrotrons are usually inferior to storage rings as SR light sources, they have properties which can be of some value for special experiments. For instance, the much simpler vacuum system ( $10^{-6}$  Torr) allows for the investigation of "dirty" gases or solids in a much easier way. Any equipment for which there is no inherent need for ultrahigh vacuum conditions can be installed much simpler and cheaper. Often the very high photon energies are used from synchrotrons since they are not produced by the present generation of storage rings (although PETRA, PEP, CESR, will be available soon), see Tables 1.1 and 1.2.

### 3.1.3 Beam Line Optics

#### General considerations

Practically any optical instrument has a certain maximum acceptance defined as the area of a real or virtual diaphragm times the maximum solid angle tolerable for the beams passing through this diaphragm. The goal of a beam line optics is to image the source in such a way onto this diaphragm that the acceptance is filled. If this is achieved the intensity throughput with a given brightness of the source is maximized. Imaging is governed by Abbe's law (Liouville's theorem). For these considerations we have ignored intensity losses in the optical elements. No further geometrical gain in intensity is then possible. There are, however, three points: (1) the goal defined above can be achieved in an elegant (say simple, efficient, low-cost) manner or in a more complicated way tolerating reflection losses of many mirrors or other components; (2) when constructing new instruments their acceptance can be increased and (3) they can be matched from the outset to the emittance of a SR source rendering additional optical coupling elements

unnecessary.

Unlike with radiation in the visible and near vacuum ultraviolet focusing elements in the soft x-ray region and even more in the hard x-ray region are restricted considerably. It is fairly common practice to avoid too many focusing mirrors at small grazing angles and bent gratings or crystals if possible.

There are several techniques which are helpful in designing optical arrangements in the vacuum ultraviolet, soft and hard x-ray regions. First order imaging properties of normal and grazing incidence focusing mirrors are described by a focal length applying the classical laws of optics. Spherical mirrors at grazing incidence usually have considerable aberrations already at fairly small apertures (see Section 3.2). Usually the imaging properties including the aberrations can be obtained in a fairly straight forward way by applying geometrical optics either analytically by taking into account higher order terms of the characteristic optical functions or by ray tracing which can be achieved with the help of modern computers. Ruled gratings are treated quite similarly with a few modifications. It should be noted that even a plane grating has imaging properties (see e.g. [3.36]). Crystals, as they are used for x-ray monochromators, are treated in first order again by ray optics. Imaging properties of crystals with surfaces cut at an angle to the lattice planes [3.37] come into play quite similarly to the just mentioned case of optical gratings (see Section 3.4).

#### The phase space method

A method which is especially useful in treating x-ray optics at a storage ring came up recently [3.38-40] and was borrowed from the theory of charged

particle beam transport systems with which it has an intimate relationship at the source point anyhow. It is a phase space technique as illustrated in Fig. 3.7. We demonstrate it here for the vertical extension of the SR source and for its vertical divergency described in a  $y$  and  $y'$  coordinate system where  $y$  is a vertical coordinate and  $y'$  is its derivative. SR is emitted at  $Z=0$  from an electron beam whose distribution in space and angle is described by gaussians. Then the contour for e.g. one standard deviation of beam intensity in the  $y, y'$  plane is an ellipse (see also Chapters 1 and 2). The emission of SR adds to the angular width, not to the vertical extension of the source. In order to be able to handle the convolution of beam and SR distributions mathematically the SR angular distribution is also approximated by a gaussian distribution. Then the convolution results in ellipses in phase space again. These are also given in Fig. 3.7 a) and describe now the properties of the SR source. Figure 3.7b) shows how the ellipses transform when we let the beam expand along its path. The area of the ellipse is an invariant (Abbe's or Liouville's theorem!). We also show the part of the ellipse which is cut out by a horizontal slit at distance  $Z=l$ . This slit can be transformed back to the origin  $Z=0$  and this is shown in Fig. 3.7b). In Figs. 3.7c) and d) we show the equivalent construction for a source point where the electron optics gives an oblique ellipse. For special applications it could be useful to consider separately ellipses for the two directions of polarization in such diagrams.

In general the transformation of a coordinate  $y_0, y'_0$  at the origin  $Z = 0$  of the source to a point  $y, y'$  at a certain position  $Z = l$  of the beam line is described mathematically by a series of matrix multiplications where different elements of the beam line correspond to a unique matrix each. There are matrices for drift sections, focusing elements and dispersive elements which can be worked out for each case [3.38-40]. The corresponding problem of finding the source coordinate  $y_0, y'_0$  corresponding to a coordinate  $y, y'$  at an instrumental aperture is solved by the inverse transformations.

### Magic mirrors

One of the important properties, especially of large storage rings, is time structure. The pulse structure of the electron current can be as short as 150 picoseconds (see Chapter 1). The question arises, how an optical system collecting light from the same bunch of electrons emitted at different times at different parts of the orbit will influence this pulse length. LÓPEZ-DELGADO and SZWARC [3.41] have shown that there exist specially shaped mirrors winding around an idealized circular storage ring (Fig. 3.8) which could collect all the light into a focus without distortion of the pulse structure. The method to treat the problem is to consider both, the time an electron travels around the orbit to a certain point (with practically the velocity of light) at which emission takes place and the time, the light needs from there on its optical path to the focus. Apart from the time structure problem, from these considerations follows the interesting result that a radiating circle with well collimated emission can be imaged to one point.

For practical purposes one can show that any other focusing optics collecting radiation from practically achievable horizontal apertures will produce only minor distortions of the pulses. As an example we calculate for DORIS that a mirror collecting 100 mrad of horizontal radiation would increase the pulse length by 3 psec. This is only a 2% increase of a 150 psec pulse. We therefore come to the conclusion that the magic mirror concept is most probably without practical importance for ordinary beam line concepts. It appears to be mainly of conceptual interest.

### 3.2 OPTICAL COMPONENTS

Every monochromator or spectrograph must have an optical element to disperse the radiation of the light source. Since several decades mechanically ruled reflection gratings have been used with various degrees of success in the spectral range of the VUV down to wavelengths of about 20 Å. At wavelengths below about 10 Å crystals are the most efficient dispersers. The newly developed transmission gratings give promise of covering the transition region. Gratings made on special blanks and bent crystals already have certain focussing properties, but in general especially shaped mirrors have to be used for a stigmatic imaging of the light source. Holographically made gratings offer the possibility of directly compensating some aberrations. In order to maximize the throughput of an optical system each component should have the highest attainable reflectivity in the desired wavelength range. In the near VUV multilayer reflective coatings may help to solve this problem.

In the following paragraphs we want to summarize some of the more important properties of the various optical components mentioned above. No in-depth discussion is intended since adequate treatments have been given in several monographs and review articles [3.10 - 3.17, 3.42 - 3.45].

#### 3.2.1 Mirrors and reflective coatings

##### General remarks

The discussion of Section 3.1 has already stressed some of the severe constraints which are imposed on mirror design for SR beamlines at high current and high energy storage rings. For a stigmatic imaging an excellent optical figure is necessary, especially due to the long beamlines and the required grazing incidence optics.

Mirrors should have very low stray light which implies extremely small rms roughness in a wavelength range of soft X-rays. Synchrotron radiation covers an enormous wavelength range which also requires high reflectivity of mirrors and reflective coatings in a broad spectral range. Furthermore, at grazing angles of a few degrees but with wide acceptance angles, large sizes are necessary which are difficult to make. In addition, the material must be suitable for UHV requirements of the beamlines and the optical instruments. And last but not least mirrors, which are close to the tangential point have to withstand power densities up to hundred watts/cm<sup>2</sup> or more depending on the angle of incidence of the light. In view of these stringent requirements it is not surprising that there is no unique answer of what one might consider as the optimum mirror. At present, extensive investigations are being carried out [3.46, 3.47] in order to clarify these problems.

We begin our discussion on mirrors and reflective coatings with a brief summary of the optical response of a solid to electromagnetic radiation.

##### Reflectivity in the Vacuum Ultraviolet

The optical response of a solid to electromagnetic radiation is, in principle, described by either of two frequency dependent complex quantities, the well-known complex dielectric function  $\tilde{\epsilon} = \epsilon_1(\omega) + i\epsilon_2(\omega)$  and the complex index of refraction  $\tilde{n} = n + ik$ . Both complex quantities are related through  $\tilde{n}^2 = \tilde{\epsilon}$  as a direct result of travelling wave solutions to Maxwell's equations for an absorbing optical medium. At normal incidence the reflectivity R of a surface with negligible surface roughness can be calculated from Fresnel's equation

$$R = |r|^2 = \left| \frac{\tilde{n} - 1}{\tilde{n} + 1} \right|^2 = \frac{(n-1)^2 + k^2}{(n+1)^2 + k^2} \quad (3.1)$$

with  $\tilde{r}$  being the complex reflexion coefficient. When  $n$  approaches one, the reflectivity can become very small. This behaviour is seen from Fig. 3.9 which displays the normal incidence reflectivity of aluminium, gold and carbon over a wide energy range [3.48]. These materials as well as others [3.48 - 53] exhibit a steep decrease in reflectivity beyond 30 to 40 eV which is approximately proportional to the fourth power of the wavelength. This simply means that normal incidence mirrors are no longer practical. However, at high angles of incidence  $\theta$  the reflectivity increases considerably according to Fresnel's equations which in this case depend on the polarization of the light. For an absorbing medium with the  $\vec{E}$ -vector of the light perpendicular to the plane of incidence the complex reflection coefficient  $\tilde{r}_s$  is [3.54]

$$\tilde{r}_s = \frac{\cos \theta - (\tilde{\epsilon} - \sin^2 \theta)^{1/2}}{\cos \theta + (\tilde{\epsilon} - \sin^2 \theta)^{1/2}} \quad (3.2)$$

and with  $\vec{E}$  parallel to the plane of incidence<sup>+</sup> one finds

$$\tilde{r}_p = \frac{\tilde{\epsilon} \cos \theta - (\tilde{\epsilon} - \sin^2 \theta)^{1/2}}{\tilde{\epsilon} \cos \theta + (\tilde{\epsilon} - \sin^2 \theta)^{1/2}} \quad (3.3)$$

As usual, the square of  $|\tilde{r}_s|$  and  $|\tilde{r}_p|$  give the reflectivities  $R_s$  and  $R_p$  respectively. For partly polarized radiation the reflectivity is obtained from

$$R = 0.5 \left[ R_p (1+P) + R_s (1-P) \right] \quad (3.4)$$

where  $P$  is the degree of polarization defined as

$$P = (I_p - I_s) / (I_p + I_s) \quad (3.5)$$

where  $I_p$  and  $I_s$  are the intensities of  $p$  and  $s$  polarized light respectively.

<sup>+</sup>Footnote: For  $p$ -polarization the validity range of Fresnel's equations has to be carefully considered. According to Kliewer [3.55] important deviations occur for simple metals.

Fig. 3.10 shows the reflectivity of Pt versus photon energy for various angles of incidence as determined experimentally with  $s$ -polarized SR-light [3.56]. The data demonstrate the dependence of the reflected intensity on the angle of incidence and convincingly illustrate the principle of using a mirror at non-normal incidence as a high energy cut-off filter. As we shall see below, this constitutes an important element in the design of monochromators and beamlines. Since the synchrotron radiation has a continuous wide-band spectrum, harmonics can seriously contaminate the radiation that have been monochromatized by a grating or a crystal.

Another property of synchrotron radiation is of importance when using mirror optics, namely the horizontal polarization of the electric vector  $\vec{E}$  of the light. In Fig. 3.11 we show the calculated reflectivity  $R_s$  and  $R_p$  for Pt as a function of the angle of incidence. As already stated the reflectivity is quite small at normal incidence, but for  $R_p$  it is even smaller at intermediate angles, namely at the well-known Brewster angle. For little absorption, i.e. small  $k$ ,  $R_p$  is considerably smaller than  $R_s$ . Obviously, this has to be considered in the design of beamlines and optical instruments in order to enhance the intensity and the degree of polarization.

Eqs. 3.2 and 3.3 are the exact Fresnel equations and thus are also valid for the soft X-ray region. But they are often simplified by treating the unit decrements to the complex refractive index  $\delta$  and  $\beta$  in  $\tilde{n} = 1 - \delta + i\beta$  as small quantities (typically of the order  $10^{-3}$  to  $10^{-6}$ ) which implies that their squares and products can be neglected. Furthermore, for small grazing angles one can

replace  $\sin \theta$  by the angle  $\theta$  and can neglect the polarization dependence, thus obtaining a single expression for the reflectivity in the X-ray region [3.13, 3.58, 3.59]. This rather lengthy expression which we do not want to write down, is valid for the wavelength region below 10 Å. However, at longer wavelength the approximate theory can introduce significant errors [3.60], since the reflectivity is no longer the same for both states of polarization.  $\delta$  is roughly given by [3.58]

$$\delta = 2.74 \times 10^{-6} \frac{Z^2 \rho}{A} \lambda^2, \tag{3.6}$$

where  $Z$  is the atomic number,  $A$ , the atomic weight (in g) and  $\rho$  the density (in g/cm<sup>3</sup>) of the material.  $\lambda$  is expressed in Ångström units. The parameter  $\delta$  determines that glancing angle  $\theta_c$  where total external reflection sets in at a particular wavelength  $\lambda_c$ . With decreasing  $\delta$  the real part of  $\tilde{n}$  gets closer

to 1 for a given  $\beta$  and thus the refraction becomes smaller. Therefore total reflection occurs with increasing  $\delta$  at increasingly larger glancing angles  $\theta_c$ .

The free electron theory of simple metals can be utilized to obtain a relation between the wavelength and the critical glancing angle of total reflection, namely,

$$\sin \theta_c = \lambda \cdot \left( \frac{N \cdot r_0}{\pi} \right)^{1/2} \tag{3.7}$$

where  $N$  is the number of electrons per cm<sup>3</sup> and  $r_0$  is the classical radius of an electron ( $r_0 = 0.28 \times 10^{-12}$  cm). Combining Eqs. 3.6 and 3.7 gives the proportionality  $\theta_c \sim \delta^{1/2}$ , as discussed above. It is also clear from Eq. 3.7 that a material with high electron density reflects a shorter wavelength at a given glancing angle than does a low density material. This is the reason why one uses for instance gold and platinum as coating materials for mirrors and gratings. It also explains why a surface which has become contaminated by cracked hydrocarbons of pump oil and vacuum grease shows a strong decrease in reflectivity at the short wavelength limit. Eq. 3.7 can only give a guide line in order to determine the short wavelength limit and the cut-off angle, respectively. This expression does not depend on the complete dielectric constant as it should. Moreover such effects as surface roughness are by no means included. As we shall see below this is of great importance. It is our experience that Eq. 3.7 results in a too optimistic value for  $\theta_c$  when the total number of electrons is counted. It is more reasonable to use an effective electron density which is determined by the number of electrons which can be excited with light of wavelength  $\lambda$ . The effective electron density can be estimated from sum rule plots as given by HAGEMANN et al. [3.48]. Although considerable efforts

in utilizing the X-ray part of SR have been undertaken in the various SR-laboratories, no recent systematic investigation of the cut-off angle as a function of wavelength and material appears to be available. The agreement between theory and the experimental data up to about 1965 has been thoroughly discussed by SAMSON [3.10].

The  $\beta$ -parameter in the expression for  $\bar{n}$  corresponds to the absorptive part of the complex index of refraction. Therefore  $\beta$  determines the shape of the onset of total reflection. It is a steep step-like threshold for small absorption ( $\beta \sim 10^{-6}$ ) and a weak threshold for high absorption ( $\beta \sim 10^{-3}$ ). This is illustrated in Fig. 3.12 which depicts the calculated reflectivity of fused quartz and of platinum versus the dimensionless quantity  $(\theta - \theta_c)/\theta_c$  [3.40, 3.59]. At  $\theta_c$  the more strongly absorbing platinum (which is also the high electron density material, see discussion above) has a reflectivity only about 0.4 times that of quartz. For mirror design this should be kept in mind.

#### Coating materials and multilayer coatings

Very often the optical surfaces of mirrors are overcoated with a thin layer of a different material in order to enhance the reflectivity. The choice of the material depends on various criteria: Obviously the wavelength range to be covered and the angle of light incidence have to be considered, but also the ease of reproducible production of thin layers is of importance as well as the strength of adhesion to the substrate. Further constraints are due to the UHV requirements imposed by the vacuum of storage rings. Finally, the coating must be resistant to contamination and oxidation.

From the discussion in the previous paragraphs we know that mirrors at near normal incidence can be used efficiently to photon energies up to 30 to 40 eV. The energy range of the near UV up to about 12 eV is the domain of Al mirrors which are overcoated with 100 to 250 Å of  $MgF_2$  or LiF for oxidation protection. Such mirrors can now be obtained commercially with a reflectivity up to 90 % at energies below 10 eV. At higher energies the reflectivity deviates considerably from that shown for pure Al in Fig. 3.9 due to the dielectric coating [3.44, 3.10, 3.61]. It should be noted that the performance of Al mirrors is also influenced by surface roughness and losses due to surface plasmons [3.62, 3.67].

At higher photon energies between 10 eV and 40 eV one is better off with coatings of noble metals such as gold and platinum (see Figs. 3.9 - 3.11) which offer maximum reflectivities for Au and Pt of 17 % and 23 %, respectively [3.48, 3.49, 3.57]. These materials have proven to show reproducible reflectivities even after various bake-out cycles.

It is well known that the maximum reflectivity of Au increases with increasing film thickness up to about 200 Å and then decreases again for thicker films [3.56, 3.65, 3.66]. The explanation for this effect is that thin gold films deposited in high vacuum have an island structure which grows as the average film thickness increases to become a continuous film at about 100 - 300 Å. Thicker films are thought to become less smooth due to the formation of conglomerates. However, this strongly depends on the preparation conditions. It is believed that evaporation under ultrahigh

vacuum conditions results in smoother films [3.46] if the substrate material is smooth. Polishing defects, for instance, with fairly broad structures (10 - 20  $\mu\text{m}$ ) and rms heights below 100  $\text{\AA}$  are accurately replicated by thin coatings [3.67, 3.68]. The structure of the coating itself has typical dimensions of a few atomic layers in height.

Other materials which have been used as thin film coatings include Rh, Pd, Ir, Os and others. The reflectivity of these materials are given in Refs. 3.10, 3.49 - 3.53, 3.56 and 3.57. General information on the preparation of thin film coatings is presented in Refs. 3.10, 3.12, 3.69 and 3.70.

Recently an interesting new material has been suggested [3.71]. At least up to 25 eV SiC' prepared by chemical-vapor deposition, has a significantly higher reflectivity than any other material investigated to date (see Fig. 3.13). According to Rehn et al. [3.72] this is very likely due to the extremely smooth surfaces and the high volume plasmon energy of 22 eV of SiC. We want to stress that the data of Fig. 3.13 are experimentally determined and not the result of a Kramers-Kronig conversion of transmittance data to reflectivity data as has been done by HAGEMANN et al. [3.48]. That data (see Fig. 3.9 for some of those results), shows for Au and Cu a somewhat higher reflectivity than determined experimentally.

For the design of the Flipper monochromator at the DESY laboratory an extensive test program on reflectivities of various materials has been carried out. Evaluations are underway [3.73]. Preliminary statements are that carbon and tungsten are other high reflectivity coatings in the

energy range 10 to about 40 eV.

As previously described, we have to use grazing incidence optics at energies above  $\sim 40$  eV. The same materials, i.e. Au, Pt, Ir, W and C then also give good coatings. Depending on the angle of incidence, the reflectivity can be 70 to 80 % for energies below about 150 eV (see Fig. 3.10).

Quite recently it has been shown [3.74] that the reflectivity at near normal incidence can be enhanced substantially by interference effects in the reflectance of multilayer films using layered structures of Au/C and Cu/C. This technique is well known in the visible and of extremely widespread application there [3.69].

The basic idea of using a sequence of alternating films of two materials with high and low absorption coefficients is to place the strong absorber in thin layers at the nodes of the desired wavefield. This implies that a fairly large penetration depth of the wavefield can be achieved with a participation of many layers in the reflection process [3.75]. The experimental values (Fig. 3.14) obtained thus far were by a factor 7 higher than those of a single opaque gold film at energies around 70 eV. Further improvements seem to be possible [3.74, 75, 3.45]. But as with other interference systems there will be only a fairly limited wavelength interval which is efficiently reflected. This means that one would have to use a big set of differently coated mirrors in order to work in a wide spectral range. Since the thickness of the single

layers have to be in the order of the desired wavelengths to be reflected, the practical limitation of the useful spectral range, at least in the near future, will certainly be at wavelengths above about  $50 \text{ \AA}$  due to the enormous problems of reproducibly producing thin smooth layers. Nevertheless, the technique of multilayer interference coatings in the far VUV appears to be one of the most promising mirror technologies.

Obviously, a knowledge of the optical constants and reflectivity of various materials is necessary for a proper design of optical systems for use in the extreme VUV. But there is still only very little experimental information available at photon energies between 200 and 600 eV. It is noteworthy that a large fraction of the data has been obtained with use of characteristic line sources i.e. without SR. Once again, most of the literature up to 1965 has been reviewed by SAMSON [3.10]. Since that includes the relevant literature, we just want to add a few comments. The most comprehensive study of the optical constants is due to LUKIRSKII and coworkers [3.76 - 3.79]. In the wavelength range 7 to  $190 \text{ \AA}$  they investigated the angular dependence of the reflectivity of more than 15 metals, semiconductors and insulators. In Fig. 3.15 we reproduce their results for Au and for C. As expected, the reflectivity of C drops faster with increasing grazing angle than does Au. It should be mentioned that the data of LUKIRSKII and coworkers [3.76 - 3.79] were obtained on air exposed samples. But firstly, the penetration depth of the light is fairly large and secondly, we are interested in the behaviour of materials useful as coating materials of optical components in air-exposed systems, and thus we consider the data as very useful.

The wavelength range around the carbon K edge at  $44 \text{ \AA}$  is experimentally the most difficult range to work at. As already mentioned previously, this is due to the fact that after prolonged use of mirrors a contamination layer of cracked hydrocarbons builds up resulting in a decrease of reflectivity. The build-up is a product of light intensity, time, and residual gas composition. At the DESY synchrotron laboratory, for instance, the beamlines are operated at a relatively high pressure of  $\sim 10^{-6}$  Torr and then it takes only a few days, until a sizeable intensity drop, i.e. reflectivity drop, is observed. Even at the DORIS laboratory with beamlines operating in the  $10^{-9}$  Torr range this effect is seen to occur. However, much longer exposure times have to be accumulated. As an illustration for the contamination as well as on other radiation induced effects we show a beam-splitter mirror in Fig. 3.16 which has been used in the beamline of the DORIS laboratory. In addition to the surface effects a discoloration is seen inside the mirror material. It is interesting to note that the visual inspection of a Cu beamsplitter mirror of the Stanford SR Laboratory did not show evidence for carbon build-up even after about 2 years of normal use under clean UHV conditions [3.80]. In contrast to the glass mirror at DORIS the Cu mirror is held at a constant temperature slightly above room temperature [3.81].

Quite generally, the soft X-ray region is served best with mirrors at grazing incidence. In particular for the performance in the high energy range the coating material and the substrate material are of importance. There is some experimental evidence that surface roughness can be an even more important parameter. In the next section this question shall be studied in somewhat more detail.

### Scattering and stray light

Any non-ideal surface shows diffuse reflectivity of VUV radiation, i.e. scattering [3.83]. Until recently mainly scattering measurements with visible light have been done showing a spectral dependence of the fraction of scattered light intensity proportional to  $\lambda^{-4}$  [3.82,83]. This wavelength dependence indicates a Rayleigh-type scattering with the characteristic fourth power law. From diffraction by random irregularities, which is a second kind of scattering mechanism, one expects a proportionality to  $\lambda^{-2}$ . Measurements on extremely smooth SiC surfaces with a rms roughness of 4 to 15 Å (Fig. 3.17) show very little scattering in the VUV up to 25 eV. The data of Fig. 3.17, replotted versus  $\lambda^{-2}$ , do not show a Rayleigh-type scattering for the SiC mirror in contrast to the Mo coated quartz mirror, where the Rayleigh scattering is dominating. The total scattered intensity was found to be less by about a factor of 10 to 20 compared to the metal-coated highly polished quartz surfaces and about a factor of 100 less than from a Pt coated Cu-mirror [3.80].

As it appears, the available theories on the scattering of VUV light are not yet sufficiently sophisticated [3.72, 83, 84]. But the scarce experimental results indicate that the scattering strongly depends on the angle of incidence. Furthermore, for a given surface roughness the optical scattering rises monotonically with increasing photon energy and reduction of scattering becomes increasingly important for high photon energy applications. In fact, a Pt coated Cu mirror used for an extended period in the primary SR beam at SPEAR was found to have a rms roughness of about 186 Å and a cut-off energy of about 500 eV with a monochromatization ratio of approximately 10:1 at 300 eV, whereas the corresponding numbers for a new Cu mirror having a rms roughness of 30 Å were 60:1 at about 280 eV and a high energy cut-off of at least 600 eV [3.80]. See also Fig. 3.31.

All one can say at present about scattering in the VUV from the available data is that it appears to be of crucial importance for the soft X-ray range. But even in the range below 300 eV one should care for smallest available surface roughness.

### Mirror substrate materials

From spectroscopy in the visible and infrared a highly developed technology of glass mirrors is available. But those mirrors do not have to fulfill all the requirements which are necessary for mirrors in storage ring SR beamlines. Rather the constraints on materials for VUV mirrors are closer to those in advanced laser technologies. The main reason is the high power density of SR on mirrors. Half of the total power of SR is emitted at shorter wavelengths than  $\lambda_c$  (see Chapter 1). For high energy storage rings and synchrotrons with  $\lambda_c$  of  $\sim 10$  Å this means that most mirrors working at not too grazing angles absorb about half the power which is emitted into that solid angle. Obviously, this causes problems with heat dissipation and additionally problems with distribution of charge due to photoeffect in insulators. At the DORIS storage ring, for instance, it was observed that glass mirrors (see Fig. 3.16) become cracked at the surface even at a distance of about 20 m. Thus mirror cooling of metal substrates is necessary for mirrors close to the electron orbit. At the Stanford SR laboratory platinum-plated ultra-smooth copper mirrors have been installed in such positions and they have proven very successful [3.80, 3.81]. The Pt coating did not show signs of peeling or other deterioration which has been observed on conventional glass mirrors with metal coatings.

In a recent comparison [3.71] of laser mirror substrate materials it turned out that SiC also has excellent VUV mirror characteristics. It has a relatively high electrical conductivity and, as already mentioned, it can be polished to a supersmooth surface with rms roughness of about  $7 \text{ \AA}$  which is very stable and extremely hard. Moreover, the reflectivity at wavelengths above  $\sim 500 \text{ \AA}$  is higher than that of any other material measured so far [3.72].

For all mirrors in a SR beamline behind the very first one, glass ceramic appears to be the most favourable material<sup>†</sup>. These ultralow thermal expansion materials [3.85, 3.86] guarantee the highest precision optical figures and the smoothest surfaces of mirrors even under UHV conditions and moderate SR power densities. Table 3.1 gives the thermal expansion coefficients as well as the long time dimensional stability for a number of glass ceramics. For comparison also some metals have been included.

#### Imaging in VUV

Some general considerations on imaging problems in the VUV are given in Sect. 3.1.3. Also the properties of the so-called magic mirror are discussed which is an optical element capable of collecting all the light of a wide solid angle into a focus without time distortion of the pulse structure of synchrotrons and storage rings [3.41]. Detailed discussions are presented in the literature for normal and grazing incidence optics [3.10, 3.15, 3.16, 3.88, 3.89]. Here we just want to touch on some aspects which are related to the properties of SR.

<sup>†</sup>Footnote: According to most recent results by NIEMANN et al. [3.86] there are indications that the optical figure of the surfaces of Zerodur mirrors undergoes irreversible changes after irradiation by hard x-rays.

It is well known that focussing is best achieved with ellipsoidal mirrors or with off-axis paraboloids. However, due to the very grazing angles of incidence often used in the VUV very large ratios of the semi-axis of the ellipsoids (typically 10 - 100) occur. Therefore these mirrors are extremely difficult to make with the necessary high accuracy of the optical figure. If one is able to get them at all, then they can be quite expensive. In many cases toroidal mirrors are used which come closest to the more complex elliptical mirrors. Quite generally one has the possibility to use two mirrors instead of one, e.g. two cylindrical mirrors with curvatures at right angles with respect to each other which will fully correct for one of the major aberrations of a spherical mirror at grazing incidence, namely the astigmatism. The other important aberration, the spherical aberration has to be considered anyhow. In a wavelength region say above  $50 \text{ \AA}$  one can afford two grazing incidence reflections without too much intensity loss (see above). The use of two mirrors may save cost and time (of delivery) in addition to obtaining a smoother surface which can be produced more easily on surfaces of simpler shapes. Various attempts have also been made to bend mirrors with a simpler optical figure to obtain a more complex figure, e.g. to bend a cylindrical mirror in order to approximate an ellipsoidal mirror [3.90] or to bend an appropriately shaped plane mirror to also obtain an elliptical mirror by simple adjustment of a single set-screw [3.66]. These kind of systems have proven to be extremely useful in illuminating the entrance slit of normal and grazing incidence monochromators [3.91]. Perhaps more often bent mirrors have been utilized in the X-ray region (see Sect. 3.4.3) of the SR spectrum in order to enhance the acceptance of crystal monochromators or to focus the radiation. It is also quite common to directly focus with bent crystals.

### 3.2.3 Dispersive Elements

#### Reflection grating dispersors

The most commonly used type of dispersor in the VUV is the reflection grating. The simplest system is the plane grating which consists of a number of equidistant lines or grooves ruled on a smooth mirror-like surface. The basic grating equation is obtained by considering the condition for constructive interference between two parallel rays diffracted by two consecutive lines of the grating. The result is [3.10, 3.16]

$$+ m \cdot \lambda = d(\sin \alpha + \sin \beta) \quad (3.8)$$

where  $m$  is an integer specifying the diffraction order and  $d$  is the spacing between the lines. If  $W$  is the ruled width then  $d = W/N$ , where  $N$  is the total number of lines.  $\alpha$  and  $\beta$  are the angles of incidence of the incoming light and the diffracted light, respectively. The sign convention is such that the negative sign applies when the spectrum lies between the central image (where  $\alpha = \beta$ ) and the tangent to the grating ("outside order"). The positive sign must be used, if the spectrum lies between the incident beam and the central image ("inside order"). If one considers the path difference between rays originating from opposite sides of the grating one can work out the theoretical resolving power  $R_0 = \lambda/\Delta\lambda$  of the grating by applying Rayleigh's criterion. This gives

$$R_0 = (W/\lambda) (\sin \alpha + \sin \beta) = \frac{W \cdot m}{d} \quad (3.9)$$

which shows that a high resolution grating must have a large width  $W$  for a given wavelength and that it should be operated at large angles of incidence. The resolving power of a grating also increases with the spectral order number  $m$ . This can be seen from Eqs. 3.8 and 3.9. How close the theoretical limit is approached strongly depends on the quality of the grating. For a spherical concave grating which shall be discussed in detail in the next section Eq. 3.9 does not hold [3.10]. Here one has to introduce an optimum width  $W_{opt}$  [3.10] of the grating to get an optimum resolving power  $R_{opt}$  equal to  $0.92 \cdot W_{opt} (m/d)$ .

The angular dispersion of the grating is obtained by differentiation of Eq. 3.8 with respect to the diffraction angle  $\beta$

$$\frac{d\beta}{d\lambda} = \frac{m}{d \cos \beta} \quad (3.10)$$

Plane gratings already have certain imaging properties due to the dispersion of the light causing the beam cross-section to change after reflection. Simultaneously the virtual size and distance of the light source changes. This is of importance for plane grating grazing incidence monochromators working at SR sources without entrance slit as we shall see below (Sect. 3.3.1).

#### Spherical concave grating

It was Rowland [3.92] who realized that the focusing properties of a mirror and the dispersive properties of a grating can be combined in a single optical component to give a monochromatized stigmatic image of a light source. In Fig. 3.18 Rowland's basic idea is illustrated for a concave spherical grating with radius  $R$ . A circle of radius  $R/2$  which is tangent to the surface of the grating at its center and lying in a plane perpendicular to the direction of the grooves,

is called the Rowland circle. A point light source lying on this circle will be focussed on this circle. Since Rowland's comprehensive treatment the theory of the concave grating has been discussed extensively in the literature. In particular we want to mention the work of BEUTLER (3.93) and NAMIOKA [3.94, 3.95] and, more recently, the work of WERNER [3.96] who was able to give a general focusing condition in a more complete formulation of the theory for all types of ruled surfaces. Also several reviews on the grating theory have been presented [3.10, 3.12, 3.16, 3.43, 3.84]. Here we want to briefly outline the general ideas and introduce the notation in order to have a basis for the later discussion on monochromators.

In Fig. 3.18 we also show the conventional Cartesian coordinate system with the origin in the center of the diffraction grating. An incident ray from point A to point P on the grating surface is diffracted towards point B. Within the geometrical theory of the concave grating a characteristic light pass function F is defined [3.93 - 3.96] as

$$F = \overline{AP} + \overline{BP} + m \cdot w \cdot (\lambda/d) \quad (3.11)$$

In addition to the optical path length  $\overline{AP} + \overline{BP}$  a third term is included which ensures that rays from different grooves of the grating reinforce one another, where  $w$  is a coordinate perpendicular to the grooves along the surface. The light pass function can be expanded as a power series in terms of the coordinates of the grating pupil and the spectral image information can be evaluated by applying Fermat's principle which says that the diffracted point B is located in such a way that the light pass function has a stationary value for any point P on the grating surface. Thus, in order to find the focusing conditions one has to take the partial derivatives of F with respect to the pupil coordinates which then can be related to the aberrations of the concave gra-

ting. WERNER [3.96] gives an extensive discussion on the choice of the coordinate system, in particular if one uses an off-plane mounting [3.97]. In the vicinity of the meridional plane [3.93-95] the expression for the various terms of the light path function can be simplified due to approximations. The resulting equations are still very lengthy and we do not write them down. With increasing power of the series expansion of F the expressions contain successively higher inverse powers of R, r and r' with r and r' being the central rays in the meridional plane (see Fig. 3.18). Since the grating dimensions are small compared to these parameters, the higher order terms in the expansion rapidly decrease in magnitude. These higher order terms can be associated with certain types of aberrations [3.10, 93-96] i.e. with astigmatism, with coma, spectrum line curvature and with spherical aberration, respectively. The first order term of the partial derivative of Eq. 3.11 with respect to the pupil coordinates gives [3.107]

$$\left(1 + \frac{x^2}{r^2}\right)^{1/2} (\sin\alpha + \sin\beta_0) = \frac{m\lambda}{d} \quad (3.12)$$

$$\text{and} \quad \frac{x}{r} = \frac{x'_0}{r'_0} \quad (3.13)$$

with  $(r'_0, \beta_0, x'_0)$  being the coordinates of the image point for the central ray. Since  $x^2/r^2 \ll 1$ , Eq. 3.12 which represents the grating equation for the concave grating, is the same as Eq. 3.8 for the plane grating.

The second order term of the series expansion gives the general image equation for the diffraction grating. In the dispersion plane which is usually called the horizontal focal plane, the focusing properties are described by

$$\frac{\cos^2\alpha}{r} - \frac{\cos\alpha}{R} + \frac{\cos^2\beta}{r'_h} - \frac{\cos\beta}{R} = 0. \quad (3.14)$$

For the properties of the vertical focal plane, i.e. perpendicular to the dispersion plane, one finds

$$\frac{1}{r} - \frac{\cos\alpha}{R} + \frac{1}{r'_v} - \frac{\cos\beta}{R} = 0, \quad (3.15)$$

where  $r'_h$  and  $r'_v$  are the distances to the horizontal and vertical foci respectively.

Eqs. 3.14 and 3.15 have the well-known Rowland circle and Wadsworth mountings as special solutions.

For the Rowland mounting the solution of Eq. 3.14 is

$$r = R \cos \alpha \text{ and } r'_h = R \cos \beta \quad (3.16)$$

which is the equation of a circle (the Rowland circle) expressed in polar coordinates. For the Rowland mounting the entrance and exit slits and the grating lie on a circle with radius  $R/2$ . An appropriately bent photographic plate could be used, for instance, to record the full spectrum simultaneously. The solution of Eq. 3.15 allows to calculate the astigmatism i.e. the difference between the horizontal and vertical foci and is given by

$$r = \frac{R}{\cos \alpha}, \quad r'_v = \frac{R}{\cos \beta} \quad (3.17)$$

Rowland mountings offer optical advantages, since lower order aberration terms, for instance coma, become indentionally zero and spherical aberration remains as the major image distortion. Therefore, this mounting is preferred for high resolution monochromators. At SR sources, where the light source direction is fixed, a scanning Rowland monochromator either generates a spatially varying exit beam which is obviously not desirable, or a fixed exit beam with a complex mechanical linkage of various optical components in addition to the grating. As already pointed out, there exists an optimum grating width for the concave grating  $W_{opt}$  [3.98] which is due to the rapid increase of the spherical aberration term with increasing grating width.  $W_{opt}$  depends on the angles  $\alpha$  and  $\beta$  and on  $R$ , the radius of curvature, but also on  $\lambda$ . Consider a 2 m grating with 1200 grooves per mm. The optimum width at 100 Å wavelength then is 104, 38 and 24 mm for angles of incidence

of 7, 45 and 80 degrees, respectively. The maximum resolving power for a grating illuminated with a point source is [3.98]

$$R_{opt} = 0.92 \cdot W_{opt} \cdot \frac{m}{d} \quad (3.18 a)$$

For a grating much wider than the optimum width the resolution decreases to about 0.8 times  $R_{opt}$ . These theoretical limits are, however, usually not reached, since they require infinitely small slits or at least slit widths  $S$  smaller than  $R \cdot \lambda / W_{opt}$ . The examples for  $W_{opt}$  used above imply a slit width of 0.2, 0.5 and 0.8  $\mu\text{m}$ , respectively or less. The resolution for a spectrograph which is limited by the entrance slit widths is obtained from

$$R_{slit} = 0.92 \cdot \frac{R \cdot \lambda \cdot m}{S \cdot d} \quad (3.18 b)$$

At  $\lambda = 100 \text{ \AA}$  the 2 m, 1200 gr/mm grating would give  $R_{slit}$  of about 500 with 50  $\mu\text{m}$  slit width in contrast to  $R_{opt}$  of more than  $2.6 \times 10^4$ .

A second solution of Eqs. 3.14 and 3.15 is described by

$$r = \infty \text{ and } r'_h = \frac{R \cos^2 \beta}{\cos \alpha + \cos \beta} \quad (3.19)$$

for the focus in the dispersion plane and

$$r = \infty \text{ and } r'_v = \frac{R}{\cos \alpha + \cos \beta} \quad (3.20)$$

in the orthogonal plane. This is the Wadsworth mounting [3.93] which places the source at infinity. This type of mounting is the basis for a large number of monochromators which have been installed at SR laboratories at large accelerators or storage rings (see Sect. 3.3), where one easily finds the ratio of  $r/r' \gtrsim 30$ . If one is working close to normal incidence (i.e.  $\cos \beta \sim 1$ ), then  $r'_h \sim r'_v$  and one obtains a point focus. At this point, we want to note that Wadsworth mountings use the electron or positron beam width as entrance slit which therefore determines the attainable resolution.

Approximate solutions of the equations obtained by setting partial derivatives of the light pass function zero have been given, e.g. the well known Seya-Namioka mounting which minimizes aberrations by the choice of the sum of the angles  $\alpha + \beta$  to be  $70.5^\circ$  [3.10,99,100]. We also want to mention the asymmetric mounting due to POUHEY [3.84,101]. Various monochromator mountings shall be described in Sect. 3.3, but there we do not want to elaborate further on the complex mathematics of imaging properties but rather shall present their advantages and shortcomings.

Aspherical concave gratings

So far we have confined our discussion on spherical concave gratings. However, by various theoretical efforts [3.102,103,104] it has been shown that with aspherical gratings some aberrations occurring with spherical gratings vanish or are at least diminished by a large extent. With elliptical surfaces the ratio  $a/b$  of the half-axis can be determined in such a way that for a given angle of incidence the astigmatic aberration term is minimized for a range of diffraction angles. With  $a/b = 0.134$  NAMIOKA [3.105] was able to reduce the astigmatism to about 25 % of that of a spherical grating. However, it should be kept in mind that aspherical mirror surfaces are difficult to polish and it is even more difficult to rule on elliptical surfaces. Perhaps the future will bring progress with holographically produced gratings. This fairly new promising technique shall be described later on.

Efficiency and blaze

It is of particular importance to know which fraction,  $s$ , of the light intensity incident on a grating is going into the various orders.

While the groove spacing of a grating determines the angular separation of the spectral orders and wavelengths, it is the groove shape which controls the partition of the incident intensity into the spectral orders. As discussed in Sect. 3.2.1 the total reflected intensity is determined by the coating material of the grating. It is this question of grating efficiency which we want to discuss in this paragraph.

Gratings having a sawtooth shape of the grooves are called blazed gratings with the blaze angle being the angle between the normal of the individual groove facet and the overall surface normal. The blaze angle helps to enhance the intensity in a certain wavelength region. This occurs, if the direction of the diffracted lightbeam coincides with the direction of the beam specularly reflected from the groove facets. At near normal incidence the relevant blaze wavelength  $\lambda_B$  is obtained from

$$\lambda_B = 2 \cdot d \cdot \sin \theta_B. \tag{3.21}$$

For a general angle of incidence  $\alpha$  the blaze wavelength  $\lambda_B^+$  is given by

$$\lambda_B^+ = \lambda_B \cdot \cos (\alpha - \theta_B). \tag{3.22}$$

Quite often a grating blazed for the visible or ultraviolet is also blazed for an appropriate VUV wavelength at a grazing angle of incidence. The grating is also blazed for the wavelengths  $\lambda^+/m$  in  $m$ -th order. In the VUV region blazed gratings proved to be superior to lightly ruled gratings. Theoretical calculations on the grating efficiency as a function of groove shape have been performed to various degrees of sophistication. Here we just want to mention the comprehensive most recent work of LOEWEN, NEVIÈRE and MAYSTRE [3.106] and that of HUNTER and co-workers [3.107], which also provides more references. Since the actual groove shape is so important, however, an experimental determination of the efficiency is superior to any theoretical prediction. Experimental set-ups for this purpose are described e.g. in 3.10, 3.66, 3.106, 3.107. Basically, one measures the diffracted intensity

with a suitable reflectometer for a monochromatized beam of light impinging under fixed angle onto the grating in an in-plane mounting. In Fig. 3.19 we reproduce some of the results obtained by HAELBICH et al. [3.10] at 194 Å wavelength for various angles of incidence. The gratings were commercial Bausch and Lomb blazed plane replica gratings, i.e. an epoxy replica of an originally ruled grating, which were either new, used, or used and recoated with Au to restore the reflectivity.

The new replica 9-2 and 10-1-1 of the same master grating with 1200<sup>gr</sup>/mm show efficiencies with strong blaze maxima for the +1 (inside) order. The efficiency is between 12 % and 14 % for these conditions, the highest observed efficiencies were about 20 %. One of the used gratings has been recoated with 600 Å of Au. Under the assumption that different replica from the same master are similar, one finds a deterioration by a factor of 25 from Fig. 3.19 and, this is important to note, after recoating with gold the original efficiency values are practically regained. As a general reference source for efficiency measurements we refer to the proceedings of the last VUV conferences [3.2,3,9,108,109]. We also reproduce a very recent compilation by JOHNSON [3.11] of the efficiencies of various (commercially or not) available gratings in Fig. 3.20 (see also Table 3). This data collection by JOHNSON [3.11] comprises both mechanically ruled gratings and holographically produced gratings. We shall talk about the latter gratings in somewhat more detail later on. But here we see that both types have about the same efficiencies. This result was also obtained by HAELBICH et al. [3.10]. We also learn that the efficiency decreases with increasing line density. The data of Fig. 3.19 and 3.20 were obtained with in-plane mountings, i.e. incoming and diffracted rays are in the meridional plane of the grating. Very interesting off-

plane mountings for grazing incidence have also been considered [3.16,3.96,3.97]. In extreme off-plane mountings the incoming light strikes the grating grooves almost parallel to their direction and not perpendicular as usual. This is called conical diffraction [3.11] and it gives rise to a reflection/diffraction contribution of the whole groove even at grazing incidence which is not the case for in-plane mountings. By these techniques WERNER [3.9] was able to get absolute efficiencies of 30 % in the +1 order at 44 Å wavelength at grazing angles of 0.5 to 6°. This is certainly promising and warrants further investigations. However, only a fairly moderate resolution (~100) can be obtained this way. For certain kinds of secondary spectroscopies as for instance fluorescence this might be sufficient.

#### Holographic gratings

The basic idea of present day advanced holographic grating technology is the relationship between interference fringes and the rulings of a grating. It was already in the last century that CORNU [3.112] realized that a grating with a systematic variation of the grating constant  $d$  has certain focussing properties and he was already able to demonstrate it experimentally. In the following decades various attempts have been made to produce such gratings, but in general those gratings were not useful for spectroscopic purposes [3.43]. In 1966 LABEYRIE [3.113] suggested the method of recording the interference fringes of two coherent laser light beams. In 1967 RUDOLPH and SCHMAHL [3.114] were able to produce a grating by recording the interference fringes of a laser beam in a positive photoresist material which was a thin layer on a flat optical substrate. By a special dissolution technique the exposed resist was converted into a laminar type grating structure which was useful for spectroscopy. In the same year the French company Jobin-Yvon signed the first commercial holographic grating. [3.43]. This company gave considerable impetus on the design of the modern holographic gratings which now actually have imaging properties.

Of course, various other laboratories were also involved in the development of the theory and technology of the holographic grating. For example, SHANKOFF [3.115] and SHERIDON [3.116] succeeded in producing blazed holographic gratings. Because of lack of space we are not able to review all these valuable efforts. For a recent review the reader is referred to Ref. 3.117. The main advantages of holographic gratings are as follows [3.43, 3.106, 3.117]:

- The spectra are completely free of ghosts which are known to occur to various degrees of magnitude on ruled gratings due to periodic irregularities in the groove spacing.
- Spectra have much lower stray light level and better signal to noise ratio.
- The size of gratings only depends on the optics used to produce the interference pattern (up to ~ 45 cm diameter is available).
- Steeply curved substrates (aspherical surfaces) can be used to produce the gratings (at least in principle).
- Wider choice of groove spacing is available ( up to 6000 gr/mm).
- Finally and perhaps most importantly there is the possibility of introducing focussing properties when designing a grating.

Obviously this is a long list of advantages. It is legitimate, however, to ask for disadvantages or, in other words, for which application is the regular grating still the better choice? There is one important point to mention, namely at present, it is not possible to produce all-metal holographic gratings which are as good as described above. However, for certain applications in UHV beamline systems all-metal gratings might be a necessity. Recently RUDOLPH and SCHMAHL [3.117] developed a method for producing gratings with all-metal structures. First tests performed at DESY indicate that the efficiency along the grating surface is not constant [3.107]. This is, however, a technical problem which can be overcome.

To date Jobin Yvon is the main supplier of holographic gratings of various types. According to the gratings' properties they define 4 different types of gratings [3.43]:

- Type I is identical in terms of aberrations to a conventionally ruled grating and is therefore exchangeable.
- Type II has already some aberration compensations built in for certain types of monochromators. For instance, astigmatism reducing gratings are available for Seya-Namioka monochromators.
- Type III and IV are practically complete monochromators in themselves. They can act as a collimator, a diffraction grating and a focussing element even with aberration corrections. Wavelength scanning is achieved by a simple rotation of the grating.

A monochromator for the spectral range 1500 Å to 150 Å based on a Type IV grating is in operation at the LURE SR laboratory with great success [3.118] and at present various other systems of this kind are under construction [3.119,120] for wavelength between 2000 Å and 20 Å. For extreme VUV light holographic gratings now appear to have higher efficiencies than ruled gratings [3.66,110].

The theory of the holographic grating has been worked out in detail in the last few years [3.118-122]. The light pass function (see Eq. 3.11) of the regular concave grating is extended in order to include also such terms which contain the coordinates of the optical arrangement used to produce the gratings. Then the procedure described above is applied: i.e. power series expansion of the light path function and application of Fermat's principle which then yields additional terms which are due to the special geometry of the grating lines. For a detailed description

of the theory the reader is referred to the original literature [3.43, 3.117, 3.120, 3.123].

Zone plates and transmission gratings

Besides the reflection type dispersers which we discussed above in the VUV also transmission type dispersers exist. Until recently [3.10, 3.124] Fresnel zone plates have not been used for practical purpose in the VUV. A zone plate is a "thin-film-optical-element" which consists of an array of concentric rings which alternatively are opaque and transparent to the incident radiation. The widths of the zones or equivalently the radii of circles  $r_n$  are chosen in such a way that the distance from the circumference of a given circle to an image point P on the symmetry axis of the zone plate differs from that of adjacent circles by  $\lambda/2$ . For this geometry and an illumination with parallel light of wavelength  $\lambda$  an enhancement of light intensity at the image point P will occur. The zone plate acts as a lens and the imaging properties are described by the well-known focal equation for a lens. The focal length f of a zone plate for a wavelength  $\lambda$  is given by [3.124]

$$f = \frac{r_1^2}{m \cdot \lambda} \quad \text{with } m = 1, 3, 5, \dots \quad (3.23)$$

if  $\lambda/16 \ll f$ . This is a direct result of the equation describing the radii  $r_n$  of the n th ring

$$r_n^2 = f \cdot n \cdot \lambda + \frac{n^2 \lambda^2}{16} \quad n = 1, 2, 3 \quad (3.24)$$

To a good approximation the attainable resolution  $\Delta$  is given by

$$\Delta = \frac{1.22 \cdot \lambda}{D} \cdot \frac{f}{m} = 1.22 \frac{\lambda}{2 \cdot r_n} \quad (3.25)$$

with D the diameter of the zone plate. For an amplitude zone plate with equal width of opaque and transparent zones the maximum efficiency is  $1/(\pi^2 m^2)$ . SCHMAHL and collaborators [3.125] used holographically made zone plates at wavelengths of 46 Å to 23 Å to focus SR onto a sample for microscopy purposes. The condenser zone plate for instance was made up of 2600 zones with  $r_1 \sim 50 \mu\text{m}$  (see also Sect. 3.6.1). Recently it was suggested [3.126] to prepare fairly thick zone plates by the technique of X-ray lithography in order to use the channels between adjacent zones as reflectors with blaze properties. Also the possibilities of using phase zone plates [3.127] and zone plates with curved surfaces [3.128] have been discussed.

Transmission gratings are closely related to zone plates which disperse and focus the transmitted light. In fact, one can think of the zone plate as a radial transmission grating. The convention more or less is to name laminar amplitude transmission gratings simply as transmission gratings, i.e. an array of wires with approximately rectangular cross-section. In the last two to three years the technology of producing such gratings for use in the X-ray and VUV region has been developed by DIJKSTRA and LANTWAARD [3.129]. Basically it is the same kind of holographic process as is used in the production of zone plates. Typical dimensions of state of the art gratings [3.42, 3.130] are a thickness of about 0.2  $\mu\text{m}$  and 1000 lines per mm. In order to be rigid enough over a large area there is a coarse support structure of about 2  $\mu\text{m}$  thickness. It is believed that the gratings can be constructed to achieve first order transmission up to 25 % in the region of anomalous dispersion [3.130]. The efficiency of a transmission grating can be evaluated as follows. The count rate of a detector which is received in a given order m as a function of photon energy or wave vector q is calculated from the N-slit diffraction pattern taking into account the

modulation by the simple slit diffraction pattern related to the particular fractional slit opening  $a/d$  [3.42, 3.130]. Since the "opaque" thin lines also have a certain transmission in the VUV also the interference between waves passing through transparent parts and those waves attenuated and phase shifted coming through the wire have to be included. With known optical constants the efficiency versus photon energy has been calculated and compared with experimental data. Fig. 3.21 a) shows the ratio of efficiencies of  $m$ -th to 1-st order, part b) displays the first order to zero order ratio values and c) gives the absolute efficiency of the 1st order. The existing discrepancies are believed to be due [3.42, 3.129] to the difficulties in obtaining absolute normalization to the incident beam. One of the potential advantages of transmission gratings is to obtain an optimum efficiency performance for a given energy region by a suitable choice of the grating material and its thickness. In Sect. 3.6.1 we shall discuss monochromator arrangements which have been proposed or already been used. The properties of a transmission grating behind a grazing incidence telescope for cosmic ray spectroscopy are discussed at some detail [3.131].

### 3.2 Crystals for monochromators

The wavelength region where crystal diffraction can be used to monochromatize SR extends in principle up to wavelengths above  $100 \text{ \AA}$ . If  $d_{\infty}$  is the geometrical distance between atomic planes then  $\lambda_{\text{max}} = 2d_{\infty}$  is the maximum usable wavelength. Table 3.3 gives  $d_{\infty}$  for a few useful materials. The anorganic crystals extending to gypsum are usually quite resistive to the primary SR beam. High resolution can be achieved quite easily if the angular divergence of the incoming radiation is small (see Section 3.4). For a perfectly parallel beam the resolution depends only on the single crystal reflection curve as shown in Fig. 3.22. The relative photon energy resolution  $\Delta\epsilon/\epsilon$  for zero crystal absorption depends thus only on the choice of the proper Bragg reflection [3.132] and is independent of the photon energy

$$\frac{\Delta\epsilon}{\epsilon} = \frac{4r_e}{\pi a} F_h d_{\infty}^2 \quad (3.26)$$

where  $F_h$  is the structure factor,  $r_e = e^2/mc^2$  and  $a$  is the lattice constant. Table 3.4 gives calculated resolutions [3.41, 3.132] for a wide range of Bragg reflections ( $F_h$  is set constant here).

In some cases the very high resolution of such perfect crystals is not necessary and even not welcome, since it leads to a considerable loss of intensity. In some cases crystals with a mosaic spread [3.58], namely a crystal consisting of individual subcrystal slabs which are thin compared to the absorption length and having a certain variation in orientations about a mean orientation, can serve to pass a wider wavelength band. Crystals of pyrolytic graphite [3.133] with a mosaic spread of about 10 mrad can serve such a purpose. The disadvantage of using such crystals is an accompanying increase in the divergence of the beam after monochromatization. This could be avoided by producing a strong gradient in the lattice constant of a crystal in a depth smaller than the absorption length [3.134]. Alloying of a single crystal with a gradient in composition appears to be an appropriate method [3.135].

For use with very long wavelengths we mention the so-called soap crystals listed at the end of Table 3.3 [3.136 - 3.139]. These crystals have not found any widespread applications with SR yet due to their low resolution which is reported to be 0.03 - 0.016 [3.138]. Reflectivities are in the order of 1 - 5 % for typically 100 layers in the 20 - 120 Å region [3.138]. For some applications, however, the large band-pass associated with the low resolution could be quite desirable. These crystals are on the borderline to the evaporated multilayer structures mentioned above (Section 3.2.1).

Focussing with crystals can be achieved by bending them either cylindrically or even spherically [3.140, 3.140']. Usually the bending introduces defects which leads to a somewhat enlarged single crystal reflection curve compared to the ideal values as shown in Fig. 3.22. A reduction in the size of a bundle (with an associated increase in its angular spread according to Liouville's theorem) can be accomplished by asymmetric cuts of a crystal [3.37] as shown in Fig. 3.23.

### 3.2.3 Filters and Polarizers

#### Filters and higher order problems

Synchrotron radiation continuously covers the wavelength range from the infrared to the X-ray region. Therefore the spectrum of an optical disperser will contain an admixture of higher harmonics in addition to the fundamental wavelengths. Sometimes higher orders are used to improve the resolution of a monochromator, but generally the higher order contribution is an unwanted effect. In Sect. 3.2.1 we described the method of utilizing a mirror at a grazing angle of incidence as a high energy cut-off filter. Recently this technique has been extended to a system of two plane parallel mirrors. With a simple rotation of the mirrors the cut-off wavelength can be changed to a certain extent maintaining the direction of a slightly displaced exit beam [3.141]. However, often such a system does not provide the necessary spectral purity in particular in the longer wavelength region say above 100 Å due to the missing of a pronounced short wavelength cut-off. On the other hand the transmittance of thin films of some materials does show the desired window-type spectral characteristic in limited wavelength intervals. For example, thin films of Al with a thickness of a few thousand Å (see Fig. 3.24) have the property of transmitting a portion of the VUV spectrum from 72 eV (~ 170 Å) to about 18 eV (~ 680 Å), while blocking the longer wavelengths up to the visible and the short wavelengths down to about 50 Å. This transmission characteristic makes Al one of the most useful transmission filter materials in the VUV. Practically no higher order radiation is present behind an Al filter in the energy range 36 eV to 72 eV.

The transmittance curves  $T(h\nu)$  of Fig. 3.24 have been calculated for film thicknesses  $d = 1000 \text{ \AA}$  and  $3000 \text{ \AA}$  according to the equation  $T = I/I_0 = \exp(-\mu d)$ ,

$$T = I/I_0 = e^{-\mu d} \tag{3.26}$$

where  $I$  and  $I_0$  are the transmitted and incident intensities, respectively, and  $\mu$  is the linear absorption coefficient of the material which is related to the optical constants by

$$\mu = \frac{4\pi k}{\lambda} \quad (3.27)$$

$T = \exp(-\mu d)$  is only valid, if the reflectance  $R \ll 1$  and  $k^2 \ll n^2$ . This is the case for Al for wavelengths up to about 620 Å [3.48]. At longer wavelengths a full treatment has to include possible interference effects which cause  $T$  and  $R$  to exhibit oscillatory behaviour as a function of  $d/\lambda$  [3.48, 3.69, 3.142]. In fact, in the near VUV interference effects in multi-layer systems are used to produce transmission filters with small bandwidth and high transmission [3.61, 3.69, 3.143].

For an exact determination of the transmittance of thin films the optical constants of the materials in question have to be known. At present only very little data sets are available in the VUV [3.48, 3.144]. Recently, a comprehensive collection and tabulation of available absorption data for alkali halides has been published, [3.145]. Compilations of this kind can well serve as starting points for an evaluation of optical constants and sum rules [3.48, 3.146]. In the x-ray region extensive data compilations [3.147] for the mass absorption coefficient are available. However, one should realize that the data are often incorrect at photon energies below about 1000 eV [3.68]. The reason is simply due to the fact that in most cases extrapolated data had to be used rather than measured ones.

In the near VUV data have been accumulated on the transmissivity of thin metal films useful as transmission filters, SAMSON [3.10] presents an overview of the available data up to 1965. Virtually none of these data have been obtained with SR. In subsequent experimental studies with monochromatized SR often

considerable differences have been found in the fine structure of the spectra [3.27, 148-150]. Nevertheless, the compilation of Ref. 3.10 still provides a very useful guide for the selection of transmission filters. In Tab. 3.5 we give the useful wavelength ranges of several often used materials along with the resp. references. Some of the materials are affected by contamination and oxidation resulting in change of transmittance, in formation of pinholes and ultimately in a destruction of the filter. In such cases (e.g. Pr.) a protective overcoating of a very thin ( $\sim 50$  Å) carbon layer has proven to be extremely useful [3.48]. The standard way of preparing VUV filters is by means of various evaporation techniques [3.69, 70]. HUNTER [3.151] also gives a thorough discussion on the influence of pinholes, substrate material, supporting mesh, contamination, aging effects etc. on the transmission characteristic of filters. With Rowland monochromators and some other types of instruments it is hardly possible to keep the spectra free of higher order contributions over large wavelength regions. In such cases the ratio of first to higher orders can be estimated by measuring pronounced absorption edges as discussed in Refs. 3.17, 154. Another method has been proposed by HOWELLS et al. [3.155] based on photoelectric measurements with retarding potentials in order to stop electrons arising from high energy photons from higher order harmonics. It should also be mentioned that under certain circumstances predispersers of any kind can be utilized to select the various orders [3.36, 156].

### Polarizers

The SR sources are the only ones in the VUV emitting highly polarized radiation (compare Chapt. 1 of this volume). The polarization state depends on the elevation angle  $\psi$  between the electron orbit and the observer. For vanishing angle  $\psi$  the radiation is linearly polarized with the electric field vector in the orbital

plane. With increasing elevation angle the perpendicular field component increases with a relative phase difference of plus or minus  $\pi/2$  above or below the orbital plane, respectively. The absolute values of the electric field components are determined by the absolute value of the angle  $\Psi$  (see Chapt. 1).

There is an increasing number of experiments using polarized synchrotron radiation in a variety of applications; for instance, the determination of optical constants with the reflectivity versus angle of incidence technique [3.56, 3.150] (see also Chapter 7), the study of selection rule effects on optically excited electronic transitions [3.157, 3.158] and especially in the field of photoelectron spectroscopy [3.149, 3.159]. All these experiments make use of a known degree of the polarization of the monochromatized light. There is another class of experiments in which the degree of polarization and the phase difference between the mutually perpendicular electric field components is determined, i.e. the ellipsometry technique. This technique is a standard method of determining optical constants in the visible and near UV [3.160]. However, in the VUV at wavelengths below the LiF cut-off (1050 Å) there appears to be only one experimental investigation of this kind [3.161]. This is certainly due to the fact that it is necessary to use reflection polarizers/analyzers in order to analyze the polarization of the reflected light [3.10, 3.162]. Reflection polarizers are not as efficient as transmission polarizers which are in common use in the visible and in the near VUV. However, they are not limited to a certain wavelength range. Furthermore, they can have a high degree of linear polarization, if more than one reflection occurs at an appropriate angle.

The principle of reflection polarizers is evident from Fig. 3.25 where the reflectivity of Pt is plotted versus angle of incidence. If unpolarized light is reflected at an angle near to the so called principal angle of incidence  $\theta_B$ , the degree of polarization of the reflected light acquires a maximum value

depending on the optical constants of the reflecting material as a function of wavelength. If the reflecting material is a non-absorbing ( $k=0$ ) dielectric this occurs at the Brewster angle  $\theta_B$  which is related to the index of reflection by Brewster's law. Then the reflected light is completely plane polarized, since  $R_p$  equals zero. This is not the case for the optical constants of a material as shown in Fig. 3.11 ( $k \neq 0$ ). Here one has to include the absorptive part of the complex index of refraction and one defines a principal angle of incidence  $\theta_B$  for which the phase change is  $90^\circ$  in analogy to the ordinary Brewster law ( $k=0$ , [3.163]). DAMANY [3.164] gives an analytical equation for the angle  $\theta_p$  for which the polarization becomes a maximum and HUMPHREYS-OWEN [3.165] obtained a general solution for the angle  $\theta_m$  where the minimum in  $R_p$  occurs. For example, for the 16.8 eV curves of Fig. 3.11 these three angles span a range of about  $10^\circ$ .

Various types of reflection polarizers have been described in the literature including three (Fig. 3.25a) and four-mirror configurations. Experimenters have used metal (mostly Au) coated mirrors [3.161-165] and combined metal and dielectric mirrors [3.162, 166]. The later configuration is particularly useful in a wavelength range where for the dielectric a true Brewster reflection occurs ( $k=0$ ), since it implies that the  $R_p$  component is zero for the appropriate angles of incidence. Three and four mirror polarizers are built in such a way that the beam is transmitted without deviations (see Fig. 3.25a). For the three mirror system this implies that  $2\alpha - \beta = 90^\circ$  holds with  $\alpha$  and  $\beta$  approximating the Brewster angles in the desired wavelength interval. For the four mirror system all angles are equal.

HASS and HUNTER [3.167] have designed a three mirror system applying two Al and a  $MgF_2$  reflection at angles  $\alpha = 73.5^\circ$  and  $\beta = 57^\circ$  which is approximately the Brewster angle for  $MgF_2$  at 1500 Å. They calculated the ratio  $R_s/R_p$  in the

wavelength range 2000 Å to 300 Å and the throughput  $R_s$  of the system. As expected their results (Fig. 25 b) for  $R_s/R_p$  show a pronounced spike at 1500 Å. But even for wavelengths below 900 Å there is a useful polarization.

Transmission polarizers make use of birefringence and their degree of polarization and throughput are much larger than for reflection type polarizers. However, they are limited in wavelength to about 1200 Å or 10 eV. Various types of transmission polarizers have been described in the literature including Rochon- [3.167], Wollaston- [3.168] and Sénarmont prisms [3.169] and others [3.10, 3.162].

It should also be noted here that Bragg reflection at the appropriate angles is a good method to obtain polarizers and analyzers for the x-ray region.

### 3.3 VUV Monochromators

#### 3.3.1 General Considerations

In the preceding section we have described the most important properties of various optical components, e.g. mirrors, dispersers, filters etc. In this section we want to discuss the design characteristics of monochromators and spectrographs which are in use or have been used at the various SR laboratories.

It is quite common to make a distinction between a monochromator, a spectrometer and a spectrograph (although these terms are sometimes also used equivalently nowadays). All three systems generally work with an entrance slit and a grating in one or the other stigmatic mounting as discussed in Sect. 3.2.2. Both, a monochromator and a spectrometer also have an exit slit to separate out the desired band pass to be used in a subsequent experiment in case of a monochromator or to be measured by a suitable detector (Sect. 3.5) in case of a spectrometer. In contrast, in a spectrograph the whole spectrum is recorded at once on a photographic plate detector. The sample to be analysed generally has to be mounted in front of a spectrograph or spectrometer. This already implies that the choice of a specific system depends on the experiment itself (see Sect. 3.6 for various examples). It is certainly correct that monochromators have to be considered more as general purpose systems. Therefore we essentially describe monochromator systems in this section.

As pointed out already, there exist certain constraints which have to be considered when designing a monochromator for use with SR. For convenience we summarize the most important constraints in Table 3.6, along with some implications depending on the SR light sources. Table 3.6 clearly shows that, in contrast to conventional spectroscopy, at SR facilities the light source, the beam line with the relevant optical components, the monochromator and the experimental set-up itself have to be considered as a whole in order to maximize the flux of monochromatized photons onto the sample. In Sect. 3.1.3

general ideas on beam lines and beam transport have been presented. In summarizing and extending that discussion a bit, there are a few main factors which govern the attainable flux  $N_s(\lambda)$  at the sample:

- The source with a photon flux  $N_k(\lambda)$  per horizontal angle and spectral bandwidth  $k = \lambda/\Delta\lambda$  and with characterizing horizontal and vertical emittances  $\epsilon_{sx}$  and  $\epsilon_{sy}$ .
- The beam line and beam line optics, which transform the source emittances into the beam line emittances  $\epsilon_{Bx}$  and  $\epsilon_{By}$  at the monochromator, having a transmission coefficient  $T_B$  due to reflection efficiencies of the mirrors.
- The beam line acceptance angle, where in general only the horizontal angle  $\theta_x$  is of importance due to finite beam line diameters and size of optics.
- The monochromator with horizontal and vertical acceptances  $\alpha_x$ ,  $\alpha_y$ , resp., and a transmission coefficient  $T_M$ .
- The sample with its effective area. In these terms the monochromatized flux  $N_s(\lambda)$  falling onto the sample is given by [3.17Q]

$$N_s(\lambda) = N_k(\lambda) \cdot \theta_x T_B T_M (\alpha_x / \epsilon_{Bx}) \cdot (\alpha_y / \epsilon_{By}), \quad (3.28)$$

where  $\alpha_i / \epsilon_{Bi}$  are always smaller than one. Assuming an infinite vertical slit which is appropriate due to the collimation of SR,  $N_k(\lambda)$  for an horizontal angle  $\theta_x$  can be derived from Eq. 1.6. Quantitative estimates on the various other quantities of (3.28) are given by BROWN et al. [3.17Q].

Traditionally the various VUV monochromators fall into two classes, namely into normal incidence monochromators (NIM) for the spectral range from about 6 eV to about 50 eV photon energies and into grazing incidence monochromators (GIM) for the range of about 30 eV to 600 eV. Nowadays GIM's at fairly large grazing angles are frequently also used in the photon energy range down to 10 eV

Nevertheless, in the following we shall subdivide the presentation into NIM's in Sect. 3.3.2, GIM's in Sect. 3.3.3 and new design concepts in Sect. 3.3.4.

### 3.3.2 Normal Incidence Monochromators

Three NIM mountings are commonly used with SR sources, the standard NIM, the Seya-Namioka monochromator and the so called modified Wadsworth monochromator. These three types are the conventional mounts of concave spherical gratings with the focussing properties determined by the second order terms of the series expansion of Eq. 3.11 as discussed in Sect. 3.2.2. But monochromators based on newer optical designs with spherical gratings have also been built; for instance, a mount using higher order focussing derived from a generalized focussing condition [3.84, 3.10U] or an asymmetrical mounting [3.17U]. For a long time conventionally ruled concave gratings have been used in these instruments. Nowadays, they are more and more replaced by holographically produced gratings due to the various reasons discussed in Sect. 3.2.2. In Fig. 3.26 we give a schematic diagram of some of the important NIM's being used for SR light sources. In Tab. 3.7 further information is provided including references to the original work. In the literature a variety of other NIM's is discussed [3.10-3.13, 3.16, 3.43] which, to the author's knowledge, have not been used with SR light sources.

The standard NIM is a monochromator operating in a mode close to the Rowland the focussing conditions determined by Eqs. 3.16 and 3.17. These are accurately given by Eqs. 3.14 and 3.15. The monochromator itself has only one optical component, namely the grating. This is the same with the other NIM's to be discussed. In order to vary the wavelength the grating has to be rotated and, for maintaining focussing, it has to be

translated at the same time. Thus the basic principle of the scanning mechanism of a standard NIM consists in a movement of the grating along the bisector of the angle which is subtended by the entrance and exit slit at the center of the grating with a simultaneous rotation about a vertical axis tangent to its center [3.10]. The most widely used system is that of the McPherson company [3.17] which uses an angle of 15 degrees. This system has the capability of high resolution with its ultimate value depending on the gratings' constant and on the radius of curvature. With a 3 m focal length a resolution of  $0.03 \text{ \AA}$  independent of wavelength has been achieved with 10  $\mu\text{m}$  wide slits and the 1200gr/mm grating illuminated over an area of about  $82 \times 60 \text{ mm}^2$  [3.173,174]. This NIM (McPherson) is installed at the DORIS storage ring SR laboratory (compare Sect. 3.1 and Figs. 3.2a and b) and has proven as an invaluable instrument for high resolution spectroscopy [3.174]. For a proper optical matching to the source a focussing mirror has to be installed in front of the entrance slit. The magnification of this optical system should be chosen in such a way that the image of the orbiting electrons just fills the width of the entrance slit. If the slit width is smaller than the image of the source, one loses intensity but the resolution is not affected. Usually one has to make a compromise due to the requirements of different resolution, i.e. slit width, for different experiments and also due to problems in finding an appropriately figured mirror (see Sect. 3.2.1) in VUV quality.

The focussing conditions of the Wadsworth mounting are approximately expressed by Eqs. 3.19 and 20. It requires the light source to be at infinity for an optimum performance in producing a point like stigmatic focus. Thus, this mounting exploits one of the particular properties of SR, namely the small divergence. SKIBOWSKI and STEINMANN [3.175] were the first to build a Wadsworth monochromator at the DESY laboratory

in 1967. Since that time a large number of such monochromators has been designed with slight modifications [3.155,3.176-3.181]. It is appropriate to say that the Wadsworth monochromator is the work horse of the NIM's. The basic layout of such an instrument is shown in Fig. 3.26; features of particular monochromators are given in Tab. 3.5. The instrument operates without a real entrance slit which actually is substituted by the electron beam. Wavelength scanning is achieved by a simple rotation of the grating. In order to compensate for the severe defocussing when working with a fixed exit slit, one uses an excentric pivot for rotation of the grating similar to the Johnson-Onaka mounting [3.10]. The optimum off-axis position depends on the grating parameters and the sum  $B$  of the angle of incidence and refraction. This is shown in Fig. 3.27 for a 2 m concave grating. The straight line is drawn as a best fit to the focussing curve for the desired angle  $B$  and the required pivot length can be derived from the plot Fig. 3.27 [3.155].

The attainable resolution of the Wadsworth monochromator is determined by the remaining defocussing and the finite image size of the source point which is horizontally about 5 times as wide as vertically for most SR sources. Thus, by vertical mounting of the dispersion plane one increases the resolution [3.176,3.177]. In addition, the degree of light polarization is improved by the s-reflection. Typical resolutions are between 0.5 and  $2 \text{ \AA}$  for vertical mounting and standard gratings. For grating protection often premirrors are introduced [3.155, 3.176-3.180], which also offer the possibility of giving the monochromatized light a convenient direction in the laboratory. Of course, the latter goal can also be achieved by using mirrors behind the exit slit in connection with refocussing [3.176,3.180]. Type I holographic diffraction gratings have been used with great success [3.178]. Fig. 3.28 shows two spectra obtained with a ruled grating and a holographic grating in a vertically dispersing mounting at the DORIS storage ring [3.179]. Also, by using corrected holographic gratings, the characteristic of a monochromator has been considerably improved [3.181].

The Seya-Namioka monochromator (Fig. 3.26) with its real entrance and exit slits is designed to have the simplest scanning mechanism, i.e. single rotation of the grating about an axis through the center of the grating. Seya and Namioka [3.99, 3.100] have shown that deviations from the Rowland circle can be minimized by choosing the angle between the incident and diffracted beam to be  $70.5^\circ$ . Due to the fairly large angle of incidence the most severe aberration of this monochromator is its astigmatism, if a point light source is used near the entrance slit. This drawback can be corrected for by utilizing additional focussing mirrors [3.182] or by using appropriately corrected holographic gratings. By an asymmetrical illumination of the grating one can also improve the degree of defocalization and thus improve the resolution [3.171]. In the standard Seya-Namioka mounting the distances  $r$  and  $r'$  of the slits to the center of the grating (see Fig. 3.18) are equal. A corrected Seya-Namioka-mounting [3.101, 3.183] is obtained by making  $r$  and  $r'$  slightly unequal. Using SR the aberrations of the standard mounting can be reduced by long focal length and astigmatic source optics when illuminating the entrance slit [3.81]. With a vertically dispersing instrument at the Stanford SR source a resolution of  $0.18 \text{ \AA}$  has been obtained with a one meter 1200 1/mm grating and 20  $\mu\text{m}$  slits. Nowadays in general vertically dispersing instruments are used and planned with a layout as that given schematically in Fig. 3.26.

A fourth type of mounting included in Fig. 3.26 is due to POUÉY [3.84, 3.101] and is based on higher order focussing derived from a generalized focussing condition. Some of the characteristics of this mounting are [3.101]:

- A fixed angle  $2\theta$  subtended by the fixed slits at the grating which can be chosen between  $10^\circ$  and  $170^\circ$  depending on the grating.
- The luminosity resolution product reaches a maximum at low  $\theta$  values (between  $14^\circ$  and  $17^\circ$ ) for a 1200 1/mm grating and increases with the number  $N$  of lines for  $\theta$  values larger than  $35^\circ$ .

- Optical correction allows an improved resolution even for the simple rotation wavelength scanning mechanism.
- To one object (or image distance) correspond two  $\theta$  values above and below  $35^\circ$ .

These characteristics as well as others [3.101] lead to the design and construction of a monochromator with four exit slits used with SR at the LURE laboratory.

Also other monochromators operating with a simple rotation of the grating and working with corrected holographic gratings at near normal incidence have been designed [3.184]. We are not aware, if such systems have been built for use with SR. A similar system operating at grazing incidence will be described in Sect. 3.3.4.

### 3.3.4 Grazing Incidence Monochromators

A survey on grazing incidence monochromators (GIM) was given by one of the present authors in 1973 [3.17]. Several general aspects of GIM's have been discussed in that paper, as for instance the importance and effects of the acceptance window, the size of the source, the distance from the source, higher orders, straylight, etc. In view of this discussion and the various comments and remarks, which we have included in the previous paragraphs, we confine ourselves in this subsection to a description of the various types of grazing incidence monochromators which have been used in conjunction with synchrotron radiation. Some types, which have been abandoned again due to the design of more convenient instruments, are still included in the discussion, since they illustrate the development of the techniques to the present day's highly sophisticated grazing incidence wavelength scanning systems. However, it is neither intended nor possible within limited space to give a complete discussion of all instruments. Similar to the report on NIM's, we outline the principle of operation and give some comments on their performance. Figs. 3.29, 30 and 32 give a survey of plane grating monochromators, Rowland-type monochromators and Non-Rowland monochromators with focussing gratings, respectively. A comparison of the different instruments is given in Table 3.8.

#### Plane grating monochromators

Fig. 3.29 a shows the simplest possible instrument [3.56, 3.186] with only one optical surface, a plane grating. Wavelength change is achieved by means of rotating a Soller slit system around an axis parallel to the grating grooves. Of course, only very moderate resolution is attainable and higher order suppression is only given in limited wavelength ranges. The latter can be improved by installing a plane mirror in front of the grating, a provision which at high energy SR sources is anyhow necessary for protecting the sensitive gratings from direct

exposure to SR [3.56]. It should be realized that this mounting belongs to the "historical ones" which are no longer used.

The instrument shown in Fig. 3.29 b uses a plane grating and a spherical mirror [3.187]. The grating is rotated by small angles so that the sum of entrance and exit angles is fixed. The exit beam is spatially fixed which allows the installation of complex experiments. With one spherical mirror two different optical arrangements are possible, if different values for the sum of entrance and exit angles are allowed with a fixed mirror. The two arrangements yield the same position of the exit beam. Only one of the two possibilities is drawn in Fig. 3.29 b. Suppression of higher orders is achieved only in a limited wavelength range by a suitable choice of the angles of incidence at the grating and the concave mirror. For best higher order reduction it is preferred to work in negative orders. It also determines the choice of the two possible mounting configurations. On the basis of this design a vertically dispersing monochromator has been built at Daresbury Laboratory [3.188] with provisions made to test both mounting possibilities. The operation of the instrument proved successful in practice also for the position which has less higher order reduction capability. Therefore a new instrument has been designed at Daresbury implementing the option of using two different focussing mirrors by means of a precision translation stage [3.189]. Also with this system it is common to use a grazing incidence premirror.

The instrument in Fig. 3.29 c was built to operate at the DESY synchrotron [3.190]. It utilizes a plane mirror, a plane grating and a paraboloid mirror for focussing and produces a fixed exit beam. The motion of the premirror and the grating is coupled in a fairly complex way. In its simplest mode of operation the premirror travels along the incident beam and rotates at the same time in such a way as to illuminate always the center of the grating. Simultaneously the grating rotates so that it remains parallel to the premirror. Zero order emerges parallel to the incoming beam while light at a fixed angular separation from the zero order

beam is accepted by the exit slit. This type of wavelength change is favourable for the suppression of higher orders, since the longer wavelengths are taken at the steep angles. Indeed with a 1200 lines/mm grating and the other parameters (e.g. coating material of the components) properly chosen higher order light can be efficiently suppressed over the whole range of operation. Moreover, this instrument is set up to always operate at the blaze maximum independent of wavelength. With additional "non-parallel" modes of operation, where the order suppression is less effective, the DESY instrument covers the energy range 15 - 280 eV. The maximum intensity is around 100 eV with a resolution of 1:400 to 1:800. Since the system operates without entrance slit, the width of the electron beam in the synchrotron is the limiting factor for the resolution. This complex coupled motion is accomplished, if a complicated mechanical coupling can be used within the vacuum system. This is, however, impossible for UHV monochromators as they are installed at high energy storage rings such as e.g. DORIS. Therefore the design of the plane grating monochromator c) had to be modified in such a way that a series of 6 plane premirrors at different angles of incidence can be used alternatively instead of the single traveling and rotating mirror in Fig. 3.29c [3.19]. Each premirror allows a wavelength scanning by a simple rotation of the grating. Due to a careful selection of the mirror coating materials (see Sect. 3.2.1, 3.73) and appropriate angles of incidence onto the premirror and the grating the monochromator offers mutually overlapping wavelength ranges with extremely small higher order contributions. Since the source width at DORIS is smaller and much more stable than at the DESY synchrotron and due to a high quality manually ground parabolic mirror [3.19] the resolution ( $E/\Delta E$ ) reaches about 3000 at some wavelengths. In general, such a high resolution can only be obtained with Rowland type mountings.

### Rowland mountings

Fig. 3.30 schematically shows six different instruments based on the Rowland circle mounting (Sect. 3.2.2, Eqs. 3.16 and 17) [3.19]. Entrance slit, grating and exit slit are all located on the Rowland circle to minimize aberrations. In principle, this mounting provides the best resolution for grazing incidence monochromators.

The simplest version of a Rowland mounting is illustrated in Fig. 3.30 a. The disadvantage of this conventional instrument is the travelling exit slit. Apart from a few exceptions, mainly absorption measurements are possible with the samples in front of the spectrometer. For absorption type experiments the Rowland spectrograph is extremely useful, since the photographic plate detectors allow the whole spectrum to be taken at a single exposure. Rowland instruments can be operated to fairly short wavelength of about  $10 \text{ \AA}$  which already approaches the domain of crystal spectrometers. However the standard regime is for wavelengths above  $\sim 25 \text{ \AA}$ . The usual way to illuminate a conventional Rowland instrument with SR is by means of a focussing premirror at grazing incidence. Again, in order to maximize the available intensity behind the exit slit, one has to take care of a proper matching of the image of the source to the slit. We note that for grazing incidence spherical optics the spherical aberration induced increase in focal size is of limiting importance.

The instrument shown in Fig. 3.30 b was constructed by CODLING and MITCHELL [3.194] at Reading and used at Glasgow and Daresbury. It combines the advantages of a Rowland mounting with the property of having a fixed exit beam. Entrance and exit slits are fixed while the grating slides along the Rowland circle. The directions of the incoming and outgoing beams are changed by a rotating mirror-slit-combination. A fourth focussing mirror is needed to illuminate the entrance slit. A disadvantage of the present arrangement lies in the fact that the longer

wavelengths pass the instrument at more grazing angles. This can cause considerable problems with higher orders.

A new type of grazing incidence spectromonochromator [3.156, 3.195] has been built by JAEGLÉ and coworkers for use with SR of the LURE laboratory and for plasma research. The layout of the instrument is based on a two-grating principle. Two gratings,  $G_1$  and  $G_2$ , with the same radius of curvature are mounted on the same Rowland circle. A mirror FM, with the same radius, is also mounted on the Rowland circle between the two gratings. A prefocussing concave mirror in front of the entrance slit allows to vary the grazing incidence angle on the first grating  $G_1$ . The instrument can be used in a one or two-grating mode and provides a fixed exit beam. In the two grating mode, shown in Fig. 3.30 c) the prefocussing mirror and  $G_1$  are fixed. The wavelength scanning is achieved by a coupled displacement of the intermediate mirror and the second grating  $G_2$  along the Rowland circle. The exit slit is a special rotating system with a mirror and a single slit jaw. The advantage of the two grating mode lies in its order-sorting capability and its resolution. In the one-grating mode the intensity throughput is about 100 x higher [3.156]. However, in this mode the monochromatized radiation is not always free of higher orders. In this mode wavelength scanning is achieved by a rotation of the prefocussing mirror which is connected with the displacement of  $G_1$  along the Rowland circle [3.195]. Apparently this instrument works quite satisfactory, since three more copies are under construction [3.156]. It is however a question how the complicated driving mechanism behaves under UHV requirements.

The instrument shown in Fig. 3.30 d) is a double-Vodar monochromator which has been installed at the Stoughton storage ring [3.196]. The two spherical gratings,  $G_1$  and  $G_2$ , together with the entrance slit of the second sub-instrument (exit slit of the first one) are connected rigidly by a bar. This unit is con-

strained in such a way that the exit slit and the second grating move on straight lines which meet at the position of the exit slit. The focussing mirror and the first entrance slit move together along the incoming beam so that the first grating is always illuminated. The two gratings must have the same number of lines/mm but not necessarily the same curvature. The two Rowland sub-instruments operate in tandem yielding a fixed exit beam. The unpredictable aspect of this instrument lies in the gratings one of which is used in negative order.

The monochromator given in Fig. 3.30 e) is in the testing stage at the Bonn synchrotron (3.197, 19<sup>a</sup>). The original idea was to restrict the number of reflections to two, which means that it is not possible to generate a fixed exit direction of the beam. However, the position of the exit slit is fixed. The toroid mirror moves along the incoming beam and rotates at the same time. Simultaneously the coupled entrance slit grating unit undergoes a complicated motion. The coupled motion is determined by the following constraints: 1. Rowland condition has to be fulfilled and 2. the toroid mirror has to illuminate the grating with its focus being at the entrance slit. The focussing in the direction perpendicular to the plane of dispersion is only fulfilled approximately. It is intended to use this instrument for photoelectron spectroscopy on gases.

The instrument shown in Fig. 3.30 f) is one of the first bakeable UHV systems built for use at the Stanford storage ring laboratory [3.170]. The optical principle is related to that introduced by SALLE and VODAR [3.199]. A one meter Rowland circle rotates about the exit slit  $S_2$  to give a fixed exit beam. The grating is mounted on an arm connecting the entrance slit FM (similar to that described for the Jaeglé mounting Fig. 30 c) and the grating and pivots about the entrance slit-mirror-combination together with  $M_1$  which translates parallel to the incoming beam [3.170]. The necessary high precision is achieved

by means of a linear air bearing which is referenced to a ground marble slab. The monochromator delivers a spectral bandwidth of  $0.15 \text{ \AA}$  at a scanning range 20 eV to zero order. With a 600 1/mm grating blazed at  $1^{\circ}31'$  the total photoyield of a Au emitter has been measured up to 700 eV (Fig. 3.31). The focussing all-metal premirror (not shown in Fig. 3.30 f) had a measured rms roughness of about  $165 \text{ \AA}$  for the lower curve in Fig. 3.31 whereas a new superpolished Cu mirror had a rms roughness of about  $30 \text{ \AA}$ . Note the drastic intensity increase for energies above the carbon K edge. As pointed out earlier this is also due to hydrocarbon build-up on used mirrors. In the last 3 years this instrument has been utilized for a variety of experiments. A second copy of this monochromator (named "Grasshopper") is presently tested at the PSL laboratory [3.119] with important improvements incorporated (e.g. variable slits).

#### Non-Rowland monochromators

The principle of two further instruments in which the electron beam is used as the entrance aperture is sketched in Fig. 3.32, Part a) shows how it is possible to change the alignment of a conventional Rowland instrument in such a way that it can be used without an entrance slit [3.1, 3.154]. The focal curves for the illumination of a grating with parallel light are lemniscates [3.93]. The grating of a Rowland monochromator can be tilted so that the path of the exit slit intersects this focal curve, at a wavelength position where optimum resolution is desired. This mounting yields high intensity because the light undergoes only a single reflection. However there are problems due to the direct illumination of the grating and due to higher order contributions.

At the NBS an instrument has been built with only a single optical element, having a fixed exit beam (Fig. 3.32 b). With the special geometry at the NBS synchrotron it could be shown that combinations of entrance angles and exit angles exist (in negative order), where a slight rotation of the grating causes

only second order focussing errors. With a grating ruled on a toroidal surface an almost stigmatic focus could be achieved.

#### 3.3.4 New Concepts

The various mountings discussed in the preceding sections can be realized with mechanically ruled gratings. In this section we briefly want to describe new mounting concepts utilizing holographic and transmission gratings.

In Fig. 3.33 a) the principle of a toroidal holographic grating monochromator is shown. A type III Jobin Yvon grating is used (see Sect. 3.2.2) to achieve the whole monochromator action by a simple rotation of the grating at a grazing angle of incidence of the light. The aberrations inherent with ruled gratings are largely compensated for by the special arrangement of lines obtainable only with the holographic production techniques [3.120]. A small 30 cm focal distance instrument is successfully operating at the ACO storage ring [3.118] in the energy range 15 eV to 100 eV with a high efficiency and a relatively good resolution ( $0.7 \text{ \AA}$  for 100  $\mu\text{m}$  slits). New designs have been worked out to extend the energy range to higher energies and to improve on the resolution. Prototype instruments have been built and are being tested at the ACO ring [3.120]. Three monochromators are under construction with toroidal gratings with entrance length of about 1.1 m and exit length of 1.8 m and an angle of  $150^{\circ}$  between the beams. Two interchangeable gratings are held in special flip over grating holders as indicated in Fig. 3.33 a). With a 1800 gr/mm grating a useful energy range 40 eV to 150 eV is obtained at a calculated resolution of 0.2 to  $0.3 \text{ \AA}$ . With 450 gr/mm grating the useful energy range is about 10 eV to 40 eV at a resolution of  $0.8 \text{ \AA}$  to  $1.2 \text{ \AA}$  [3.119]. These instruments give promise for improved intensities in the monochromatized beams.

The energy range 300 eV to 1000 eV is still the most problematic range to work at due to the various reasons given above. A monochromator design based on a transmission grating has been suggested for use with SR. The layout of Fig. 3.33 is thought [3.42, 3.130] to work also in this problematic energy range. However, since mirrors have to be used for focussing purposes anyhow, contamination, surface roughness and other problems still remain. At present, it appears that more experience with these dispersing elements has to be collected. A first transmission grating monochromator for work with light from resonance lines is in operation at energies below 40 eV. The whole crude monochromator essentially consists of the transmission grating which is tilted for varying the wavelength [3.202].

### 3.4 X-Ray Monochromators

#### 3.4.1 Plane Crystal Instruments

PARRATT [3.203] in 1959 appears to have been the first to note the excellent matching of a double crystal monochromator (Fig. 3.34) to the SR source. Double crystal monochromators in the parallel mode keep the direction of SR fixed while generating only a parallel displacement of the beam. They are nowadays most widely used for high resolution spectrometers with groove cut crystals which are ideally suited for continuous scanning of a spectrum [3.204, 3.204']. CAUCHOIS and coworkers [3.205] were the first to use a fairly simple monochromator in connection with SR at Frascati consisting of one single crystal.

BEAUMONT and HART [3.132] and BONSE et al. [3.206] have discussed and tested several plane crystal arrangements with SR as shown in Fig. 3.35. While the former have concentrated their effort to calculate resolution and to test several quite different multireflection arrangements the latter [3.206] have attacked especially the problem of higher order rejection. The classical highly dispersive (+,+) setting of the double crystal monochromator (Fig. 3.34), as it was first proposed by EHRENBERG and MARK [3.207] in 1927, could never be used with sufficient intensity, since its angular acceptance in the dispersive direction is of the order of the width of the single crystal reflection curve (see Fig. 3.22). For this arrangement the high brightness of SR is of crucial importance and very high resolution can be obtained by selecting the appropriate reflections (see Table 3.3).

When scanning wavelength with a (+,+) spectrometer as shown in Fig. 3.34 a fairly complicated mechanism is necessary to achieve a continuous scan. The second crystal has to be rotated around the first one and the detector again around the second crystal. In addition, first and second crystals must be rotated around an axis lying in their surfaces, all with different angular

speeds. Before we discuss how to overcome these problems we want to describe the (+,-) setting of the double crystal monochromator.

The (+,-) arrangement is shown in Fig. 3.34. In this case the arrangement is not any more a perfect angle selector. Different energies are transmitted for different angles of incidence. In practice this spectrometer is equivalent to a spectrometer consisting of a single crystal with the advantage that the second crystal deflects the radiation back to its original direction. Thus scanning of a spectrum involves only small lateral displacements of the beam, but no angular deflection. The resolution of this arrangement is usually determined by the geometrical arrangement. The size of the aperture in the dispersive direction, the distance from the source and source characteristic as described in Sect. 3.1.3 determine an acceptance angle  $\Delta\theta$ , which according to

$$\frac{\Delta\lambda}{\lambda} = \frac{\Delta\varepsilon}{\varepsilon} = \cotg \theta \Delta\theta \quad (3.29)$$

defines the resolution. Detailed estimates of the resolution based on (3.29) have been made e.g. by PIANETTA and LINDAU [3.39] and BONSE et al. [3.206]. If  $\Delta\theta$  is very small, however, in addition to the geometrical effect the width of the single crystal reflection curve should also be taken into account. Typical values for this (+,-) arrangement are  $\Delta\varepsilon/\varepsilon = 10^{-4}$  to  $10^{-3}$  [3.206]. LINDAU and PIANETTA [3.39], however, have obtained  $2.5 \cdot 10^{-5}$  by using very narrow collimators. Such a good collimation, on the other hand costs a lot of intensity.

One particular problem encountered with this type of monochromator is a phenomenon which KINCAID [3.204] calls "glitches". Always, when the rotation of the monochromator leads to additional oblique lattice planes coming into the reflecting position for the same wavelength as the main lattice planes, an *Umweganregung* to the intensity in the main channel takes place, with several complex geometry determined effects on the measured signal.

Often these glitches can be eliminated during data evaluation. But it should also be possible to control these unwanted structures, perhaps even eliminate them, by using specially cut groove crystals or spectrometers made from two individually cut crystals [3.208].

The (+,-) arrangement is widely applied for EXAFS-spectrometers [see e.g. 3.204]. The main goal in EXAFS is to measure the extended x-ray absorption fine structure above the x-ray edges. These structures are a modulation of the absorption coefficient with a periodicity length of several tens of eV extending up to 1000 eV above the edge (see Sect. 3.6.2). Only moderate resolution is needed in order to resolve this structure. In this case a vertically deflecting double focussing mirror which gives a 1:1 image of the SR source is tolerable in front of the monochromator. The increased angular divergence reduces the resolution to about  $5 \cdot 10^{-4}$  which, however, is sufficient. In return a gain in flux density on the sample by about two orders of magnitude is obtained [3.209]. Higher order radiation usually contributes only to the flat structureless background. This background can cause troubles when quantitative amplitude information is desired.

A very convenient arrangement of a monochromator with four reflections and zero beam deviation is shown in Fig. 3.35a. This arrangement is a combination of the (+,-) and the (+,+) double crystal monochromator. This instrument combines highest resolution with simple scanning and independence of position fluctuations of the source. Such an instrument was first built at Daresbury [3.210] and is presently installed at DESY. According to BONSE and HART [3.210] such multiple reflections serve to suppress the tails in the single crystal reflection curves (Fig. 3.22) and thus the resolution function is improved. Some of the other proposed monochromators (Fig. 3.35) serve this purpose while others give intentional deflections to the monochromatic beam in order to avoid the direct beam of SR in cases of difficult shielding and even others have high mechanical

stability. Quite obviously additional arrangements are possible and will find applications under special circumstances.

As an example of the phase space methods introduced in Section 3.1.3 we show in Fig. 3.36 the acceptance for the antiparallel (+,+) spectrometer at the source ellipse for a vertically dispersing instrument. This spectrometer generates a pure angular slit with a width determined by the single crystal reflection curve. If properly aligned the slit picks the central position of the SR emission pattern [3.39, 3.40].

#### 3.4.2 Higher Order Rejection

Unwanted effects in all the monochromators of Fig. 3.35 and also the focussing instruments described in Section 3.4.4 are the admixture of higher order wavelengths namely in addition to  $\lambda$  also  $\lambda/2$ ,  $\lambda/3$ , etc. In special cases like e.g. the Si or Ge (111) reflections the second order reflection is avoided due to special structure factors, e.g. (222) has zero intensity. This, however, does not provide a general method for higher order rejection. As in the equivalent cases with ruled gratings in the vacuum ultraviolet the problem of higher orders depends on the type of experiment performed. Higher orders can be suppressed already in the monochromator or in the detector or just by the special experimental arrangement in use. There are, however, cases in which a fairly small contribution of higher order radiation can be enhanced and thus can have disturbing effects on the experimental results. Therefore we shall describe here one of the methods to suppress higher order radiation in more detail. BONSE et al. [3.206] suggest to use a spectrometer as it is shown as an insert of Fig. 3.37. Such a monochromator uses reflections from two different types of crystals, Si and Ge in this case. Small wavelength shifts and shifts of the effective angle of diffraction occur, because the

index of refraction differs from 1 between the inside and the outside of the crystal. Thus, for a fixed direction crystal reflection does not occur exactly for harmonics of the fundamental frequency but for slightly detuned frequencies. This detuning depends on the wavelength, the angle of incidence and on the electronic density of the monochromator crystals. The angle of incidence on the Ge crystal in Fig. 3.37 can be slightly detuned in such a way that the first order radiation coming from the Si crystal is still reflected while the higher orders are not. In Fig. 3.37 it is demonstrated [3.206] that an alignment which maximizes the fundamental frequency suppresses higher harmonics while in an alignment in which the first harmonic is maximized also the higher harmonics and the fundamental frequency are present.

A similar method was applied by BONSE et al. [3.206] in connection with their interferometer. In this case Si (1 $\bar{1}$ 0) reflection are used first in the Bragg (reflection) case second in the Laue (transmission) case. Since the radiation penetrates into the crystals at different angles with respect to the surface there is again a separation of orders possible.

MATERLIK et al. [3.211] have built a groove cut monochromator of the type Fig. 3.34(a) which has the first reflector cut at an angle which is oblique compared to the lattice planes (see Fig. 3.23). A slight angular detuning again serves to maximize the fundamental and suppresses higher harmonics. In addition such arrangements serve to concentrate the beam (see Section 3.2.2).

Another means of suppressing harmonics is reflection from mirrors (see Section 3.2.1). With an appropriate choice of the angle of incidence harmonics can be effectively suppressed. Problems arise with scanning monochromators for which also the angle of incidence onto the mirror needs to be scanned. This technique up to now is mainly applied with focussing instruments for which the

mirror also serves to achieve focussing in one or two planes when it has the appropriate curved shape [3.212-3.215].

### 3.4.3 Bent Crystal Monochromators

If a crystal, cut with the reflecting lattice planes parallel to the surface, is bent in one direction it focuses radiation emerging from a source point on the Rowland circle back to an image lying again on the Rowland circle [3.58, 3.212, 3.213]. In contrast to a grating monochromator this condition is fulfilled only for one wavelength (and higher harmonics) at specular reflection. For work involving SR the distance to the crystal is large and consequently the image point would lie at the same distance from the crystal. Scanning of the spectrum is prohibitively complicated. No such monochromators have been built up to now.

ROSENBAUM et al. [3.213, 214] were the first to build a focusing monochromator with asymmetric distances between the source and the crystal and the crystal and the focus at the DESY synchrotron. Two more instruments applying practically the same principle have been built in the meantime by WEBB et al. [3.215-3.217] at SPEAR and by HASELGROVE et al. [3.218] at Daresbury. All these instruments are used for small angle diffraction from biological samples. Therefore the band pass of the monochromator is not of such a critical importance. It is easily verified that with a white source like SR a crystal bent to any radius will reflect radiation like a mirror. If the bending radius deviates from the appropriate Rowland radius different portions of the crystal will reflect different wavelengths. Thus focussing at a shorter distance (and correspondingly a demagnification of the source) can be achieved at the cost of resolution.

With the focal distance of 1.5 m aimed at by ROSENBAUM et al. [3.213] and the source distance of 37 m the wavelength spread with useful apertures would have been prohibitively large. As mentioned above, GUINIER [3.37] has shown that the focal distance can be reduced when cutting the crystal surface at an angle  $\sigma$  with respect to the lattice planes as shown in Fig. 3.23. Then the source and the image lie still on the Rowland circle, but the distance to the source  $g$  and the distance to the focus  $f$  are given by

$$g = R \sin (\theta + \sigma), f = R \sin (\theta - \sigma), \tag{3.30}$$

where  $R$  is the radius of curvature and  $\theta$  the Bragg angle. For  $\lambda = 1.5 \text{ \AA}$ ,  $\theta = 13^\circ$  with quartz ( $10\bar{1}1$ ) reflecting planes,  $\sigma = 7^\circ$  was chosen [3.213]. This would give a focus at 11.3 m with  $g = 37$  m distance and a bending radius  $R = 108$  m according to [3.213]. Further bending to a radius of about 30 m is necessary to bring down the focal length to 1.5 m. As a consequence the band width of the radiation reflected by the 45 mm long crystal is about  $3 \cdot 10^{-3} \text{ \AA}$ . This is not to be confused with the transmitted band width for one direction relative to the lattice planes which depends only on the single crystal reflection curve. This band width is estimated to be  $\Delta\lambda = 2.4 \cdot 10^{-4} \text{ \AA}$  [3.213]. An increase of this band width by introducing artificial mosaic spread or gradients in the lattice constant as mentioned in Section 3.2.2 would be highly desirable in order to increase the reflected intensity in such monochromators.

Focussing in the perpendicular direction and higher order rejection is achieved by a mirror bent to a radius of 1000 m giving total reflection at a glancing angle around 4 mrad (see Sect. 3.2.1). The focal spot has a size of 200  $\mu\text{m}$  with a gain in speed at the photographic plate of more than two orders of magnitude over classical instruments [3.213, 3.214] already at a synchrotron like DESY.

### 3.5 Photon Detectors

In this section we present a survey on photon detection systems which are currently utilized in the VUV and in the x-ray region. Several systems to be described operate in both spectral ranges due to the underlying basic physical processes, e.g. photoionisation, photoemission, etc. Therefore some detectors appear twice in our tables, namely, in Table 3.9 which summarizes VUV detectors and in Table 3.11 which gives an overview of x-ray detectors.

#### 3.5.1 Detectors for the Vacuum Ultraviolet

The last few years have seen an enormous progress in detection systems for use in the VUV. We only mention the very small, but easy and reliably to operate channeltron and microchanneltron plate systems with a time response fast enough to allow for the investigation of excitation and decay processes (see Sect. 3.6) in the subnanosecond regime. Furthermore, by utilizing monochromatized SR the absolute detection efficiency of vacuum diodes have been calibrated. The wealth of information is summarized in a first Table 3.9 which provides an overview over various detection systems. More detailed information on photomultiplier systems is presented in Table 3.10. It is almost unnecessary to say that the latter table is by no means complete.

The photographic detection was invented by SCHUMANN in 1892 [3.10] who realized that for VUV photons in order to be detected with silverhalide crystals the gelatin base of the photoplates had to be diluted. (The strong hydrocarbon absorption in the VUV is evident from Fig. 3.8.) The resulting "Schumann plates" made by hand were extremely sensitive to mechanical damage. Eastman Kodak produced the first Schumann emulsion on a filmbase (Eastman Kodak SWR) about 50 years later, followed by Kodak Pathé with more sensitive films (SC-5 and SC-7). At present the most advanced VUV emulsions are Eastman Kodak 101 and the slower, but finer grained emulsion 104. A comprehensive report on the VUV performance of these emulsions has recently

been given by VAN HOOSIER and collaborators [3.219].

Photon counters and ionisation chambers allow absolute intensity measurements of VUV radiation. For wavelengths shorter than about 100 Å proportional counters or Geiger-Müller counters [3.10, 3.12] (see also the following Sect. 3.5.2) can well be utilized as standard detectors provided the corrections are known which have to be applied to account for absorption in the window materials of the moderately pressurized (several Torr depending on the filling gas [3.10]) counting cells. In principle photon counters can be used to wavelengths well above 1000 Å. However, in the spectral region  $\sim 1000$  Å to 200 Å one has problems in finding a suitable radiation transmitting window material to withstand the differential pressure. In addition, the energy resolution and sensitivity is reduced. Especially for the range 100 Å to 300 Å SASAKI et al. [3.220] constructed a photon counter with an incorporated channeltron multiplier (to be discussed later-on) to gain sensitivity.

Rare gas ionisation chambers are commonly used at wavelength above 200 Å up to  $\sim 1000$  Å. This method, developed by SAMSON [3.10] is based upon the fact that one photon absorbed in a rare gas produces just one electron-ion pair which can be measured by means of a collector electrode and a high sensitivity electrometer amplifier. At wavelength below  $\sim 250$  Å corresponding to twice the ionisation potential of He ( $2 \times 24, 58$  eV) one has to consider the effect of secondary ionisation by ejected photoelectrons and of multiple photoionisation. However, by measuring the pressure dependence of the detector gas on the ion current the first effect can be quantitatively determined. If in addition the photoionisation yield is known, the absolute spectral intensity can be evaluated. The most appropriate gas for this application is He because its double ionisation cross-section can effectively be neglected in the range 250 to 20 Å [3.221]. By this method [3.222] the absolute photon flux of a grazing incidence

monochromator at DESY was determined in the energy range 20 eV to 170 eV with an experimental set-up shown in Fig. 3.39 [3.223].

Below 50 eV the ionisation chamber is operated in the well-known 2-chamber mode [3.10] and above 50 eV the two chambers are connected to facilitate the measurements at low gas pressures. Behind the ionisation chamber photocathodes are mounted at normal incidence to be calibrated as secondary detector standards in the range 30 to 170 eV. The total photoelectric current leaving the cathodes is measured. The cathodes were prepared as thin films from standard high purity materials except for Al<sub>2</sub>O<sub>3</sub> which was evaporated from 99.5 % Al<sub>2</sub>O<sub>3</sub> ceramic. The cathodes were then kept at normal atmospheric pressure, but free from dust, for a few days before the measurements were performed. The absolute photoelectric yield of a 1000 Å thick Au film and a 150 Å thick Al<sub>2</sub>O<sub>3</sub> film on polished stainless steel is shown in Fig. 3.40a). Fig. 3.40b) depicts the photoyield of a 2000 Å thick CsI film and of a 1800 Å thick LiF film. For comparison other experimental data points have been included [3.224]. In particular we mention the yield data of SALOMON and EDERER [3.225] of an Al<sub>2</sub>O<sub>3</sub> cathode prepared by anodic oxidation. The Al<sub>2</sub>O<sub>3</sub> calibrated diode which has proven to be stable to within 5 - 10 %, is now regularly available from the NBS. The photoyield of Au depends on contamination [3.226]. However, after heating in an UHV system it appears to be reproducible to within 20 % [3.144b, 3.226]. The photoyield of LiF and in particular CsI is less stable and reproducible with preparation conditions than that of Al<sub>2</sub>O<sub>3</sub> and Au. However, it should be noted that the absolute yield of the alkali halides is higher by a factor of 10 to 50. Thus, if a sensitive diode or detector is needed, one should consider these materials. The photoelectric yield of various other materials has been reported [3.144b, 3.10, 3.12, 3.224 - 3.228] in the energy range 10 eV to several hundred eV. Notably the work of LUKIRSKII and coworkers in the high energy range has to be mentioned [3.224d, 3.229].

The photoelectric yield also depends on the angle of incidence of light with respect to the surface of the emitter. This is shown in Fig.3.41 for an evaporated (*in situ* in UHV) Au film for photon energies ranging from 22 eV to 190 eV [3.230]. The photoyield  $\gamma(\theta)$  normalized to the yield  $\gamma(0^0)$  at zero degree angle of incidence shows a drastic increase with increasing angle for photon energies above about 90 eV. With increasing energy one also observes a shift of the maximum to more grazing angles. This behaviour is well understood and can be explained on the basis of the step model for photoemission [3.144b, 3.228, 3.230]. At oblique angles of incidence Eq.3.27, the linear absorption coefficient  $\mu$ , has to be generalized in order to include the refraction of the intensity flux in an absorbing medium

$$\mu' = \frac{4\pi}{\lambda} \text{Im} \{(\epsilon_1 + i\epsilon_2) - \sin^2 \theta\}^{1/2} \quad (3.31)$$

It can be shown [3.144b, 3.223] that the relative spectral behaviour of the photoyield and to a certain extent also the absolute spectral response is given by

$$\gamma(E) \approx P \{1 - R(E, \theta)\} M(E) \frac{\mu'(E, \theta) \cdot L(E)}{\mu'(E, \theta)L(E) + 1} \quad (3.32)$$

where P is an escape probability factor for the photoelectrons,  $R(E, \theta)$  is the reflectivity at the photon energy E and angle  $\theta$  and  $M(E)$  is a smoothly varying multiplication factor approximately given by  $M(E) \sim E/\epsilon$  with  $\epsilon$  the average energy of the released photoelectrons.

The data of Fig. 3.41 can be quantitatively fitted [3.230] with (3.31) and (3.32), with known optical constants [3.48]. In fact, one can work out the average escape length of the photoelectrons from  $\gamma_N = \gamma(\theta)/\gamma(0^0)$  since P and  $M(E)$  cancel. At high energies the absorption is weak and the refractive index approaches one. Therefore one can approximate (3.31) by

$$\mu' = \mu / \cos \theta \quad (3.27')$$

with  $\mu$  given by (3.27). Eq. 3.32 then becomes

$$\gamma(E) \approx P(1 - R) \cdot M \cdot \mu \cdot L \cdot \sec \theta \quad (3.32')$$

From Fig. 3.41 we see that the high energy data are well described by the  $\sec \theta$  law [3.229] up to angles close to the inflection point of the curves which is determined by the onset of the total external reflection (see Sect. 3.2.1). At low energies the enhancement in the photoyield is limited due to refraction effects in the absorbing medium. Clearly, for a detector design the angle of incidence dependence of the yield has to be considered.

A wide variety of photoelectron multiplier systems is in use as seen from Tables 3.9 and 3.10. The first multiplier systems were built with mechanically formed metal dynodes (mostly CuBe) mounted separately (5.41 in Table 3.9 and 10). Then strip dynodes have been designed which consist of semiconducting thin films ( $\text{SnO}_2$ , C) on glass plates with two of the plates in parallel. An electric field is generated across the continuous strip dynodes by an applied potential which gives rise for an electron avalanche to move along the dynodes (see Fig. 3.42a). The main advantages of continuous dynodes are the reduced number of necessary different potentials and vacuum feed throughs and the smaller size. Various photomultiplier systems of this kind have been described in detail by SAMSON [3.10].

The latest achievement with this type of detectors, the channeltrons, also have continuous dynodes. The basic channel electron multiplier (CEM) consists of a semiconducting glass channel having an internal diameter of only a few mm and a ratio of length to diameter in the order of 50:1. The channel has a resistance of typically  $10^9 \Omega$  which allows an output pulse of the order of  $10^8$  electrons to be collected by an anode at an applied potential of 3-4 KV. In general, the channel of the CEM is bent in order to inhibit the acceleration of positive ions towards the photocathode. These could otherwise generate further electrons and thus spurious output signals. The output characteristic of CEM's is determined basically by space charge effects [3.227, 228, 3.23]. In order to enlarge the size of the photo sensitive area of the cathode to a size larger than the basic channel dimensions, CEM's are built with large cones up to several  $\text{cm}^2$  added to the front end of the CEM. The striking advantages of CEM's include: extremely small size, fairly large count rate capability, the requirement of (for specific types) only two leads, the compatibility with UHV requirements.

Recently TIMOTHY and LAPSON [3.227, 3.228] gave a comprehensive report on the use of CEM's as secondary standards in the VUV spectral range. They compared and tested various CEM models with different photocathode materials for the CEM to investigate their efficiency and spectral response. The absolute detection efficiency of an  $\text{MgF}_2$ -coated CEM and an uncoated CEM (Mullard B 419 BL) is shown in Fig. 3.42b) in the wavelength range from 44 Å to 1216 Å. As expected at an angle of incidence of  $45^\circ$  [3.228], the efficiency of the coated CEM is slightly higher in the range 70 Å to 900 Å than the uncoated one. For both types, the absolute efficiency is higher than 10 % (see Fig. 3.42b).

Very many channels with diameters as small as  $\sim 10 \mu\text{m}$  have been manufactured

in a way to form an area of microchannels [3.231] covering a plate of up to 10 cm diameter with thickness (i.e. channel length) of about one mm. Such devices allow the detection of photons and electrons at an extremely fast time response ( $\approx$  50 psec) with high uniformity in the sensitive area (see Sect. 3.6.1). Even curved microchannel plates (MCP) are available from different suppliers with a spherical or elliptical figure. The present state of the art are MCP's in high-gain chevron configuration located in parallel to each other. By using a resistive anode encoder readout behind the MCP, opposite to the light source or electron source, it can be utilized as a position sensitive detector. A spatial resolution of about 60  $\mu$ m has been reported [3.232].

### 3.5.2 X-Ray Detectors

We cannot give here a complete survey on all properties of x-ray detectors but rather would like to discuss those properties which are closely related to the special conditions of a SR source, namely high intensity, higher harmonic rejection and pulsed structure. Various kinds of detectors are listed in Table 3.11. General information on detectors is given in [3.239-243] while the special problems involving SR are treated in Refs. 3.244,245.

For any detector which is used in the counting mode it should be considered that the maximum count rate which is tolerable under certain predetermined count loss and resolution conditions,  $N_{\max}$ , has to be multiplied by the duty cycle  $\delta$ , namely the fraction  $\delta$  of time during which radiation is emitted. This results in an effective maximum count rate

$$N_{\max}^{\text{eff}} = N_{\max} \cdot \delta \tag{3.33}$$

For 30 keV photons from a synchrotron like DESY at 7 GeV, with a repetition period of acceleration of 20 msec, hard x-rays are emitted only for the last 2 msec, giving  $\delta \approx 0.1$ .

Another kind of problem arises with storage rings like DORIS or SPEAR when operating in the single bunch mode (see Sect. 1.2.3). With DORIS a 150 - 400 psec long light pulse is regularly emitted every 1  $\mu$ sec. There is no detector available which can resolve two or more events arriving within 400 psec. Thus, assuming Poisson statistics for the probability of multiple emission from one bunch to the experiment we obtain for the actual count rate

$$N = n(1 - e^{-N_0/n}), \tag{3.34}$$

where  $N_0$  is the true event rate and  $n$  is the number of bunches per second. We recognize that  $N = N_0$  for low count rates while it approaches  $n$  for very high event rates. In this case every light pulse leads to one counted event. We have assumed that the detector is capable of resolving events originating from adjacent bunches.

With e.g.  $N_0/n = 0.1$  a count loss of 5 % results.

The most interesting and frequently used detectors are the lithium drifted silicon and germanium semiconductor counters (Si(Li) and Ge(Li)). They have the highest energy resolution due to the fact that only 3 - 4 eV are needed for producing one electron-hole pair. The useful count rate is limited to about 50.000 Hz, if no deterioration of the energy resolution is tolerated. If the count rate is too high the energy resolution suffers, because on an incomplete collection of the charges. In Table 3.11 we summarize the available detectors quoting both a "dead time" and "time resolution". The "dead time" is just the minimum time between adjacent pulses under which significant count loss or loss of information (pile-up) occurs, while "time resolution" is the time accuracy with which an event can be located from the steep rising part of the pulse. The numbers quoted are only typical, since the technical development of detectors and the perhaps even more important subsequent electronics is going at a very fast pace.

Scintillation counters usually have a very poor energy resolution. This is due to the fact that about 400 eV are needed for NaI(Tl) and 2000 eV for plastic scintillators in order to produce one photoelectron at the multiplier cathode [3.239 - 3.244]. Especially the organic scintillators, however, have very short decay times down to 0.5 nsec. This is an important property for experiments with very high count rates.

Proportional counters [3.239, 3.241] are especially useful in the soft x-ray region up to  $\sim 6$  keV. With very thin windows they can have a high overall efficiency combined with an energy resolution which is just sufficient to allow for a certain suppression of higher harmonics.

Experiments which take full advantage of the very high intensities in the primary beam, like absorption measurements (EXAFS) (see section 3.6.2), cannot be operated with digital electronics. Ne-He (9:1) [3.204] filled or just plain air filled [3.246] ionisation chambers are used. There are flow systems and sealed chambers in usage. The current is collected and amplified by a dc amplifier. Such amplifiers have usually a sensitivity limit of  $10^{-14}$  A. For the common gases an average of 25 - 35 eV is needed for producing one ion pair. At high intensities, typically above  $10^6$  photons/sec, the noise is determined by photon statistics only.

The efficiency of all the systems described above depends on matching the size of the sensitive part of the detector including its shape to the mean free path of the detected photons. With higher x-ray energy the mean free path in general increases and the size of the pressure of the detector have to be increased too. As a consequence e.g. for Si(Li) and Ge(Li) detectors the energy resolution is becoming worse [3.240] and also the dead time which depends on the collection time for the charges produced is increased.

Table 3.11 lists also the most important position sensitive detectors. Photographic film is used in topography, where nuclear emulsions [3.239] with highest resolution are needed (down to 0.3  $\mu$ m). For other applications like the registration of diffraction patterns films with lower resolution (up to 100  $\mu$ m) but higher sensitivity can be applied. With photographic recording no real time experimentation is possible and absolute intensity determination is usually a problem. Another difficulty arises with non-uniform film shrinkage when precision measurements are required.

There are several attempts to divide ionisation detectors into small subsections which allow for a localization of individual events. Linear solid state detectors [3.247] and proportional counters [3.248, 3.249] are used in such a way. The

collector is subdivided into small sections and the signal is fed into a parallel delay line. The signals travel to both ends and the times of arrival are monitored and translated to a position for the event. Resolutions of 1 mm or less are possible.

Multiwire proportional chambers [3.214, 3.250, 3.251] serve as two dimensional detectors, some are equipped with crossed wires making also use of the positive signal from the ion current. Separation of the wires can be as low as 1 mm. By a careful measurement of the charge on neighboring wires interpolation calculations can give a positional accuracy of about 0.15 mm. Readout of individual wires into the computer allows very high count rates. This is, however, quite expensive. Slower but cheaper systems are working again with the help of delay lines [3.252]. A special type of two dimensional detector is the spherical drift chamber developed by CHARPAK and coworkers [3.51] (see Fig. 3.43). This detector is centered at a sample and collects the electronic charge at one point developed along a radial path corresponding to one scattering angle. This instrument has a high conversion probability for the photon and does not suffer from the position uncertainties of inclined paths in planar chambers. In summary, many of the techniques which originally have been developed for high energy physics can usefully be applied also in the x-ray region.

Finally we want to mention the use of TV cameras using a fluorescent screen and an image intensifier [3.253 - 3.256]. Such a system can be used with high and low intensity signals. They are of considerable interest, since they make use of the highly developed TV techniques. On the other hand cathode homogeneity, geometric distortion and noise constitute problems which have to be overcome. Further the computer interface needs considerable care, since the TV output originally is an analog signal.

### 3.6 Typical Experimental Arrangements

After having discussed the individual optical components to build spectrographs and monochromators for spectroscopy and various types of detector systems efficient for wavelengths from the visible to the x-ray region, we now turn to a brief description of complete experimental arrangements. The purpose of this section is to make the reader acquainted with some typical experimental set-ups which can be found in more or less similar arrangement in several SR laboratories. Simply for reasons of convenience we heavily use material from our laboratory. However, we also include some unique experimental set-ups to illustrate the possibilities of SR spectroscopies and to show up possible future trends.

#### 3.6.1 Experiments in the Vacuum Ultraviolet

A general summary on experimental methods in the VUV is given in Table 3.12. For convenience, some references are included to provide an easy access to an in-depth information on the various physical and instrumental aspects. For references we also refer the reader to the bibliography on SR [3.258] and to the proceedings of the recent VUV conferences [3.2,3.3,3.5,3.9,3.108,3.109].

##### 1) Absorption, reflection, ellipsometry

Absorption and reflection spectroscopy on solids are now standard techniques to determine the optical constants by means of Kramers-Kronig analysis of absorption or/and reflectivity data or directly from appropriate reflectance measurements. Moreover, these techniques provide standard means of locating optical transitions. There is no need to give special references. As mentioned earlier (Sect. 3.2.3) ellipsometry is more difficult to use for the determination of optical constants due to lack of easy to operate VUV polarizers [3.160 - 1.69].

In Fig. 3.44 we show an apparatus for absorption measurements of transition metal and rare earth metal vapors [3.259,260] in the energy range of the outermost core excitations (50 eV to 200 eV). By comparing the spectra of free atoms and those in solids important correlation effects can be studied. The central instrument is a standard Rowland spectrograph which allows the detection of the full absorption spectrum of the vapor in front of the spectrograph at a single exposure. A spectrograph is preferred here, since it is difficult to maintain very stable conditions in an absorption oven operating up to about 2500°C. The heating element is a Ta tube powered with 40 kW. The metal vapor is confined to the oven by means of thin VUV filters (Sect. 3.2.3) and by a buffer gas. The SR is collimated by a toroidal mirror and after passing the oven it is focussed onto the entrance slit of the spectrograph.

## 2) Luminescence, fluorescence

The investigation of secondary processes is developing rapidly especially with the higher fluxes from storage rings which become more and more available now [3.21,22]. In soft x-ray fluorescence experiments [3.260] the valence electron structure of a variety of materials has been studied including organic materials which are easily decomposed, if high energy electrons are used for the excitation of primary core vacancies. At the DORIS laboratory SR, pre-filtered by a grazing incidence mirror, is the exciting source giving rise to fluorescence radiation in the range up to 600 eV to be detected by a standard Rowland spectrometer.

Fluorescence and luminescence experiments with secondary radiation energies up to 50 eV have been reported at various laboratories [3.261]. The investigation capability of decay processes [3.262] in insulators and molecules is greatly enhanced by use of the pulse structure of storage rings (Chap. 1). For example, at the DORIS ring operating in the multi-bunch mode the time structure due the single electron and positron bunches corresponds to light flashes of 250 psec duration separated by about 8 nsec. An experimental arrangement for luminescence studies

is shown in Fig.3.45 (3.263). SR from DORIS is monochromatized by a Wadsworth monochromator (W) and focussed onto the exit slit. The refocussed light forms a small image on the sample under investigation. This light spot is then used as the entrance slit for a second Seya Namioka (SN) monochromator which analyses the luminescence radiation (PM). A simultaneous reflection measurement (RE) is also included as well as a monitor for the incoming primary radiation (R). Materials studied include solidified rare gases (by means of a He cryostat (HK)) and organic molecules in rare gas matrices.

## 3) Photoionisation, photofragmentation

The investigation of the decay of excited molecular states is performed by fluorescence and/or fragmentation. The latter is accomplished by ion mass spectrometry. In current experiments on small organic molecules [3.264] and atmospheric gases [3.265] normal incidence monochromators are utilized to initially excite or ionize the molecules. In commercial quadrupole mass spectrometers the electron beam ionisation is replaced by that with monochromatic light.

## 4) Photoemission

Photoemission experiments have become the major tool for investigating the electronic properties of solids, molecules and atoms [3.5,3.6,3.27,3.39,3.109,3.148-3.150]. The intense, polarized and continuously tunable SR allows to obtain conventional photoelectron energy distributions, both angle-integrated and angle-resolved, as well as various yield-type measurements on solids and solid surfaces [3.159]. The photon energy range provided by normal- and grazing incidence monochromators allows the investigation of valence and core electrons. Also a crystal monochromator has already been utilized for photoelectron spectroscopy [3.39] at 8 KeV. In Fig. 3.46 we show an experimental arrangement for photoemission studies in the energy range 15 eV to 300 eV [3.191]. The monochromator is a plane grating instrument exploiting the collimation of SR at the DORIS ring. The instrument has been briefly discussed in Sect. 3.3.3. The UHV experimental chamber is built around the exit slit of the monochromator to allow photoemission measurements with highest

possible radiation density. Of course, such an arrangement also allows small samples to be used. The energy analysis of photoemitted electrons is made with a commercial double stage cylindrical mirror analyser [3.66]. For sample preparation and characterisation several tools are incorporated which are standard in modern systems, e.g. ion-sputtering, crystal cleaver, evaporating source, sample heating and cooling. Auger electron spectroscopy, low energy electron diffraction etc.

A very different photoelectron spectrometer has been built and utilized by BROWN and collaborators [3.267] to explore the angular dependence of the energy distribution (Fig. 3.47). Their time-of-flight spectrometer for photoelectrons is based on the pulsed structure of the SR (at SPEAR pulse width of 1.5 nsec and a repetition period of 780 nsec). The sample is irradiated with monochromatized light from the "Crashopper" monochromator described in Sec. 3.3.3 [3.170]. The time of flight spectrometer essentially consists of a drift tube combined with a retardation sector and a fast channelplate as the detector. The transit time along the 17.5 cm long drift distance is approximately 100 nsec for a 10 eV electron as measured with a sensitive delayed coincidence timing system [3.267]. The spectrometer can be pivoted around the sample allowing for angularly resolved photoelectron spectroscopy. The energy resolution is determined by the light pulse structure and corresponds to 0.1 eV energy resolution at 10 eV electron energy. First spectra have been obtained with this interesting new instrument. However, the complex electronics needed to take and analyse the data outweigh somewhat the simplicity of the spectrometer itself. The system yet has to prove its capabilities to be preferred over others.

#### 5) Radiometry

SR serves as a radiometric standard in the VUV, since it can exactly be calculated, if the accelerator or storage ring parameters are well known. SR is also used for calibration of rocket spectrometers including detectors [3.268, 3.269]. In Fig. 3.48 a radiometer is shown which is designed for calibrating transfer standards of the spectral radiance and irradiance for wavelength between 600 Å and 3500 Å [3.270]. The main optical components are a concave mirror with an aperture stop and two Seya-Namioka monochromators which use a pinhole as a common entrance slit. One of the monochromators is operated at a wavelength in the visible while the other is scanned through the VUV region. By measuring the ratio of the detector currents with the concave mirror first in position A and subsequently in position B (Fig. 3.48) the spectral radiance of the transfer standard can be calibrated. The ratio recording system is necessary in order to cancel effects due to fluctuations in the SR emitted by the synchrotron [3.270]. The calibration accuracy obtained is  $\sim 2\%$ . The calibration of transfer standards to shorter wavelengths is of particular importance also for plasma diagnostics.

#### 6) Microscopy

In the last years considerable progress in microscopy techniques with soft x-ray radiation has been achieved in particular through the application of high brightness synchrotron radiation, high resolution photosensitive resist materials and scanning electron microscopes. Various methods for microscopy have been introduced since 1972. They can be subdivided into two classes: namely into a class which allows "real-time microscopy" at a moderate resolution (but still better than with light microscopy) and a class, which gives potentially the highest resolution in a non-real-time mode. To the former

belong the techniques of scanning microscopy [3.90,126], the application of mirror optics [3.27] and of Fresnel zone plates [3.125]. To the latter belong x-ray holography [3.27] and contact microscopy [3.68,126]. Since scanning microscopy makes more efficient use of the radiation impinging onto the sample the scanning technique has to be preferred for studies on living biological objects because of radiation damage considerations. SCHMAHL and coworkers [3.27] who built the first imaging microscope for soft x-ray synchrotron radiation using zone plates as imaging elements (Sect. 3.2.2), were able to record x-ray pictures on photographic film of live 3T3-mouse cells at a moderate resolution. With the technique of contact microscopy various biological specimens have been investigated with a resolution as good as  $100 \text{ \AA}$  [3.68,126, 274,275]. For contact microscopy no optical components are required for imaging. In this technique specimens are placed on top of thin films of photosensitive resist material. The intensity absorbed in the resist depends on the absorption profile of the sample. Therefore a replica in relief of the specimens absorption structure is obtained via a development procedure. This can be magnified and photographed with a scanning electron-microscope. Basically, it is the same process which is used as a step in the production of electronic microcircuits [3.68,126]. Due to the good resolution obtainable with the short wavelength spectrum of SR first provisions are being made to use SR for the fabrication of further miniaturized microcircuits in the future.

### 3.6.2 Experiments in the X-Ray Range

We give here a survey on different experimental techniques which have been pursued in the x-ray region using SR. We include some references in which instrumental details can be found. The information is summarized in Table 3.13. General references which contain recent information on this topic are the proceedings of the 1977 Orsay meeting on SR instrumentation [3.9], the 1976 Quebec meeting on SR facilities [3.5], the Stanford [3.7], and the DESY [3.8] SR handbooks. In most cases we shall stress only the most important points. In a few cases we give a special example of the experimental arrangements used.

#### 1) Single crystal diffraction

Structural research with x-rays is one of its oldest and most important applications. Due to the high brightness of SR sufficient intensity can be collimated onto very small crystals. This should simplify structure determination of difficult to grow crystals from organic materials like e.g. proteins [3.276,3.277]. In principle tuning of the wavelength to the vicinity of the absorption edge of one of the constituent atoms should be a means to manipulate individual scattering amplitudes due to anomalous dispersion. This would make substitution of atoms unnecessary for solving the problem of phases in determining complicated crystal structures. The instrument consist of a crystal monochromator followed by a diffractometer operating in a vertical plane because of the polarization of SR.

#### 2) Small angle diffraction

This technique is typically used for structures with large unit cells like muscles or retina [3.213-3.218, 3.278]. It takes advantage again of the high brightness of SR. Narrow fans with good collimation are needed to have good angular resolution with small samples. Focussing bent crystal monochromators are used as described above (Sect. 3.4.3). The diffraction spots are measured with

photographic film or with one- or twodimensional detectors. The latter type of detectors are preferred, since kinematic measurements like muscle contraction are of major interest [3.213,3.214]. Fig. 3.38 shows such an instrumental arrangement [3.218].

### 3) Small angle scattering

This method is applied for the determination of the outer dimensions and possibly shapes of large organic molecules in solution (and other complexes of corresponding sizes) [3.34]. Since the method does not need a good monochromatization of the radiation ( $\Delta\lambda/\lambda \sim 1/10$  is already more than sufficient) high intensity can be available if it is possible to filter out such a broad band. As a first attempt of filtering use of the high energy cut-off of total reflection (see Section 3.2) and the low energy cut-off of an appropriate absorber is suggested [3.34]. This method could yield  $\Delta\lambda/\lambda \approx 0.3$ . With the available intensities time dependent phenomena could be investigated if the detectors can be made fast enough. According to STUHRMANN [3.34] ZVIKAM [3.279] has proposed experiments to obtain information on molecules which goes beyond the time and space averaged charge distribution. By measuring scattering fluctuations on sufficiently small samples in short times correlation functions are obtained with information on the actual shapes of individual molecules.

### 4) Mössbauer scattering

A 1 mrad wide beam of SR from DORIS operating at 4 GeV, 100 mA contains about 1000 photons in a  $10^{-8}$  eV wide energy interval at  $\sim 14$  keV photon energy (Mössbauer level of  $\text{Fe}^{57}$ ). Attempts are being made [3.280-3.282] to filter out these photons from the background of white SR. If this can be achieved without too much losses, a well collimated beam of  $0.1 \times 1 \text{ mrad}^2$  angular spread would become available with an intensity surpassing that attainable in the same solid angle

from natural  $\text{Fe}^{57}$  sources by about two or more orders of magnitude. This beam would be pulsed as the SR source and nearly 100 % polarized. Possible applications are interferometry, investigation of coherent nuclear Bragg scattering, anomalous transmission of Mössbauer radiation through single crystals, structural investigations on biological samples containing  $\text{Fe}^{57}$  markers etc. The following means of filtering have been suggested [3.280-3.282]:

- a) Premonochromatization by ordinary Bragg reflection resulting in a 1 eV wide band,
- b)  $90^\circ$  horizontal nuclear Bragg reflection from a  $\text{Fe}^{57}$  or  $\text{Fe}^{57}$  compound crystal making use of the M1 character of the nuclear transition and thus suppressing the electronic dipole scattering,
- c) utilizing the time structure of SR by gating the detectors to be sensitive only for time delayed (up to 100 nsec half width) nuclear scattering. Alternatively it is possible to use a detector which consists of a  $\text{Fe}^{57}$  fluorescent target and a photomultiplier which is gated off during the excitation process.

The methods b) and c) have efficiencies which are in the order of 10 %. Therefore a considerable overall loss of photons has to be tolerated in the course of the monochromatization process. The whole undertaking is therefore tedious and difficult. If the efforts made towards this goal will be combined one day with those towards the production of a periodic undulator producing several orders of magnitude more intensity at 14 keV (or any other appropriate Mössbauer energy) a really intense Mössbauer beam could become available.

### 5) Energy dispersive diffraction

This method [3.283-3.285] takes full advantage of the continuous spectral distribution of SR. Bragg scattering from powder materials is described by the Bragg equation

$$2d \sin \theta = 12400/\epsilon$$

where  $d_H$  is the lattice plane spacing for the planes with indices  $H$  measured in  $\text{\AA}$  and  $\epsilon_H$  is the photon energy (in eV) fulfilling the Bragg condition at a fixed Bragg angle  $\theta_0$ . The experimental arrangement is shown in Fig. 3.49. The white beam of SR hits the sample, while Si(Li) or Ge(Li) detectors (see Section 3.5.2) are employed for the energy analysis of the  $\epsilon_H$  peaks.

The speed of the method is presently only restricted by the counting limit of  $\sim 50000$  Hz of the detection system. Even with this speed the method is by a factor of about 100 faster than angular scan methods using monochromatic radiation from commercial tubes and has a better signal to noise ratio. The real advantages lie in the simultaneous appearance of all reflections which makes possible the study of structural changes in a very simple way. Large changes can be observed with a time constant of 1 sec already while fairly accurate spectra allowing for the investigation of small changes are obtainable in 10 s. If faster changes shall be investigated a repetitive technique can be applied. As a demonstration Fig. 3.50 shows phase transitions of manganese from the low temperature  $\alpha$  phase into the high temperature  $\beta$  phase. Absolute structure determination is achieved, if the spectral distribution of SR and the detector sensitivity is taken into account. These can be calibrated with known structures.

Applications to high pressure induced phase transitions have also been made [3.285]. In this case the high brightness of SR comes into play, since the small diamond windows of these instruments cut off most of the beam. Further attempts were made to investigate small angle scattering from biological samples. In this case radiation damage plays a dominant role and the method has the disadvantage that a large fraction of the radiation which is impinging onto the sample is not used for obtaining information. Other methods may be more efficient in this respect.

## 6) Interferometry

This method is described in several publications by BONSE et al. [3.206,3.286, 3.204',3.285']. An interferometer (Fig. 3.51) consists of a series of plane single crystal beam splitters which accept only very well collimated beams. Again the high gain in brightness of SR is the important factor. This experiment serves in principle to obtain the complementary information to an absorption experiment, namely the real part of the forward scattering amplitude, which is directly related to the index of refraction. Such a measurement of the scattering amplitude near absorption edges, where it shows its dispersive behaviour (anomalous scattering) is a means to obtain the primary data necessary for the application of this method to the solution of the phase problem (see Point 1). This method offers the possibility to measure the dispersion correction directly for the substance under investigation.

## 7) Absorption (EXAFS)

The popularity of the absorption measurements in a range up to 1000 eV above absorption edges (mainly K edges) is due to the new interpretation of the Kronig structure [3.204,3.287] and the simplicity with which these measurements can be performed with SR in combination with easily tunable double crystal monochromators in the (+,-) mode (see Section 3.4.1). The Kronig, or extended x-ray absorption fine structure (EXAFS), is due to the scattering of the internally excited photoelectrons in the immediate environment of specific atoms and the interference of the scattered waves with the primary wave (see also Subsection 4.2.3). EXAFS spectrometers can serve a large number of different experiments in which cryostats, ovens, high pressure cells, stop-flow devices, ultrahigh vacuum sample chambers etc. are used at the sample position [3.204,3.281, 3.282,3.288]. A fully equipped EXAFS station must also provide the necessary computer programmes to transform the spectra into nearest neighbor distances. The theoretical limitations, however, are still somewhat unclear and there is a danger of overinterpretation of the data by unexperienced users. The methods are still in the stage of development.

A promising future development appears to be the observation of secondary processes which occur after absorption, e.g. fluorescence, Auger electrons and photoelectrons. This makes the technique more selective to certain types of atomic constituents or to special regions of the sample as for instance the surface. SR beams condensed by focussing mirrors provide the necessary intensity for such investigations [3.209].

#### 8) Topography

In topography experiments a sample crystal is positioned in the undispersed white beam of SR producing Laue reflections [3.289-3.292]. Any defects inside the crystals are projected onto the film and are observable as fine structures in the Laue reflections, Fig. 3.52 gives an example. The advantages of SR are

- a) The large distance from the source which are possible because of the good collimation of SR. This distance allows either a good resolution if the film is near the sample or a larger distance between the film and the sample which is needed when applying heat, magnetic fields, low temperature etc. to the sample.
- b) The very short exposure time in the order of seconds to minutes, which can be even further reduced, allow for the investigation of non-stationary phenomena like motion of dislocations under stress, motion of domain structure with applied magnetic fields etc. The application of high speed film techniques with image converters appear to be feasible [3.293].
- c) The experimental conditions are simplified, since no tedious prealignment of the samples is needed compared to the use of characteristic x-rays from x-ray tubes.
- d) The white beam leads to a creation of many Laue reflections at the same time. This allows for a stereoscopic observation of the same defect from different angles.

In addition to the Laue transmission arrangement also reflection topographs are of interest. In this case special filters between the sample and the recording film can be helpful in order to reduce the fluorescent radiation from the sample. Although this causes troubles and the conditions differ from case to case the problems appear to be solvable.

#### 9) Standing wave excited fluorescence

A group from Aarhus, Denmark, made first tests with this method [3.294,3.295] at the DESY synchrotron [3.296]. After producing a parallel, monochromatic, higher order free beam with a spectrometer a standing-wave pattern in the Bragg case is set up in a single crystal of Si (but also any other crystal of high quality could be used) (Fig. 3.53). While the rocking curve of this crystal is scanned, the standing waves move with their maxima from the lattice plane position to the inter-lattice plane position. The fluorescence signal of impurity atoms like As is observed with a solid state detector at  $90^\circ$  horizontally in order to suppress scattered light thus making use of the polarization of SR. A signal ratio of 7 to 1 was observed when scanning through the rocking curve thereby confirming the substitutional nature of the As impurities. An ultimate goal of this method would be to apply it to surface physics. Since the standing wave pattern extends beyond the crystal surface into the vacuum the distance of absorbed atoms relative to the crystal surface could be measured. Such an experiment would certainly require the very high intensity from a storage ring.

#### 10) Fluorescence excitation

The excitation of soft x-ray fluorescence is now applied for many years at DESY for the investigation of substances which are easily damaged by electron bombardment [3.297,3.298]. Although the relative damage of electron and radiation excitation is different in different cases, there is clear evidence that the excitation with

radiation is usually less harmful per fluorescence quantum. The soft x-ray experiments involve the fairly tedious techniques of grating monochromators.

In the x-ray region proper the fluorescence excitation can compete with that of strong x-ray tubes if a favourable geometry is used. SPARKS and coworkers [3.299] have used SR of SPEAR because of the very high photon energies available for looking for the fluorescence of superheavy elements. They used a graphite crystal bent to a radius of 10 cm collecting SR from an angle of 2 mrad.

11) Compton scattering

COOPER et al. [3.300] apply radiation filtered by a crystal monochromator at 10 and 20 keV at Daresbury and DESY for a Compton scattering experiment. They find that a gain by a factor of  $\sim 10^3$  over the use of a conventional x-ray tube is obtained. There appears to be some contradiction when comparing this factor with calculations. COOPER et al. [3.300] used a solid state detector with a resolution of about 250 eV. There is obviously an apparent mismatch between the monochromaticity of the primary beam ( $\sim 1$  eV) and the resolution of the detector. A considerable improvement of the experiment should become possible by increasing the bandwidth of the primary monochromator to 20 eV (see Sect. 3.2.2) and by analyzing with a curved secondary monochromator with equivalent bandwidth.

Another direction of future development would be a transfer of the Compton experiment to the 100 keV range where interpretation is easier because of the validity of the impuls approximation. Such an experiment could compete only with conventional techniques like  $\gamma$ -ray Compton scattering, if the special advantages of SR come into play like gain of intensity by increasing the usable bandwidth, time structure, circular polarization for investigating magnetic properties etc.

12) Resonant Raman scattering

X-ray Raman scattering involves in principle the same instrumentation as Compton scattering. The only difference is that a resolution of the order of the width of the electronic transitions involved is required. This leads to a resolution of 0.2 - 1 eV which can be achieved only at the expense of enormous intensity loss. When, however, an electronic transition, like e.g. the K edge of Cu, which can be excited by the primary photon is approached, the cross section for a Raman scattering from e.g. the Cu  $L_{2,3}$  excitation can be boosted up by several orders of magnitude (see also Subsection 4.8.2). This was shown by SPARKS et al. [3.301] using characteristic radiation and varying Z, the atomic number of his scatterer. EISENBERGER et al. [3.302,3.303] could show that SR due to its tunability is an excellent tool for such an experiment. The resolution of the  $L_{2,3}$  excitation as measured with a Ge(Li) solid state detector [3.302,3.303] is yet far from being sufficient enough to obtain structural details of this transition.

13) Photoelectron spectroscopy (XPS)

The pilot experiment of LINDAU et al. [3.39,3.304,3.305] on photoelectron spectroscopy(x-ray photoemission spectroscopy, XPS with 8 keV photons) has been mentioned already in connection with their monochromator design in Section 3.4.1. Although the count rate in this experiment was extremely low, there are some arguments in favour of such an instrument. They could show that the resolution of their monochromator is extremely good, in the order of 0.2 eV. The escape depth of photoelectrons in the 8 keV range is large thereby making volume properties accessible for photoelectron spectroscopy. Volume investigations may even become feasible in the presence of oxide layers. If the technique should not be limited to very few cases, it will be necessary to increase the photon flux considerably compared to the plane crystal monochromators used now [3.30]. It is not yet clear, if bent crystal monochromators can be used without a serious reduction

of the resolution. But such instruments at smaller distances from the source should allow a large horizontal acceptance. On the other hand, powerful rotating anode x-ray generators can also be equipped with bent crystal monochromators outweighing the high brightness of SR by an even larger acceptance [3.306] (see Sect. 1.3). Rough estimates give about equal available intensities for the strongest available storage rings and x-ray sources. An effort to obtain experience with an improved photoemission equipment at a storage ring appears to be justified, because of the further possibility to gain several orders of magnitude, when the periodic wigglers will become available (see Sect. 1.2.2).

#### Acknowledgement

The authors wish to thank numerous colleagues who have provided information for this chapter. Special thanks go to G. Materlik who helped to clarify many details concerning the x-ray instrumentation and who also did a careful reading of this part of the manuscript and made valuable suggestions. We are also indebted to H. Dahl, A. Paetz and E. Thumann for their careful typing of the manuscript and to R. Fisseler, V. Fischer, W. Knaut, J. Schmidt, and M. Sörensen for their help in preparing the figures.

#### References

- 3.1 R. Haensel and C. Kunz, *Z. Angew. Physik* 23, 276 (1967)
- 3.2 G.V. Marr and I.H. Munro, eds. Proc. Intern. Symposium for Synchrotron Radiation Users, (Daresbury Nucl. Phys. Lab. Report DNPL/R26, 1973)
- 3.3 E.E. Koch, R. Haensel, and C. Kunz eds. Vacuum Ultraviolet Radiation Physics (Pergamon-Vieweg, Braunschweig, 1974)
- 3.4 E.E. Koch in: Problems of Elementary Particle Physics, Proc. of the 8<sup>th</sup> All Union School of High Energy Particle Physics (Yerevan, 1975) p. 502
- 3.5 J.Wm. McGowan and E.M. Rowe eds. Synchrotron Radiation Facilities Proc. Quebec Summer Workshop (University of Western Ontario, London, Ontario 1976)
- 3.6 A.N. Mancini and I.F. Quercia, eds. Proc. of the Internat. Summer School on Synchrotron Radiation Res., Alghero 1976 (Intern. College on Appl. Phys. and Istituto Nazionale di Fisica Nucleare, Catania 1976) Vol. 1 and 2
- 3.7 K.O. Hodgson, H. Winick and G. Chu, eds. Synchrotron Radiation Research and the Stanford Synchrotron Radiation Project (SSRP Report, Stanford No. 76/100 Aug. 1976)
- 3.8 E.E. Koch and C. Kunz eds. Synchrotronstrahlung bei DESY (DESY, Hamburg, Juli 1977)
- 3.9 F. Wuilleurmier and Y. Farge, eds. Synchrotron Radiation Instrumentation and Developments, Proc. Orsay Meeting Sept. 12-14, 1977, Special Issue Nuclear Instrum. and Methods (North-Holland, Amsterdam 1978) Vol. 15, 2
- 3.10 J.A.R. Samson, Techniques of Vacuum Ultraviolet Spectroscopy (Wiley and Sons, New York 1967)
- 3.11 N. Damany, J. Romand, B. Vodar eds. Some Aspects of Vacuum Ultraviolet Radiation (Pergamon Press, Oxford 1974)
- 3.12 A.N. Zaidel and E.Y.A. Schreider, Vacuum Ultraviolet Spectroscopy translated from the Russian (Ann-Arbor-Humphrey Science Publishers, Ann Arbor, London 1970)

- 3.13 A.C.S. van Heel ed. Advanced Optical Techniques, (North Holland Publishing, Amsterdam 1967)
- 3.14 L.V. Azaroff ed. X-Ray Spectroscopy (McGraw Hill, New York, 1974)
- 3.15 S. Flüge ed. Handbuch der Physik XXX (Springer Verlag, Berlin, Göttingen, Heidelberg, 1957)
- 3.16 G.W. Stroke in: Handbuch der Physik XXIX S. Flüge ed. (Springer Verlag, Berlin, Göttingen, Heidelberg 1967) p. 426
- 3.17 C. Kunz in Ref. 3.2, p. 68
- 3.18 D.L. Ederer and S.C. Ebner, A Users Guide to Surf (NBS, Washington)
- 3.19 P. Dagneaux et al., Ann. Phys. 9, 9 (1975)  
P.M. Guyon, C. Depautex and G. Morel, Rev.Sci.Instrum. 47, 1347 (1976)
- 3.20 Synchrotron Radiation Center Users Handbook (Physical Sciences Laboratory, University of Wisconsin, Stoughton 1973)
- 3.21 Synchrotron Radiation a Perspective View for Europe, prepared by ESF (European Science Foundation, Strasbourg, France 1978)
- 3.22 An Assessment of the National Need for Facilities Dedicated to the Production of Synchrotron Radiation (Report to the National Academy of Sciences, Washington D.C. 1976)
- 3.23 E.M. Rowe, R.A. Otte, C.M. Pruett and J.D. Steben, IEE Transactions on Nuclear Science NS-16, 159 (1969)
- 3.24 E.M. Rowe and F.E. Mills, Particle Accelerators 4, 221 (1973)
- 3.25 C. Gähwiler, F.C. Brown and H. Fujita, Rev.Sci.Instrum. 41, 1275 (1970)
- 3.26 G.W. Rubloff, H. Fritzsche, U. Gerhard and J. Freeouf, Rev.Sci.Instrum. 42, 1507 (1971)
- 3.27 F.C. Brown, Solid State Physics 29, 1 (1974)
- 3.28 M.L. Perlman, E.M. Rowe and R.E. Watson, Physics Today 27, 30 July 1974
- 3.29 E.M. Rowe and J.H. Weaver, Scientific American, June 1977, p. 32
- 3.30 R. Jean and J. Rauss, Le Vide 111, 123 (1964)
- 3.31 R.C. Wolgast and J.W. Davis, Nucl. Science 16, 954 (1969)
- 3.32 Design Study for a Dedicated Source of Synchrotron Radiation  
(Science Research Council, Daresbury Laboratory, DL/SRF/R2, 1975) P. 52
- 3.33 E.E. Koch, C. Kunz and E.W. Weiner, Optik 45, 395 (1976)
- 3.34 H.B. Stuhmann, Quarterly Review of Biophysics, to be published
- 3.34' W. Ebeling and G.W. Bennett, DESY Internal Rep. S 1-70/6 (1970)
- 3.35 W. Gudat, C. Kunz and J. Karlau, Appl. Opt. 13, 1412 (1974)
- 3.36 H. Dietrich and C. Kunz, Rev. Sci. Instrum. 43, 434 (1972)
- 3.37 I. Fankuchen, Nature, London 139, 193 (1937);  
A. Guinier, C.R. Acad. Sci. Paris 223, 31 (1946)
- 3.38 G.K. Green, Spectra and Optics of Synchrotron Radiation, BNL Report 50522,  
(Brookhaven, April 1976)
- 3.39 P. Pianetta and I. Lindau, J. of Electr. Spectr. and Rel. Phenom. 11, 13 (1977)
- 3.40 J. Hasting, in Ref. 3.5 p. 8-19
- 3.41 R. Lopez-Delgado and H. Szwarc, Optics Commun. 19, 286 (1976)
- 3.42 H.W. Schnopper, L.P. Van Speybroeck, J.P. Delvaille, A. Epstein,  
E. Källne, R.Z. Bachrach, J. Dijkstra and L. Lantwaard, Appl. Opt. 16,  
1088 (1977)
- 3.43 Diffraction Gratings-Ruled and Holographic-Handbook. ed. by Jobin-Yvon  
Company, (Longjumeau, France, 1976)
- 3.44 E. Spiller, Space Optics, ISBN-309, Nat. Acad. Sci. 1974
- 3.45 A.V. Vinogradov and B.Ya. Zeldovich, Appl. Opt. 16, 89 (1977)
- 3.46 V. Rehn, private communication
- 3.47 A mirror testing program is underway at the DESY Laboratory
- 3.48 H.J. Hagemann, W. Gudat and C. Kunz, J. Opt. Soc. Am. 65, 742 (1975)  
and DESY SR-74/7, May (1974)
- 3.49 J. H. Weaver, Phys. Rev. B 11, 1416 (1975)
- 3.50 J. H. Weaver, D.W. Lynch, and C.G. Olson, Phys. Rev. B 7, 4311 (1973)

- 3.51 J.H. Weaver, D.W. Lynch, and C.G. Olson, *Phys. Rev. B* 10, 501 (1974)
- 3.52 J.T. Cox, G. Hass, and J.B. Ramsey, *J. Opt. Soc. Am.* 64, 423 (1974)
- 3.53 J.F. Osantowski, *J. Opt. Soc. Am.* 64, 834 (1974)
- 3.54 See e.g. M. Born and E. Wolf, *Principles of Optics*, (Pergamon Press, 2nd Ed. 1964)
- 3.55 K.L. Kliewer and R. Fuchs, Theory of Dynamical Properties of Dielectric Surfaces  
in: *Advances in Chemical Physics*, Vol. 27: Aspects of the Study of Surfaces,  
Eds. I. Prigogino and S.A. Rice (Wiley, London, 1974)
- 3.56 J. Römer, *Diplomarbeit, University of Hamburg (1970)*
- 3.57 C.H. Pruett P. 8-3 in Ref. 3.5
- 3.58 A.H. Compton and S.K. Allison, *X-Rays in Theory and Experiment*, (Van Nostrand,  
New York, 1935)
- 3.59 R.W. Hendrik, *J. Opt. Soc. Am.* 47, 165 (1957)
- 3.60 B.L. Henke, *Phys. Rev. A* 6, 94 (1972)
- 3.61 E. Spiller, *Appl. Opt.* 13, 1209 (1974)
- 3.62 B.P. Feuerbacher and W. Steinmann, *Optics Commun.* 1, 81 (1969)
- 3.63 J.G. Endriz and W.E. Spicer, *Phys. Rev. B* 4, 4144 and 4159 (1971)
- 3.64 L.R. Canfield, R.G. Johnston, and R.P. Madden *Appl. Opt.* 12, 1611 (1973)
- 3.65 K. Lindsey, *Proc. Symp. X-Ray Optics, Mullard Space Science Lab. April (1973)*
- 3.66 R.L. Johnston, Ph.D. Thesis, Imperial College of Science and Technology,  
London (1975)
- 3.67 M.F. Verhaeghe, *Optica Acta*, 19, 905 (1972)
- 3.68 W. Gudat, Ref. 3.9, p. 279
- 3.69 O.S. Heavens, *Thin Film Physics*, (Methuen & Co. Ltd, London, 1970)
- 3.70 H. Mayer, *Physik dünner Schichten*, Wissenschaftliche Verlagsgesellschaft  
Vol. I, Stuttgart (1950); Vol. II Stuttgart (1955)  
H. Mayer, *Physics of Thin Films*, Complete Bibliography, Part I and II,  
Wissenschaftliche Verlagsgesellschaft, Stuttgart (1972)
- 3.71 W.J. Choyke, R.F. Forich, and R.A. Hoffman, *Appl. Opt.* 15, 2006 (1976)

- 3.72 V. Rehn, J.L. Stanford, A.D. Baer, V.O. Jones, and W. J. Choyke,  
*Proc. Taormina Research Conference on Recent Developments in Optical  
Spectroscopy of Solids, Taormina (1976)*, and  
V. Rehn and V.O. Jones, to be published
- 3.73 DESY collaboration, to be published
- 3.74 R.P. Haelbich and C. Kunz, *Optics Commun.* 17, 287 (1976)
- 3.75 E. Spiller, *Appl. Opt.* 15, 2333 (1976)
- 3.76 A.P. Lukirskii and E.P. Savinov, *Opt. Spectrosc.* 14, 162 (1968)
- 3.77 A.P. Lukirskii, E.P. Savinov, O.A. Ershov, and Yu.F. Shepelev, *Opt. Spectrosc.*  
16, 168 (1964)
- 3.78 A.P. Lukirskii, E.P. Savinov, O.A. Ershov, V.A. Fomichov, and I.I. Zhukova,  
*Opt. Spectrosc.* 19, 237 (1965)
- 3.79 O.A. Ershov, I.A. Brytov, and A.P. Lukirskii, *Opt. Spectrosc.* 22, 66 (1967)
- 3.80 R.Z. Bachrach, S.A. Flodstrom, R.S. Bauer, V. Rehn and V.O. Jones,  
*Ref. 3.9*, p. 135
- 3.81 J.L. Stanford, V. Rehn, D.S. Kyser and V.O. Jones p. 188 in Ref. 3.9
- 3.82 V. Rehn, J.L. Stanford, A.D. Baer, V.O. Jones and W.J. Choyke, *Appl. Opt.* 16,  
1111 (1977)
- 3.83 see e.g. S.M. Elson and R.H. Ritchie, *Phys. Stat. Sol. (b.)* 62, 461 (1974),  
J.O. Porteus, *J. Opt. Soc. Am.* 53, 1394 (1964) and references therein
- 3.84 M. Pouey, p. 287 in Ref. 3.11
- 3.85 J.W. Berthold III and S.F. Jacobs, *Appl. Opt.* 15, 2344 (1976)
- 3.86 J.W. Berthold III, S.F. Jacobs and M.A. Norton, *Appl. Opt.* 15, 1898 (1976)
- 3.86<sup>1</sup> B. Niemann, D. Rudolph and G. Schmahl private commun.
- 3.87 O.H. Wyatt and D. Dew-Hughes, *Metals, Ceramics and Polymers* (Cambridge University  
Press, London 1972)
- 3.88 H. Wolter, *Ann. Physik* 6c, 94 (1952) and 6, 286 (1952)
- 3.89 C.E. Winkler and D. Korsch, *Appl. Optics* 16, 2464 (1977)
- 3.90 P. Horowitz and J.A. Howell, *Science* 178, 608 (1972)

- 3.91 e.g. D.E. Eastman, W.D. Grobman, J.L. Freeouf, and M. Erbudak, Phys. Rev. B 9, 3473 (1974)
- 3.92 H.A. Rowland, Phil. Mag. 35, 397 (1893)
- 3.93 H.G. Beutler, J. Opt. Soc. Am. 35, 311 (1945)
- 3.94 T. Namioka, J. Opt. Soc. Am. 49, 446 (1958)
- 3.95 T. Namioka, J. Opt. Soc. Am. 51, 412 (1961)
- 3.96 W. Werner, Appl. Opt. 6, 1691 (1967)
- 3.97 W. Werner, Appl. Opt. 16, 2078 (1977)
- 3.98 J.E. Mack, J.R. Stehn and B. Edlen, J. Opt. Soc. Am. 22, 245 (1932) and J. Opt. Soc. Am. 23, 184 (1933)
- 3.99 M. Seya, Sci. Light, 2, 8 (1952)
- 3.100 T. Namioka, J. Opt. Soc. Am. 49, 951 (1959)
- 3.101 M. Pouey, p. 728 in Ref. 3.3  
M. Pouey, J. Opt. Soc. Am. 64, 1616 (1974)
- 3.102 T. Namioka, J. Opt. Soc. Am. 51, 4 (1961)
- 3.103 T. Namioka, J. Opt. Soc. Am. 51, 13 (1961)
- 3.104 R.C. Chase and J.K. Silk, Appl. Opt. 14, 2096 (1975)
- 3.105 E.G. Loewen, M. Nevière and D. Maystre, Appl. Opt. 16, 2711 (1977)
- 3.106 W.R. Hunter p. 683 in Ref. 3.3  
D.J. Michels, T.L. Mikes and W.R. Hunter, Appl. Opt. 13, 1223 (1974)
- 3.107 R.P. Haelbich, C. Kunz, D. Rudolph and G. Schmahl, Ref. 3.9, p. 127 and R.P. Haelbich, Internal Report DESY F 41-76/05 (1976)
- 3.108 Conf. Digest, IIIrd Int. Conf. on VUV Rad. Phys., Tokyo (1971) ed. by J. Nakai
- 3.109 Proc. Vth Int. Conf. on VUV Rad. Phys., Montpellier (1977) ed. by M.C. Castex, M. Pouey, and N. Pouey
- 3.110 R.L. Johnson, Ref. 3.9, p. 117
- 3.111 For further work on "conical diffraction" see e.g. P. Vincent, M. Nevière and D. Maystre, to appear in Ref. 3.9; D. Maystre, M. Nevière and W.R. Hunter, Ext. Abst. Vol. III p. 74 of Ref. 3.109

- 3.112 A. Cornu, Ann. Phys. Chem. 6. Reihe, 6, 114 (1875)
- 3.113 A. Labeyrie, Thesis, University of Paris (1966)
- 3.114 D. Rudolph and G. Schmahl, Umschau in Wissenschaft und Technik 67, 225 (1967)
- 3.115 T.A. Shankoff, U.S. Patent 3, 567, 444
- 3.116 N.K. Sheridan, Appl. Phys. Lett. 12, 316 (1968)
- 3.117 G. Schmahl and D. Rudolph, Holographic Diffraction Gratings in Progress in Optics, Vol. XIV, Ed. E. Wolf (1976)
- 3.118 Y. Petroff, P. Thiry, R. Pinchaux and L. Lepère, Ext. Abst. Vol. III p. 70 of Ref. 3.109
- 3.119 C.H. Pruett, E.M. Rowe, T.R. Winchard and F.H. Middleton, Ref. 3.9, p. 57
- 3.120 C. Depautex, P. Thiry, R. Pinchaux, Y. Pétroff, D. Lepère, G. Passereau and J. Flamand, Ref. 3.9, p. 101  
D. Lepère, G. Passereau and A. Thevenon Ext. Abst. Vol. III P. 67 of Ref. 3.109
- 3.121 J. Cordelle, J. Flamand, G. Pieuchard and A. Labeyrie, in Optical Instruments and Techniques, Ed. J. Home-Dickson Oriel Press (1970)
- 3.122 T. Namioka, H. Noda, and M. Seya, Sci. Light (Tokyo) 22, 77 (1973)  
H. Noda, T. Namioka, and M. Seya, J. Opt. Soc. Am. 64, 1031 (1974)
- 3.123 further references on most recent developments are contained in Ref. 3.109
- 3.124 G. Schmahl and D. Rudolph, Optik 29, 577 (1969)  
B. Niemann, D. Rudolph and G. Schmahl, Opt. Commun. 12, 160 (1974)
- 3.125 B. Niemann, D. Rudolph and G. Schmahl, Appl. Opt. 15, 1882 (1976)
- 3.126 E. Spiller and R. Feder, X-Ray Lithography in Topics in Appl. Phys. Vol. 22, ed. H.J. Queisser, Springer Verlag Berlin (1977)
- 3.127 J. Kirz, J. Opt. Soc. Am. 64, 301 (1974)
- 3.128 W.A. Kleinhaus, Appl. Opt. 16, 1701 (1977)

3.129 J.H. Dijkstra and L.J. Lantwaard, *Opt. Commun.* 15, 300 (1975)

3.130 H.W. Schnopper, L.P. von Speybroeck, J.P. Delvaille, A. Epstein,  
E. Källne, R.Z. Bachrach, J.H. Dijkstra and L.J. Lantwaard, P. 8-71 of  
Ref. 3.5

3.131 K.P. Beuermann, R. Lenzen and H. Bräuninger, *Appl. Opt.* 16, 1425 (1977)

3.132 J.H. Beaumont and M. Hart, *J. Phys. E* 7, 823 (1974)

3.133 R.W. Gould, S.R. Bates and C.J. Sparks, *Appl. Spectroscopy* 22, 549 (1968)

3.134 H. Maier-Leibnitz, private communication

3.135 A. Harmsen, private communication

3.136 C. Vogel, F. Wuilleumier and C. Bonnelle, *C.R. Acad. Sc. Paris* 269, 1255 (1969)

3.137 C. Vogel and M. Dpeyrat, *C.R. Acad. Sc. Paris* 270, 105 (1970)

3.138 M.W. Charles, *J. Appl. Phys.* 42, 3329 (1971)

3.139 F. Kohlrausch, *Praktische Physik*, Vol. 2, 21 ed. H. Ebert, E. Justi eds.  
(Teubner Verlagsgesellschaft, Stuttgart 1962) p. 522

3.140 A.E. Sandström, in Ref. 3.15 p. 78

3.140' D.W. Berreman, J. Stamatoff, and S.J. Kennedy, *Appl. Opt.* 16, 2081 (1977)

3.141 E.S. Gluskin, E.M. Trakhtenberg and A.S. Vinogradov, Ref. 3.9, p. 133

3.142 R.G. Buckley and D. Beaglehole, *Appl. Opt.* 16, 2495 (1977)

3.143 A. Malherbe, *Appl. Opt.* 13, 1275 and 1276 (1974)

3.144a) T. Inagaki, E.T. Arakawa, R.N. Hamm and M.W. Williams, *Phys. Rev. B* 15, 3243  
(1977); b) W. Gudat, Thesis, University of Hamburg 1974, DESY Report  
SR-74/7 (1974); c) B.F. Sonntag, Dielectric and Optical Properties of Rare Gas  
Solids, Chapt. 18 of *Rare Gas Solids II*, eds. M.K. Klein and J.A. Venables  
(Academic Press, New York 1977)

3.145 R.P. Haelbich, M. Iwan and E.E. Koch, *Optical Properties of Some Insulators in  
the Vacuum Ultraviolet Region*, Physikdaten/Physics Data ZAED, Karlsruhe,  
Germany, Vol. 8-1 (1977)

3.146 M. Altarelli, D.L. Dexter and H.M. Nussenzweig, *Phys. Rev. B* 6, 4502 (1972)

3.147 see. e.g. J.H. Hubbel, *Survey of Photon-Attenuation-Coefficient Measurements  
10 eV to 100 GeV in Atomic Data* 3, 241 (1971); B.L. Henke and E.S. Ebsu,  
*Low Energy X-Ray and Electron Absorption within Solids*, AFORS Report 72-2174,  
Univ. Hawaii (1973); B.L. Bracewell and W.J. Veigle in *Developments in Applied  
Spectroscopy*, Vol. 9, ed. by E.L. Grove and A.J. Perkins, (Plenum, New York, 1971),

3.148 see e.g. C. Kunz, *Soft X-Ray Excitation of Core Electrons in Metals and  
Alloys in Optical Properties of Solids New Developments* ed. by B.O. Seraphin,  
(North-Holland, New York 1976)

3.149 E.E. Koch, C. Kunz and B. Sonntag, *Electronic States in Solids Investigated  
by Means of Synchrotron Radiation*, *Physics Reports* 29c, 153 (1977)

3.150 B. Feuerbacher, R.P. Godwin, T. Sasaki and M. Skibowski, *J. Opt. Soc. Am.* 58,  
1434 (1968)

3.151 J.C. Lemonnier, Y. LeCalvez, G. Stephan and S. Robin, *C.R. Acad. Sci. Paris*  
264, 1599 (1967)

3.152 R. Haensel, P. Rabe and B. Sonntag, *Sol. State Commun.* 8, 1845 (1970)

3.153 W.R. Hunter in *Physics of Thin Films* ed. by G. Hass, M.H. Francombe and R.W.  
Hoffman, Vol. 7 p. 43 (Academic Press, New York 1973)

3.154 R. Haensel, C. Kunz, T. Sasaki and B. Sonntag, *Appl. Opt.* 7, 301 (1968)

3.155 M. Howells, C. Norris and G.P. Williams, *J. Phys. E* 10, 259 (1977)

3.156 P. Jaeglé, P. Dhez and F. Wuilleumier, *Rev. Sci. Instrum.* 48, 978 (1977)

3.157 F.C. Brown, R.Z. Bachrach and M. Skibowski, *Phys. Rev. B* 13, 2633 (1976)

3.158 W. Gudat, Vol. II p. 76 of Ref. 3.109

3.159 see e.g. *Photoemission and the Electronic Properties of Surfaces*, ed. by B.  
Feuerbacher, B. Fitton, R.F. Willis (John-Wiley & Sons, London 1978)

3.160 D.E. Aspnes in *Optical Properties of Solids - New Developments*, ed. by B.O.  
Seraphin (North-Holland, Amsterdam 1976)

3.161 M. Schledermann and M. Skibowski, *Appl. Opt.* 10, 321 (1971)

3.162 G. Hass and W.R. Hunter, *Appl. Opt.* 17, 76 (1978)

3.163 H. Damany, *J. Opt. Soc. Am.* 55, 1558 (1965)  
H. Damany, *Optica Acta*, 12, 95 (1965)

3.164 S.P.F. Humphreys-Owens, *Proc. Phys. Soc. London* 77, 949 (1961)

3.165 R.N. Hamm, R.A. MacRae and E.T. Arakawa, *J. Opt. Soc. Am.* 55, 1460 (1965)  
G. Rosenbaum, B. Feuerbacher, R.P. Godwin and M. Skibowski, *Appl. Opt.* 7, 1917  
(1968)

- 3.166 M.B. Robin, N.A. Kuebler and Yoh-Han Pao, Rev. Sci. Instrum. 37, 922 (1966)
- 3.167 D.L. Steinmetz, W.G. Phillips, M. Wrick and F.F. Forbes, Appl. Opt. 6, 1001 (1967)
- 3.168 W.C. Johnson, Jr. Rev. Sci. Instrum. 35, 1375 (1964)
- 3.169 U. Heinzmann, J. Phys. E 10, 1001 (1977)
- 3.170 F.C. Brown, R.Z. Bachrach and N. Lien, Ref. 3.9, p. 73
- 3.171 M. Lavollée, p. 730 in Ref. 3.3
- 3.172 GCA-McPherson Company, US Patent 3 090 863
- 3.173 V. Saile, P. Gürtler, E.E. Koch, A. Kozevnikov, M. Skibowski and W. Steimann, Appl. Opt. 15, 2559 (1976)
- 3.174 V. Saile, Ref. 3.9, p. 59
- 3.175 M. Skibowski and W. Steinmann, J. Opt. Soc. Am. 57, 112 (1967)
- 3.176 W. Gudat, Diploma Thesis, University of Hamburg (1970), DESY Report F41-70/8
- 3.177 E.E. Koch, Thesis, University of Munich, (1972)
- 3.178 G.W. Grime, J.H. Beaumont, J.B. West, Appl. Opt. 14, 2317 (1975)
- 3.179 R. Brodmann, U. Hahn, G. Zimmerer, private communication
- 3.180 M. Lavollée and R. Lopez-Delgado, Rev. Sci. Instrum. 48, 816 (1977)
- 3.181 C. Depautex, M. Lavollée, G. Jezequel, C. Lemonnier and J. Thomas, Ref. 3.9, p. 69
- 3.182 N. Behfeld, U. Gerhardt and E. Dietz, Appl. Phys. 1, 229 (1973)
- 3.183 M. Pouey, Opt. Commun. 3, 158 (1971)
- 3.184 M. Pouey, Appl. Opt. 13, 2739 (1974)
- 3.185 C.H. Pruett, N.C. Lien and I.D. Steben, p. 31 a A2-5 of Ref. 3.108
- 3.186 K. Nowak, Diplomarbeit, University of Hamburg (1968)
- 3.187 K. P. Miyake, R. Kato and H. Yamashita, Sci. Light, Tokyo 18, 39 (1969)
- 3.188 J.B. West, K. Codling and G.V. Marr, J. Phys. E: Sci. Instrum. 7, 137 (1974)
- 3.189 M.R. Howells, D. Norman and J.B. West, J. Phys. E: Sci. Instrum. 11, 199 (1978)
- 3.190 H. Dietrich and C. Kunz, Rev. Sci. Instrum. 43, 434 (1972); C. Kunz, R. Haensel and B. Sonntag, J. Opt. Soc. Am. 58, 1415 (1968)
- 3.191 W. Eberhard, G. Kalkoffen and C. Kunz, Ref. 3.9, p. 81, see also W. Eberhard, Thesis, University of Hamburg (1978)

- 3.192 The mirror was delivered from Optical Surfaces Ltd., London
- 3.193 standard mountings are in operation at most SR laboratories
- 3.194 K. Codling and P. Mitchel, J. Phys. E 3, 685 (1970)
- 3.195 P. Jaeglé, P. Dhez and F. Wuilleumier, p. 788 of Ref. 3.3
- 3.196 C.H. Bruett, N.C. Lien and J. Steben, P. 31 a A2-5 of Ref. 3.108
- 3.197 K. Thimm, J. Electr. Spectr. Rel. Phenom. 5, 755 (1974), and p. 30 of Ref. 3.2
- 3.198 G. Puester and K. Thimm, Ref. 3.9, p. 95
- 3.199 M. Salle and B. Vodar, C.R. Acad. Sci. Paris, 230, 380 (1950)
- 3.200 R.P. Madden, D.L. Ederer and K. Codling, Appl. Opt. 6, 31 (1967),  
R.P. Madden and D. Ederer, J. Opt. Soc. Am. 62, 722 (1972)
- 3.201 H. Sugawara and T. Sagawa, p. 790 of Ref. 3.3
- 3.202 S.A. Flodström and R.Z. Bachrach, Rev. Sci. Instrum. 47, 1464 (1976)
- 3.203 L.G. Parratt, Review Sci. Instrum. 30, 297 (1959)
- 3.204 B.M. Kincaid, SSRP Report No 75/03 Stanford 1975
- 3.204' G. Materlik, Thesis, Universität Dortmund 1975
- 3.205 Y. Cauchois, C. Bonnelle and G. Missoni, Comptes Rendus 257, 409 (1963)  
R. Barchewitz, M. Montel and C. Bonnelle, Comptes Rendus 264, 363 (1967)
- 3.206 U. Bonse, G. Materlik and W. Schröder, J. Appl. Cryst. 9, 223 (1976)
- 3.207 W. Ehrenberg and H. Mark, Z. f. Physik 42, 807 (1927)
- 3.208 G. Materlik, private communication
- 3.209 J.B. Hastings, B. Kincaid and P. Eisenberger, in Ref. 3.9, p. 167
- 3.210 J. Bordas, I.H. Munro, R. Pettifer and G. Worgan, unpublished
- 3.210' U. Bonse and M. Hart, Appl. Phys. Lett. 7, 238 (1965)
- 3.211 G. Materlik and V.O. Kostroun, to be published
- 3.212 J. Witz, Acta Cryst. A 25, 30 (1969)
- 3.213 G. Rosenbaum, K.C. Holmes, J. Witz, Nature 230, 434 (1971)  
J. Barrington Leigh and G. Rosenbaum, J. Appl. Crystallogr. 7, 117 (1974)
- 3.214 J. Barrington Leigh and G. Rosenbaum, Annual Review Biophysics and Bioengineering 5, 239 (1976)
- 3.215 N.G. Webb, S. Samson, R.M. Stroud, R.C. Gamble and J.D. Baldeschwieler, Rev. Sci. Instrum. 47, 836 (1976)
- 3.216 N.G. Webb, Rev. Sci. Instrum. 47, 545 (1976)
- 3.217 N.G. Webb, S. Samson, R.M. Stroud, R.C. Gamble and J.D. Baldeschwieler, J. Appl. Cryst. 10, 104 (1977)

- 3.218 J.C. Haselgrove, A.R. Faruqui, H.E. Huxley and U.W. Arndt,  
J. Phys. E: Scientific Instr. 10, 1035 (1977)
- 3.219 M.E. Van Hoosier, J.D.F. Bartoe, G.E. Brueckner, N.P. Patterson and  
R. Tousey, Appl. Opt. 16, 887 (1977)
- 3.220 T. Sasaki, T. Oda and H. Sugawara, Appl. Opt. 16, 3115 (1977)
- 3.221 T.A. Carlson, Phys. Rev. 156, 142 (1967)
- 3.222 J.A.R. Samson and G.N. Haddad, J. Opt. Soc. Am. 64, 47 (1974)
- 3.223 W. Gudat, W. Lenth and C. Kunz, p. 725 of Ref. 3.3 and W. Lenth, Diplomarbeit,  
University of Hamburg (1975)
- 3.224 a) R.P. Madden, in Calibration methods in the UV and x-region of the Spectrum,  
Int. Symp. Munich 1968, b) A.P. Lukirskii, E.P. Savinov, I.A. Brytov and  
Yu.F. Shepelev, Bull. Acad. Sci. USSR, Phys. Ser. 28, 774 (1964), c) W. Pong,  
J. Appl. Phys. 40, 1733 (1969), d) P.H. Metzger, J. Phys. Chem. Solids 26,  
1879 (1965)
- 3.225 B. Saloman and D.L. Ederer, Appl. Opt. 14, 1029 (1975)
- 3.226 L.R. Canfield, R.G. Johnston and R.P. Madden, Appl. Opt. 12, 1611 (1973)
- 3.227 J.G. Timothy and L.B. Lapson, Appl. Opt. 13, 1417 (1974)
- 3.228 L.B. Lapson and J.G. Timothy, Appl. Opt. 15, 1218 (1976)
- 3.229 M.A. Rumsh, A.P. Lukirskii and V.N. Shchemelev, Dokl. Akad. Nauk, SSSR,  
135, 55 (1959), Sov. Phys. Dokl. 5, 1231 (1960)
- 3.230 W. Gudat, unpublished results
- 3.231 see e.g. Acta Electronica Vol. 14, No 2 (1971); microchannel plates, Valvo  
Technical Note 760928 (1976), B. R. Sandel, A. Lyle Broadfoot and D.E.  
Shemansky, Appl. Opt. 16, 1435 (1977). P.J.K. Langendam and M.J. Van der Wiel,  
J. Phys. E, 10, 870 (1977)
- 3.232 J.L. Wiza, P.R. Henkel and R.L. Roy, Rev. Sci. Instrum. 48, 9 (1977)
- 3.233 see e.g. the Handbooks and Application Notes of the companies RCA, EMR,  
EMI, Johnston, Bendix, Galileo Electro Optics
- 3.233' W. Schnell and G. Wiech, Microchimica Acta (Wien), Suppl. 7, 323 (1977)
- 3.234 J.D. Branch, D.W.O. Heddl and M.J.H. Mogridge, J. Phys. E, 4, 9 (1971)
- 3.235 J.A.R. Samson and G.N. Haddad, J. Opt. Soc. Am. 64, 1346 (1974),  
U. Backhaus, Universität Hamburg (1974)

- 3.237 A.L. Robinson, Science 199, 39 (1978)
- 3.238 H. Wolf, J. Vac. Sci. Technology 12, 983 (1975)
- 3.239 S. Flügge ed., Handbuch der Physik, Vol. XLV (Springer, Berlin, Göttingen,  
Heidelberg 1958)
- 3.240 W.J. Price, Nuclear Radiation Detectors, 2<sup>nd</sup> ed. (McGraw Hill, New York,  
San Francisco, Toronto, London 1964)
- 3.241 J.B. Birks, The Theory and Practice of Scintillation Counting (Pergamon  
Press 1964)
- 3.242 N.A. Dyson, X-Rays in Atomic and Nuclear Physics (Longman Group Ltd.,  
London 1973)
- 3.243 P.W. Nicholson, Nuclear Electronics (John Wiley and Sons, London, Sidney,  
Toronto, 1974)
- 3.244 G.S. Brown in Ref. 3.5 p. 10-17
- 3.245 R. Fourme and R. Kahn in Ref. 3.5 p. 10-63
- 3.246 P. Rabe, G. Tolkiehn, A. Werner, private communication
- 3.247 F. Cappellani and G. Restelli, in: Semiconductor Detectors, G. Bertolini  
and A. Coche eds. (North Holland, Amsterdam 1968) p. 187
- 3.248 C. Cork et al.  
J. Appl. Crystallogr. 7, 319 (1973)
- 3.249 C.J. Borkowski and M.K. Kopp, Rev. Sci. Instrum. 46, 951 (1975)  
Rev. Sci. Instrum. 39, 1515 (1968)
- 3.250 A. Gabriel and Y. Dupont, Rev. Sci. Instrum. 43, 1600 (1972)
- 3.251 G. Charpak, Z. Hajduk, A. Jeavons, R. Stubbs and R. Kahn,  
Nucl. Instr. Methods 122, 307 (1974)
- 3.252 V. Perez Mendez, S.I. Parker, IEEE Trans. Nuclear Sci. 21, 45 (1945)
- 3.253 J.-I. Chikawa and I. Fujimoto, Appl. Phys. Lett. 13, 387 (1968)
- 3.254 T.C. Minor, J.R. Milch, G.T. Reynolds, J. Appl. Crystallogr. 7, 323 (1974)
- 3.255 S. Kozaki, M. Hashizume, and K. Kohra, Jap. J. Appl. Phys. 11, 1514 (1972)
- 3.256 U.W. Arndt, D.J. Gilmore, S.M. Boutle, Adv. Electronics Electron Phys. 33B,  
1069 (1972)

- 3.257 Synchrotron Radiation: A Bibliography ed. by G.V. Marr, I.H. Munro and J.C.C. Sharp, Daresbury (1972) and (1974)
- 3.258 R. Bruhn, B. Sonntag and H.W. Wolff, p.20 Vol I of Ref.3.109
- 3.259 B. Sonntag, p. 9 Vol.I of Ref.3.109
- 3.260 N. Kosuch, E.Tegeler, G. Wiech and A. Faessler, to appear in Ref.3.9  
A. Faessler, p.801 of Ref 3.3
- 3.261 see e.g. G. Zimmerer in Ref. 3.6
- 3.262 R. Lopez-Delgado, A. Tramer, J.H. Munro, Chem.Phys. 5, 72(1974)  
O. Benoist d'Azy, R. Lopez-Delgado, A. Tramer, Chem.Phys. 9, 327 (1975), N. Schwentner, in Ref.3.6
- 3.263 R. Haensel, U. Hahn and N. Schwentner, p.239 of Ref.3.8: R.Haensel, U. Hahn, N. Schwentner, B. Jordan and G. Zimmerer, p.250 of Ref.3.8
- 3.264 W. Lohr, H.W. Jochims and H Baumgärtel, Ber. Bunsenges Phys.Chem.79 901(1975), D. Reinke, R. Kraessig and H. Baumgärtel, Z. Naturforschung 28a, 1021 (1973)
- 3.265 H. Hertz, H.W. Jochims, H. Schenk, W. Sroka, Chem.Phys.Lett.29,572(1974)
- 3.266 made by Physical Electronics Industries
- 3.267 R.Z. Bachrach, F.C. Brown and S.B.M. Hagström, J.Vac.Sci.Technol. 12 309 (1975); R.Z. Bachrach, S.B.M. Hagström and F.C. Brown, p.795 of Ref.3.3
- 3.268 P.J. Key, Metrologia 6, 97 (1970)
- 3.269 E. Pitz, Appl.Opt. 8, 255(1969)
- 3.270 D. Einfeld, D. Stuck and B. Wende, p. 114 of Ref.3.109, see also DESY SR 77/03
- 3.271 R.P. Haelbich and C. Kunz, p.344 in Ref.3.8
- 3.272 S. Aoki, J. Ichihara and S. Kikuta, Jap.J.Appl.Phys.11,1857(1972)
- 3.273 G. Schmahl, D. Rudolph and B. Niemann, Vol III p.40 of Ref 3.109
- 3.274 E. Spiller, R. Feder, J. Topalian, D. Eastman, W. Gudat and D. Sayre, Science 191, 1172(1976)
- 3.275 R. Feder, E. Spiller, J. Topalian, A.N. Broers, W. Gudat, B.J. Panessa Z.A. Zadunaisky and J. Sedat Science 197, 259(1977)
- 3.276 J.C. Philips, A. Wlodawer, M.M. Yevitz, and K.O. Hodgson, Proc.Nat.Acad.Sci. USA 73, 128 (1976)
- 3.277 A. Harmsen, R. Lebermann and G.E. Schulz, J.Mol.Biol. 104, 311 (1976)
- 3.278 K.C. Holmes in Ref. 3.3 p. 809
- 3.279 Zvi Kam, Macromolecules, in press
- 3.280 S.L. Ruby, Journal de Physique C6, Suppl. 12,35, CG-209 (1974)
- 3.281 R.L. Cooper, G.L. Miller, and K.W. West, Nuclear Resonance Excited by Synchrotron Radiation (Activity Report, SSRP, Stanford, Jan-June 1977) p VI-43
- 3.282 E. Gerdau, M. Mueller, R. Rüffer, W. Trautsch and H. Winkler in Ref. 38, p. 297
- 3.283 B. Buras, J. Staun Olsen, L. Gerward, Nucl.Instrum. and Methods 135, 193 (1976)
- 3.284 J. Bordas, M. Glazer and I.H. Munro, Nature 262, 541 (1976)
- 3.285 B. Buras, J. Staun Olsen, L. Gerward, G. Will and E. Hinze, J. Appl. Crystallogr. 10, 431 (1977)
- 3.285' U. Bonse and G. Materlik, Z. Physik B 24, 189 (1976)
- 3.286 U. Bonse, G. Materlik in: Anomalous Scattering, S. Ramaseshan, S.C. Abrahams eds. (Mungsgaard, Kopenhagen 1975) p. 107
- 3.287 D.E. Sayers, F.W. Lytle and E.A. Stern in: B.L. Henke, J.B. Newkirk and G.R. Mallett, eds., Advances in X-ray Analysis, Vol. 13 (Plenum Press, New York 1970), p. 248  
D.E. Sayers, E.A. Stern and F.W. Lytle, Phys.Rev.Lett. 27, 1204 (1971)  
E.A. Stern, Phys.Rev. B10, 3027 (1974)
- 3.288 B.M. Kincaid, P. Eisenberger, K.O. Hodgson, and S. Doniach, Proc.Natl.Acad.Sci. USA 72, 2340 (1975)
- 3.289 T. Tuomi, K. Naukkarinen, E. Laurila, P. Rabe, Acta Polytechnica Scand. Ph-100 (1974); T. Tuomi, K. Naukkarinen, P. Rabe, phys. stat. sol. (a) 25, 93 (1974)
- 3.290 B.K. Tanner, M. Safa and D. Midgley, J. Applied Cryst. 10, 91 (1977)
- 3.291 J. Bordas, A.M. Glazer, H. Hauser, Phil. Mag. 32, 471 (1975)
- 3.292 M. Hart, J. Appl. Crystallography 8, 436 (1975)
- 3.293 W. Hartmann, G. Markewitz, U. Rettenmaier and H.J. Queisser, Appl. Phys. Lett. 27, 308 (1975)
- 3.294 J.A. Golovchenko, B.W. Batterman and W.L. Brown, Phys. Rev. B10, 4239 (1974)

- 3.295 S. Kjaer Andersen, J.A. Golovchenko and G. Mair, Phys. Rev. Lett. 37, 1141 (1976)
- 3.296 J.A. Golovchenko, E. Uggerhøj, G. Mair and S.K. Andersen in Ref. 3.8 p. 291
- 3.297 N. Kosuch, E. Tegeler, G. Wiech and A. Faessler, Chem. Phys. Lett. 47, 96 (1977)
- 3.298 N. Kosuch, E. Tegeler, G. Wiech and A. Faessler, DESY SR-77/19 and Ref.3.9, p.113
- 3.299 C.J. Sparks, Jr., S. Raman, H.L. Yakel, R.V. Gentry and M.O. Krause, Phys. Rev. Lett. 38, 205 (1977)
- 3.300 M. Cooper, R. Molt, P. Pattison and K.R. Lea, Communications on Physics 1, 159 (1976)
- 3.301 C.J. Sparks, Phys. Rev. Lett. 33, 262 (1974)
- 3.302 P. Eisenberger, P.M. Platzman and H. Winick, Phys. Rev. Lett. 36, 623 (1976)
- 3.303 P. Eisenberger, P.M. Platzman and H. Winick, Phys. Rev. B13, 2377 (1976)
- 3.304 I. Lindau, P. Pianetta, S. Doniach and W.E. Spicer, Nature 250, 214 (1974)
- 3.305 I. Lindau, P. Pianetta, K.Y. Yu and W.E. Spicer, Phys. Rev. B13, 492 (1976)
- 3.306 K. Siegbahn, J. Electron Spectroscopy 5, 3 (1974)

Tables

- 3.1 Properties of mirror substrate materials
- 3.2 Efficiencies of holographic and ruled gratings
- 3.3 Lattice constants of monochromator crystals
- 3.4 Calculated resolution of crystals
- 3.5 VUV-Filters for higher order rejection
- 3.6 Constraints on monochromator design
- 3.7 Normal incidence monochromators
- 3.8 Grazing incidence monochromators
- 3.9 VUV detectors
- 3.10 Properties of multipliers, channeltrons etc.
- 3.11 X-ray detectors
- 3.12 Types of experiments in the VUV
- 3.13 Types of experiments in x-ray region

Table 3.2 Grating efficiency  $\lambda = 44 \text{ \AA}$

	Radius	Origin	Catalogue No.	Serial No.	Type
17	2m	B & L	35-52-37-800	2553-6-1-1	Shallow Blazed. Ruled. Replica.
22	plane	J.Y.	-	-	Holographic.
23	2m	B & L	35-52-40-700	2517-2-4-5	Shallow Blazed. Ruled. Pt. Replica.
24	2m	B & L	35-52-40-700	2517-2-5-8	Shallow Blazed. Ruled. Pt. Replica.
25	2m	B & L	35-52-40-400	2278-32-1-3	Shallow Blazed. Ruled. Pt. Replica.
44	2m	B & L	35-62-41-800	1194-6-3	Shallow Blazed. Ruled. Pt. Replica.
47	2m	B & L	35-52-41-800	1194-5-2	Shallow Blazed. Ruled. Au. Replica.
53	5m	N.P.L.	-	156	Laminar. Ruled. Au.
67	plane	Göttingen/IC.	-	18	Laminar. Holographic. Au.
73	2m	Göttingen/IC.	-	25	Laminar. Holographic. Au.
74	2m	Göttingen/IC.	-	26	Laminar. Holographic. Au.
76	2m	Göttingen/IC.	-	34	Laminar. Holographic. Au.
77	1m	B & L	55-72-36-900	1068-1-1-1-4	Shallow Blazed. Ruled. Au. Replica.
80	5m	Göttingen/IC.	-	21	Laminar. Holographic. Au.
84	5m	Göttingen/IC.	-	37	Laminar. Holographic. Au.
87	5m	Göttingen/IC.	-	43	Laminar. Holographic. Au.
94	plane	N.P.L.	-	194	Shallow Blaz. Holographic. Au.
99	plane	N.P.L.	-	177	Shallow Blaze. Holographic. Au.
100	5m	N.P.L.	-	173	Laminar. Ruled. Original. Au.
101	2m	B & L	35.52.40.700	2517-2-6-3	Shallow Blazed. Ruled. Pt. Replica.
180	1m	Hyperfine Inc.	-	320	Shallow Blazed. Au. Ruled. Original.
197	1m	Ion Tech. Ltd.	-	-	Shallow Blazed. Holographic. Au.
B	2m	B & L	35-52-40-400	2278-30-2-6	Shallow Blazed. Ruled. Pt. Replica.
F	plane	N.P.L.	-	83	Laminar. Ruled.

Table 3.1 Thermal properties of mirror substrate materials

material	average daily length change $\Delta L/L \cdot 10^{-9}$	thermal expansion, range $100^\circ\text{C} - 30^\circ\text{C}$ $\alpha \cdot 10^7 (\text{C}^{-1})$	thermal conductivity, at $27^\circ\text{C}$ ( $\text{W/m}^\circ\text{C}$ )
Corning 7940 fused silica	$-0.51 \pm 0.03^a$	$+4.4 - 4.7^a$	$1.4^c$
Owens-Illinois Cer-Vit C-101 glass ceramic	$0.50 \pm 0.03^a$	$(-0.3) - (-1.2)^a$	$1.7^c$
Heraeus-Schott Zerodur glass ceramic	$0. \pm 0.03^a$	$(-0.4) - (0.5)^a$	$1.7^c$
Heraeus-Schott Homosil fused silica	$-0.56 \pm 0.03^a$	$+4.5 - 5.0^a$	$1.4^c$
Simonds Saw & Steel Super Invar	$0. \pm 0.03^a$	$(-3.0) - (-1.7)^a$	-
SiC reaction bonded	-	$43^b$	$180^b$
Cu	-	$168^b$	$400^b$
Mo	-	$51^b$	$140^b$

<sup>a</sup> Refs. 3.85 and 3.86

<sup>b</sup> Ref. 3.71

<sup>c</sup> Refs. 3.87 and Vol. III of Ref. 3.139

Table 3.3 Useful values of lattice constants in X.U. ( $\approx 10^{-3}$  Å).

We give here the geometrical distance between atomic planes,  $d_{\infty}$ , not corrected for the index of refraction

crystal	$d_{\infty}$ (X.U.)
silicon (220)	1920
germanium (220)	1997
quartz (11 $\bar{2}$ 0)	2451
NaCl (100)	2814
calcite (100)	3029
silicon (111)	3135
germanium (111)	3262
quartz (10 $\bar{1}$ 1)	3336
quartz (10 $\bar{1}$ 0)	4246
gypsum (010)	7585
lead stearate	50300
cerotic acid	72500

Table 3.4 Energy resolution for various Bragg reflections (3.41, 3.130)

crystal	hkl	$\Delta\epsilon/\epsilon$
germanium	111	$3.2 \cdot 10^{-4}$
	220	$1.5 \cdot 10^{-4}$
silicon	111	$1.33 \cdot 10^{-4}$
	220	$5.6 \cdot 10^{-5}$
	400	$2.3 \cdot 10^{-5}$
	440	$8.9 \cdot 10^{-6}$
	333	$8.1 \cdot 10^{-6}$
	444	$4.6 \cdot 10^{-6}$
	660	$2.2 \cdot 10^{-6}$
	555	$1.4 \cdot 10^{-6}$
	880	$6.6 \cdot 10^{-7}$

Table 3.5 Useful spectral range for several filter materials

material	range	reference
lime soda glass	throughout visible	3.10
	- 4 eV	
quartz glass	- 7,5 eV	3.10
MgF <sub>2</sub>	- 10.5 eV	3.10
LiF	- 11.5 eV	3.10
ln	11 - 16.5 eV	3.10
Al	17 - 72 eV	3.48, 3.27
Te	20 - 40 eV	
Mg	20 - 49 eV	3.48
Si	- 100 eV	3.27
C	45 - 270 eV	3.48
hydrocarbon films	45 - 270 eV	3.144, 3.27
Pr	60 - 110 eV	3.48, 3,152

Table 3.6 Constraints on the design of monochromators for use with SR (a similar table is given in Ref. 3.155)

<u>Constraints</u>	<u>Implications</u>
1) The light source is fixed in position and in many cases also the experiment	Constant deviation optics is required for the system: beam-line - monochromator-experiment. In the grazing incidence regime in general a complex coupled motion is required for high resolution
2) SR beam is coming horizontally	Horizontal reflections and dispersion planes are more convenient than vertical ones
3) SR beam is highly polarized with the electric vector in the horizontal orbit plane	Vertical reflections and dispersions are preferred due to higher intensity (no Brewster-case) and polarization
4) The SR source width is several times its height (typ. $(5-10 \times 1-2)\text{mm}^2$ )	Vertical dispersion gives higher resolution for monochromators without entrance slit and in general allows for better optical coupling (intensity, slit-efficiency factor)
5) High energy machines present a large flux of hard x-rays (with $\lambda$ of few $\text{\AA}$ or less)	First optical components of beam-lines can be severely radiation-damaged (blistering of grating and mirror coating materials, cracking of glass-mirrors) and generally a coating of components with cracked hydrocarbons can occur, importance of easy-to-replace-components
6) Radiation hazards exist at high energy machines	Remotely controlled equipment might be necessary (DESY), access to the experiment is restricted, long beam pipes are necessary (at DESY about 40 m)
7) High collimation of SR and long beam pipes give nearly parallel light	Allows for special monochromators to work without entrance slits and requires condensing mirror at slit-systems
8) At synchrotrons the light intensity can considerably fluctuate with time due to different fillings	Suitable intensity monitors are required for compensation, beam-splitter technique might be necessary for high accuracy experiments
9) The vertical beam position may be unstable depending on accelerator electron optics and energy	Short time fluctuations (due to beam oscillations) determine the attainable resolution in monochromators without entrance slits, the effects can be reduced by either using slits close to the source point or by large demagnifying optics
10) UHV in storage rings and HV in synchrotrons	Often the vacuum requirements on beam-lines and monochromators disallow for instance small motors and lubrications inside vacuum systems and in turn determine the complexity of scanning systems
11) One beam pipe often feeds several instruments	The instrument has either to be removed as a whole or at least part of the incident beam has to continue through the instrument

**Table 3.8** Survey on different mounts of grazing incidence monochromators for use with SR experiments

Fig. No.	Type	Accelerator	Number of Reflections	Grating	Exit Beam	Resolution	References
3.29a)	plane grating	DESY (Nowak et al.)	1	plane	moving	low	3.186
3.29b)	plane grating	INS-SOR (Miyake et al.)	2	plane	fixed	medium	3.187
3.29b)	plane grating	DNPL (West et al.)	2	plane	fixed	medium	3.188
3.29b)	distant source	DNPL (Howells et al.)	2	plane	fixed	medium	3.189
3.29c)	plane grating	DESY (Kunz et al.)	3	plane	fixed	medium	3.190
3.29c)	distant source	DORIS (Eberhardt et al.)	3	plane	fixed	high	3.191
3.46							
3.30a)	Rowland	all labs	2	spherical	moving	high	3.197
3.30b)	Rowland	Glasgow/DNPL (Codling et al.)	4	spherical	fixed	high	3.194
3.30c)	Rowland	ACO (Jaeglé et al.)	5	spherical	fixed	medium	3.195
3.30d)	Rowland-Vodar	Stoughton (Pruett et al.)	3	spherical	fixed	high	3.196
3.30e)	Rowland	Bonn (Thimm et al.)	2	spherical (two)	fixed	high	3.197
3.30f)	spherical grating	Stanford/Stoughton (Brown et al.)	4	spherical	fixed	medium	3.170
3.31a)	parallel illumination	DESY (Haensel et al.)	1	spherical	moving	medium	3.1
3.31b)	distant source	NBS (Madden et al.)	1	toroidal	fixed	medium	3.200

**Table 3.7** Survey on normal incidence monochromators with concave gratings and with fixed exit beams for SR experiments

Type	grating motion	focal length and dispersion plane	resolution	reference	remarks
<u>standard</u>	rotation and translation	0.3 m horiz.	low	p. 49 of 3.21	
<u>normal incidence monochromator</u>	"	1 m vert.	medium	3.185, 3.20	
	"	3 m horiz.	high	3.173 p. 50 of 3.21	
	"	10 m	very high	p. 49 of 3.21	under construction
<u>Seya-Namioka</u>	rotation	0.5 m vert.	low	3.	
	"	0.5 m horiz.	low	3.20	
	"	1 m vert.	medium	3.81, 3.119 p. 49 of 3.21	
	"	1 m horiz.	medium	3.20, 3.91	
	"	1 m		3.171, 3.101	with asymmetrical illumination of grating and asymmetric beam length
<u>Wadsworth</u>	rotation and translation	1 m horiz.	low	3.175, 3.155	
	"	0.5 m vert.	low/medium	3.176, 3.180	
	"	1 m vert.	medium	3.174, 3.177; 179; 263, 264	premirrors are used and refocussing toroidal mirror (3.180)
	"	1.5 m horiz.	medium	3.178	holographic, Au coated grating was used
		corrected holographic grating		3.181 p. 34 of 3.21	correction for astigmatism
<u>Pouey</u>					
<u>higher order focussing</u>	rotation	4 exit beams with different focal lengths	medium/high	3.101 p. 4 of 3.21	

Table 3.9 Detectors for the Vacuum Ultraviolet

	approx. spectral range ( $\text{\AA}$ )	references	remarks, examples
1. Photographic plates or Films	visible - x-rays	3.10,12,219	see also Table 3.11, Eastman-Kodak SWR 101, 104, Kodak-Pathé SC-5, SC-7, Ilford Q
2. Photon Counters			
2.1 Geiger-Müller Counter }			
2.2 Proportional Counter }	300 - x-rays	3.10,12	see also Table 3.11, useful for absolute intensity measurements, primary standards
2.3 Ionization chamber and channel-detector }		3.220	
3. Ionization chambers			especially for absolute intensity measurements, see also Table 3.11, useful as primary intensity standards
3.1 Single Ion Chamber	1000 - 250 (50)	3.10	
3.2 Double Ion Chamber	1000 - 250	3.10,222,223	
4. Open and closed photodiodes	2500 - x-rays	3.10,12	useful as secondary standards
5. Photoelectron-multipliers	visible - x-rays		see also Table 3.10
5.1 Phosphor with standard multiplier (S-11)	~ 3500 - (50)	3.10,235	Sodium salicylate, Liumogen, Terphenyl, Coronen etc.
5.2 Scintillation by accelerated photoelectron and multiplier	visible - x-rays	3.235,10	
5.3 Multiplier with transparent envelope or window	see Table 3.10	3.233	facilitates operation since solar blind
5.4 Windowless open multipliers	2500 - x-rays	3.10,233	photocathodes determine spectral characteristic
5.4.1 Divided dynodes	"	3.10,233	see Table 3.10, standard type multiplier: RCA, EMI, EMR, Johnston etc.
5.4.2 Strip dynode	"		
1. Crossed electric and magnetic field	"	3.10	Bendix
2. Electric field	"	3.233'	
5.4.3 Channel dynodes	"		nowadays most widely used
1. Channeltron	"	3.227,228,231	with capabilities up to $\mu\text{A}$ anode current
2. Microchanneltron plates	"	3.228,231	the most advanced available systems today
6. Miscellaneous			
6.1 Thermopiles	visible - (500)	3.10,236	basically for total absolute intensity measurements, useful as primary standard
6.2 Photovoltaic devices	visible - 250	3.10	

Table 3.11

X-Ray Detectors /3.239 - 245/.

The numbers quoted are typical values.

		Ref.	FWHM energy resolution	dead time	time resolution	Remarks
1	Crystal scintillation counters (NaI(Tl))	3.239-241,244	~4000 eV	0.3 $\mu$ s	10 ns	
2	Plastic scintillation counters	3.240,243,244	~8000 eV	2-4 ns	1 ns	low efficiency
3	Si(Li)	} 3.240,244,247	200 eV	10 $\mu$ s*	10 ns	some have even better resolution
4	Ge(Li), and intrinsic Ge					
5	Proportional counters	3.239,240,242,244	1000 eV	0.5 s	25 ns	especially for low energies
6	Geiger-Müller counters	3.239,240,244	--	0.1 ms		
7	Ionization chambers	3.204,244	--	--	--	for more than $10^7$ photons/s
<u>Position sensitive detectors:</u>						
8	Photographic film (nuclear emulsions)	3.239	--	--	--	reduced sensitivity with higher energy, shrinkage of film, resolution 0.3 $\mu$ m
9	Linear semiconductor detector	3.247	--	--	--	
10	Linear proportional chamber	3.248,249	~1000 eV	0.5 $\mu$ s	25 ns	resolution > 0.150 mm
11	Multiwire proportional chamber	3.214,250,252		1 $\mu$ s		0.15 - 0.7 mm FWHM resolution
12	Spherical drift chamber	3.521		200 ns		
13	X-ray TV camera	3.253-256	--	--	--	

\* This is a typical value. Smaller values are possible if a deterioration of the energy resolution is tolerated

Table 3.10 Some Properties of Multipliers

Code No. Table 3.9	Typ	Spectral range	High-voltage	typical Gain	typical dark current	size of cathode	beakable
5.0	EMR, EMI, RCA etc. side on		< 1.5 KV	~ $10^6$	$3 \times 10^{-9}$ A	~ 10 mm $\emptyset$	no
5.3	EMR 541 F	~ 3000 - 1450 $\text{\AA}$	< 2.5 KV	~ $10^6$	$4 \times 10^{-11}$ A	~ 25 mm $\emptyset$	no
5.3	EMR 541 G	~ 1900 - 1450	< 2.5 KV	~ $10^6$	$6 \times 10^{-12}$ A	~ 25 mm $\emptyset$	no
5.3	EMR 542 G	~ 1900 - 1050	< 2.5 KV	~ $10^6$	$6 \times 10^{-12}$ A	28 mm	no
5.4.1	Johnston MM 1	~ 2500 - x-rays	< 5 KV	~ $10^8$ at 3.5 KV	< $10^{-13}$ A	~ 32 mm $\emptyset$	350 $^\circ$ C
	MM 2	~ 2500 - x-rays	< 5 KV	~ $10^6$ at 3 KV	< $10^{-13}$ A	13 mm $\emptyset$	350 $^\circ$ C
5.4.1	Balzers SEV 117	~ 2500 - x-rays	< 3.5 KV	~ $10^8$ at 3.5 KV		10 x 6 mm <sup>2</sup>	400 $^\circ$ C
5.4.2.1	Bendix M 306	~ 1500 - x-rays	< 2 KV	> $10^6$	$10^{-12}$ A	15 x 18 mm <sup>2</sup>	170 $^\circ$ C
5.4.2.2	"Schnell"	~ 1200 - x-rays	< 3.5 KV	$5 \times 10^6$ at 3 KV	$1 \frac{\text{cts}}{\text{sec}}$	$0.5 \times 10 \text{ mm}^2$	
5.4.3.1	Bendix EM 401 channeltron	~ 1500 - x-rays	< 4 KV	$5 \times 10^7$ at 3 KV	< $0.05 \frac{\text{cts}}{\text{sec}}$	1 mm $\emptyset$	< 300 $^\circ$ C
5.4.3.1	Mullard B 419 BL	1500 - x-rays	< 5.5 KV	$5 \times 10^7$ at 3.5 KV	< $0.1 \frac{\text{cts}}{\text{sec}}$	10 mm $\emptyset$ 2 mm $\emptyset$ channel	200 $^\circ$ C
5.4.3.1	Galileo 4510 WL	1500 - x-rays	< 4.5 KV	> $10^7$	< $0.1 \frac{\text{cts}}{\text{sec}}$	24 x 24 mm <sup>2</sup>	200 $^\circ$ C
5.4.3.2	Mullard G 40 - 25	1500 - x-rays	< 4.5 KV 2.5 KV	$10^6$	< $0.01 \frac{\text{cts}}{\text{sec}}$	25 mm $\emptyset$	

Table 3.13 Types of experiments in the x-ray region

	References	Important properties of SR				Remarks
		Tunability	Brightness	Pulses	Total Int.	
<u>Methods for structural investigation</u>						
1) Single crystal diffraction	3.276,277	(+)	+			tunability only for anomalous dispersion
2) Small angle diffraction	3.213-218,278		+	+		
3) Small angle scattering	3.34		+	+		
4) Mössbauer scattering	3.280-282	+	+	+		
5) Energy dispersive diffraction	3.283-285	+	+			
6) Interferometry	3.206,286	+	+			
7) Absorption (EXAFS)	3.204,209,210,287,288	+	(+)		+	brightness allows simple monochromators, pulses could be of interest
8) Topography	3.289-292	+	+	+		
9) Standing wave excited fluorescence	3.294-296					
<u>Methods for investigating electron states</u>						
10) Fluorescence excitation	3.297-299	+			+	
11) Compton scattering	3.300		+		+	
12) Resonant Raman scattering	3.302,303	+			+	with wiggles also non-resonant process of interest
13) Photoelectron spectroscopy (XPS)	3.40,304,305				+	

Table 3.12 Experiments in the vacuum ultraviolet

	References	Important Properties of SR					Remarks
		Tunability	Brightness	Pulses	Polarization	Total Intensity calculable	
Absorption	standard see Chap.7	+				(+)	
Reflection	3.160-161	+			(+)	(+)	polarization for determination of optical constants
Ellipsometry	3.260	(+)			+	(+)	
Fluorescence	3.261-263	+		+		+	pulses for fluorescence decay experiments
Luminescence	3.264, 265	+				+	
Photoionisation Photofragmentation	3.39, 3.159, 3.267	+	+	(+)	+	+	tunability for yield spectroscopies and pulses for the time of flight spectroscopy
Radiometry Calibration	3.268-270	(+)				+	
Microscopy	3.68,90, 125, 126, 274, 275	(+)	+			+	tunability to work below and above absorption edges

Figure Captions

- Fig. 3.1a Arrangement of beam ports and experiments at the 0.24 GeV storage ring TANTALUS I at Stoughton/Wisconsin. (With permission by E.M. Rowe).
- Fig. 3.1b Photograph of the laboratory at the TANTALUS I ring. (From [3.28].)
- Fig. 3.2a Layout of the synchrotron radiation laboratory at DORIS. Shown is one quadrant of the storage ring, the beam line to the laboratory and the arrangement of the experiments. For details see text. (From (3.33)).
- Fig. 3.2b Photograph of the experimental area in the DORIS laboratory viewed in the direction towards the source.
- Fig. 3.3 Optical layout of the vacuum ultraviolet beam lines at the DORIS laboratory. The beam (from left) is split into four independent beams  $L_1$ ,  $L_2$ , D and R,  $S_1$  to  $S_4$  = plane mirrors, FM = focusing mirrors, FG = concave gratings, G = plane grating, Mi = flat mirrors, SL = entrance and exit slits respectively, FL = x-ray fluorescence experiment, X-RAY/ROW = space for an x-ray or Rowland monochromator, the monochromators HONORMI, FLIPPER and HIGITI are occupying the beams  $L_1$ ,  $L_2$  and R, respectively. (From (3.33)).
- Fig. 3.4 X-ray beam layout at the SSRL storage ring laboratory at SPEAR for "beam line II". In two cases focusing torroidal mirrors serve to concentrate up to 10 mrad of the horizontal fan onto the sample. (From (3.7)).

- Fig. 3.5 Position monitors for the vertical beam position a) photoemission monitors at the DORIS laboratory monitoring the photocurrent from three insulated metal strips where the center of the arrangement is adjusted to the ideal plane of the orbit. Either the system at the front end of the beam shutter (Monitor 2) or another one at the experimental area (Monitor 1) can be used. b) Photograph of a fluorescence screen monitor used at SPEAR at 22 m from the source point. The divisions are spaced by 1 cm. The black rectangle is cut out in the center to allow the used beam to pass to the experiments. (From (3.7).)
- Fig. 3.6 Original spectra registered simultaneously by an open photomultiplier with an  $Al_2O_3$  coated cathode measured at DESY: a) without reference monitor, b) the same spectrum divided by a reference signal obtained from a cathode surrounding the entrance aperture of the monochromator, c) the spectrum divided by a reference signal obtained from the photoelectrons of a gold coated mirror reflecting the monochromatized beam. (From (3.35).)
- Fig. 3.7 Phase space ellipses for the vertical coordinate of the electron beam alone (solid lines) and including the SR divergency (dashed lines). The source is located at  $Z = 0$ , the light beam expands in the positive Z direction. The upright ellipse for SR (a) is simply sheared while the beam moves to  $Z = l$  (b)). The invariants are the intersections with the y-axis, the projection on the y' axis and the area. A slit (with boundaries  $S_u$  and  $S_o$ ) inserted at  $Z = l$  (b) can be projected back to the origin (a)). The shaded area is an invariant also. Figures c) and d) show the same

transformation for an already tilted electron beam ellipse (divergent electron beam!)

Fig. 3.8 Two cases of the "magic mirror" arrangement which is capable of focusing SR from a circular orbit onto one point I without introducing any time distortion of the pulses. (From [3.41]).

Fig. 3.9 Normal incidence reflectivity of C, Al, and Au as calculated from a Kramers-Kronig consistent set of optical constants. For comparison experimental data are included. (After [3.48]. For references of the experimental data see also [3.40]).

Fig. 3.10 The experimentally determined reflectivity of Pt is plotted for various angles of incidence versus photon energy. (After [3.56]).

Fig. 3.11 The calculated reflectivity of Pt for perpendicular  $R_s$  and parallel  $R_p$  polarization is plotted for three different photon energies. (After [3.57]).

Fig. 3.12 The calculated reflectivity  $I_R/I_0$  versus the dimensionless quantity  $(\theta - \theta_c)/\theta_c$  with  $\theta_c$  being the angle of total external reflection demonstrates that the more strongly absorbing Pt does not show as steep an edge as fused quartz. (From [3.40]).

Fig. 3.13 The experimentally determined normal incidence reflectivity of chemical vapor deposited (CVD) SiC is about twice as high as any other material measured up to now in the energy range 5 to about 25 eV. (From [3.72]).

Fig. 3.14 Reflectivity R of a multi-layer interference mirror with 4.5 periods of Au/C on glass as a function of photon wavelength  $\lambda$ . The average periodicity is 106 Å. The angle of incidence  $\alpha$  is

varied in steps from 15° to 60°. Solid line: experimental values, dashed line: theoretical values based on optical constants of Ref. 3.48 (for the glass substrate  $\epsilon = 0.9 + 0.1 i$  was used independent of wavelength). The theoretical curve is reduced by a factor of 0.2. (From [3.74]).

Fig. 3.15 The measured reflectivity of Au and C is shown vs. the grazing angle  $\theta$  of incidence for various photon energies. Note the steep decrease in the reflectivity of C with increasing angle  $\theta$ . (After [3.77]).

Fig. 3.16 The radiation damage of SR is demonstrated. A glass beam-splitter mirror which has been used for several months in the beam-line of the DORIS SR laboratory under normal operating conditions ( $E \sim 1.7 - 2.5$  GeV,  $I \sim$  up to 300 mA) shows strong discoloration within the glass and cracks at the optical surface.

Fig. 3.17 Total scattering spectra for Mo coated fused-quartz and SiC mirrors show the superior performance of SiC as a VUV mirror material. The points joined by dashed lines are inaccurate due to stray light or second-order light. The solid curves are best fits according to the expression  $S = A/\lambda^4 + B/\lambda^2$ . (From [3.82]).

Fig. 3.18 Schematic of the Rowland Circle mounting for a concave spherical grating. Radiation from a point A is dispersed and focussed by the grating at the point B with A and B lying on the Rowland Circle having a diameter R equal to the radius of curvature R of the spherical grating.  $\alpha$  and  $\beta$  are the angles of incidence and diffraction, resp., measured in the meridional plane.

Fig. 3.19 Comparison of the efficiency of two new gratings (Bausch and Lomb (No. 2588-9-2 and 2588-10-1) and two gratings used with synchrotron radiation (No. 2588-4-6-1 and 2588-4-1-2). Grating No. 3588-4-6-1 has been coated with 600 Å of gold after use. The 0. order has been scaled down by a factor of 0.2. (From [3.107]).

- Fig. 3.20 Grating efficiencies for ruled and holographic gratings are plotted vs. grazing angle of incidence. The test wavelength is  $44 \text{ \AA}$ . Further explanations are given in Tab. 3.1 (From [3.110]).
- Fig. 3.21 The efficiency of a transmission grating is plotted. a) shows the relative efficiency of orders two through six compared to first order. b) gives the value of the first order to the zeroth order which has been used to determine the grating thickness. c) displays the absolute efficiency for the first order. (From [3.130]).
- Fig. 3.22 Single crystal reflection profile for the 220 Bragg reflection from Si at  $\lambda = 1.38 \text{ \AA}$ , calculated with and without absorption. (From [3.132].)
- Fig. 3.23 Change of beam cross section when Bragg reflected from a crystal with its surface cut at an angle  $\sigma$  relative to the lattice planes.
- Fig. 3.24 The transmissivity of Al thin films vs. wavelength demonstrates the excellent performance of Al as a VUV filter having window-type characteristic. Curves calculated with Eq. 3.26 and optical absorption data of [3.48].
- Fig. 3.25 Part a) shows a schematic diagram of a three mirror polarizer. The relation between the two angles of incidence is  $2\alpha - \beta = 90^\circ$  for a undeviated light beam. b) The calculated polarization  $R_s/R_p$  (solid line) and the throughput  $R_s$  (dashed line) is plotted for a three mirror polarizer. The angle of incidence on the first and third mirror (both Al) is  $\alpha = 73.5^\circ$ . The second angle of incidence is  $\beta = 57^\circ$  that is the Brewster angle at  $\lambda = 1500 \text{ \AA}$  for the second reflecting surface of  $\text{MgF}_2$ . (From [3.162]).
- Fig. 3.26 Schematic diagrams of various normal incidence monochromators for use with synchrotron radiation. For explanations and references see text.
- Fig. 3.27 Horizontal focussing correction for a modified Wadsworth monochromator by means of an excentric pivot for the grating rotation.  $\alpha$  and  $\beta$  are the angles of incidence and refraction, resp. with  $\alpha + \beta = B$ . The defocussing is plotted vs wavelength in nanometer. (From [3.155]).
- Fig. 3.28 The intensity behind the exit slit of a 1 m focal distance Wadsworth monochromator at the DORIS SR laboratory is plotted vs wavelength for two different gratings, a holographic grating blazed at  $1200 \text{ \AA}$  and a ruled grating blazed at  $600 \text{ \AA}$  (With permission of G. Zimmerer).
- Fig. 3.29 Three types of plane grating monochromators. The scanning motion of the elements is indicated. PG = plane grating, PM = plane mirror, FM = CM = focussing mirror. Synchrotron light is coming from the left. (From [3.17]).
- Fig. 3.30 Six types of monochromators are shown which operate according to the Rowland principle. (From [3.197]).
- Fig. 3.31 The spectral dependence of the photoyield of Au is shown as measured behind the exit slit of a grazing incidence monochromator. The effects of surface roughness of a used and a new mirror (with  $165 \text{ \AA}$  and  $30 \text{ \AA}$  rms roughness, resp.) and of hydrocarbon contamination are seen. (From [3.170]).
- Fig. 3.32 The optical layout of Non-Rowland monochromators is shown schematically. (From [3.17]).
- Fig. 3.33 Part a) depicts a toroidal holographic grating monochromator and b) a transmission monochromator. (From [3.130]).

- Fig. 3.34 Double crystal monochromators (a) in the parallel (+,-) mode and b) in the highly dispersive antiparallel (+,+) mode.
- Fig. 3.35 Monochromators as proposed and tested by BEAUMONT and HART (3.132)
- Fig. 3.36 Phase space ellipse in combination with a well aligned anti-parallel (+,+) double crystal monochromator. The monochromator defines an angular interval  $\theta_0$ . Note that this interval is invariant with shearing which has to be applied for obtaining the figure at different locations along the beam path Z. (See also Fig. 3.7).
- Fig. 3.37 Spectrum of the monochromator as shown in the insert decomposed into higher harmonics by solid state detector (SSD). Top: the harmonics are suppressed by maximizing the fundamental by small angular rotations of the Ge crystal; bottom: for comparison the spectrum obtained when maximizing the first harmonic. (From (3.206).)
- Fig. 3.38 Schematic of a double focusing mirror-crystal monochromator as it is applied for small angle diffraction from biological samples at SPEAR. (From (3.215-217).)
- Fig. 3.39 An ionisation chamber behind the exit slit of a grazing incidence monochromator is utilized to calibrate a secondary transfer standard diode. (From (3.223)).

- Fig 3.40 Part a) depicts the absolute photoelectric yield of evaporated Au and  $Al_2O_3$  at normal incidence. For comparison other experimental data are included. (Au: ■ Ref. 3.224a), ● Ref.3.224b)  $Al_2O_3$ : dashed line Ref.3.225, ■ Ref.3.224c)). Part b) shows the yield of CsJ and LiF. (CsJ: ■ Ref 3.22d, ● Ref 3.224b), LiF: ● Ref 3.10 p.227, x Ref 3.224b))(After (3.223))
- Fig 3.41 The normalized photoyield of in situ evaporated Au is seen vs. angle of incidence. For high photon energies it can be approximated by a secans  $\theta$  dependence (dashed line). At low photon energies refraction effects dominate and the secans  $\theta$  law is not valid.
- Fig 3.42 a) The multiplication of electrons in a continuous dynode multiplier is shown. b) The absolute detection efficiency of a  $MgF_2$  coated and an uncoated channeltron is plotted vs. photon energy. (From (3.228))
- Fig. 3.43 Spherical drift chamber ( 3.251) in principle. The negative charges produced by the photon at its conversion point drift to one point at the multiwire detector at the bottom irrespective of where along its path the photon is converted. (From (3.7).)
- Fig 3.44 Experimental arrangement to measure the VUV absorption of metal vapors. P-liquid sample,SI-Synchrotron radiation, F-window, Sv-rotatable beam stop, S-Ta boat, H-heating tube (Ta), W-heat-baffle(w), M-heat baffle (Mo), V-heat baffle stainless), T-vacuum system (After (3.258)).
- Fig 3.45 An experiment to study luminescence excitation in the VUV. For abbreviations see text (After (3.263)).

- Fig 3.46 An experiment to investigate the photoemission of solids with excitation in the VUV (After [3.19])
- Fig 3.47 Schematic of the time of flight spectrometer for photoelectron energy analysis (From [3.26])
- Fig 3.48 Layout of an experiment to calibrate VUV transfer standards with synchrotron radiation (From [3.27]).
- Fig. 3.49 Principle of the energy-dispersive x-ray diffraction method,  $S_1$ ,  $S_2$  collimators, D semiconductor detector. For one measurement the scattering angle  $2\theta_0$  remains fixed. (From (3.283).)
- Fig. 3.50 Manganese powder patterns obtained by energy dispersive diffraction showing a phase transformation. The temperatures are indicated at the spectra. Each spectrum was obtained in 300 sec at DESY. (From (3.285).)
- Fig. 3.51 Laue interferometer. SR is monochromatized by a double crystal groove-cut crystal. The Laue interferometer is cut from a single crystal consecutively splitting the beam, joining it again and finally superimposing it for interference. A wedge serves to produce interference fringes. The sample material is inserted only halfway into one of the beams.
- Fig. 3.52 X-ray reflection topograph of ferromagnetic domains in terbium below the Curie temperature of 222 K obtained at NINA, 4 GeV, 4 mA, 3 minutes exposure,  $3\bar{1}\bar{2}1$  reflection. Domain walls run horizontally, i.e. perpendicular to the  $c$  axis. (From (3.290).)
- Fig. 3.53 Schematic drawing of the triple-crystal spectrometer for standing wave excited fluorescence. Shown are two settings for different energies. (From (3.296).)

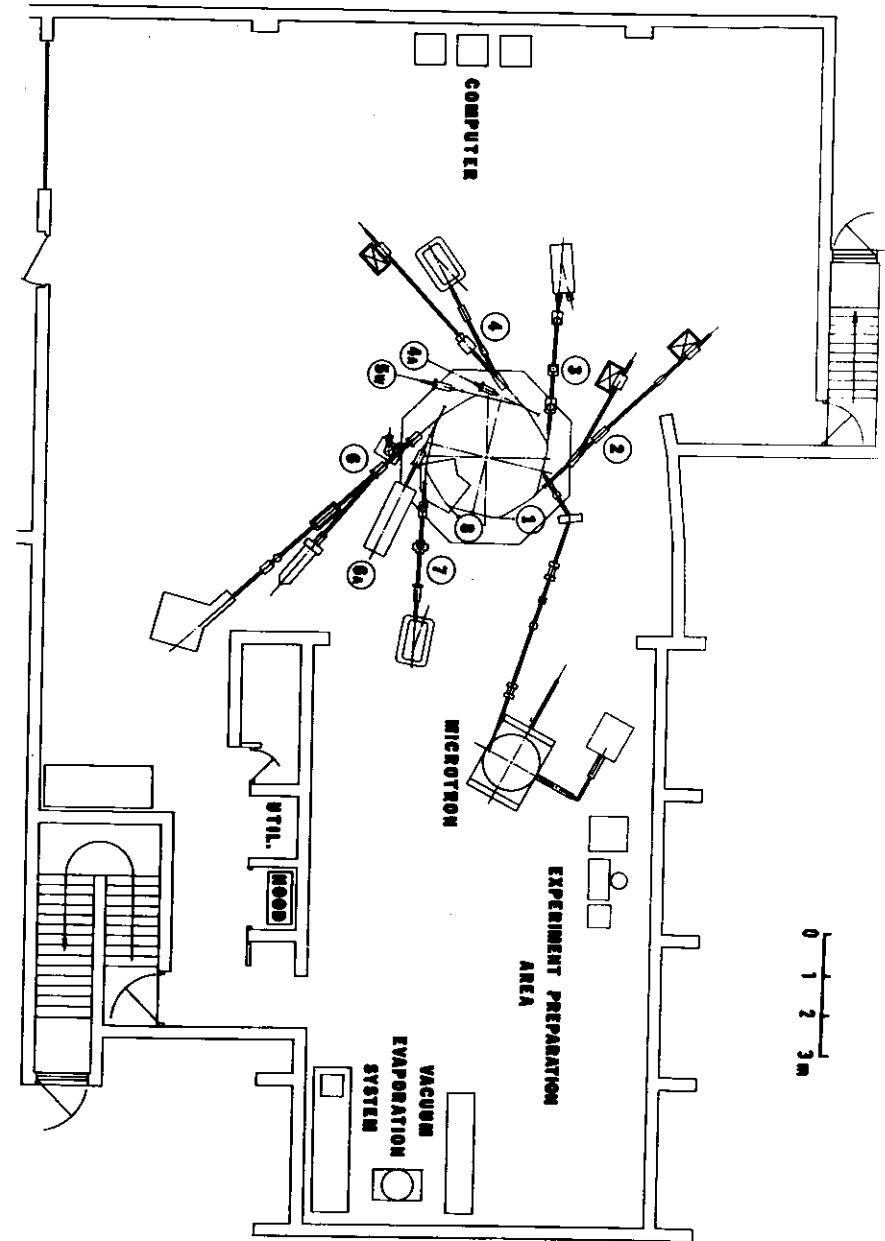


Fig. 3.1a)



Fig. 3.1b)



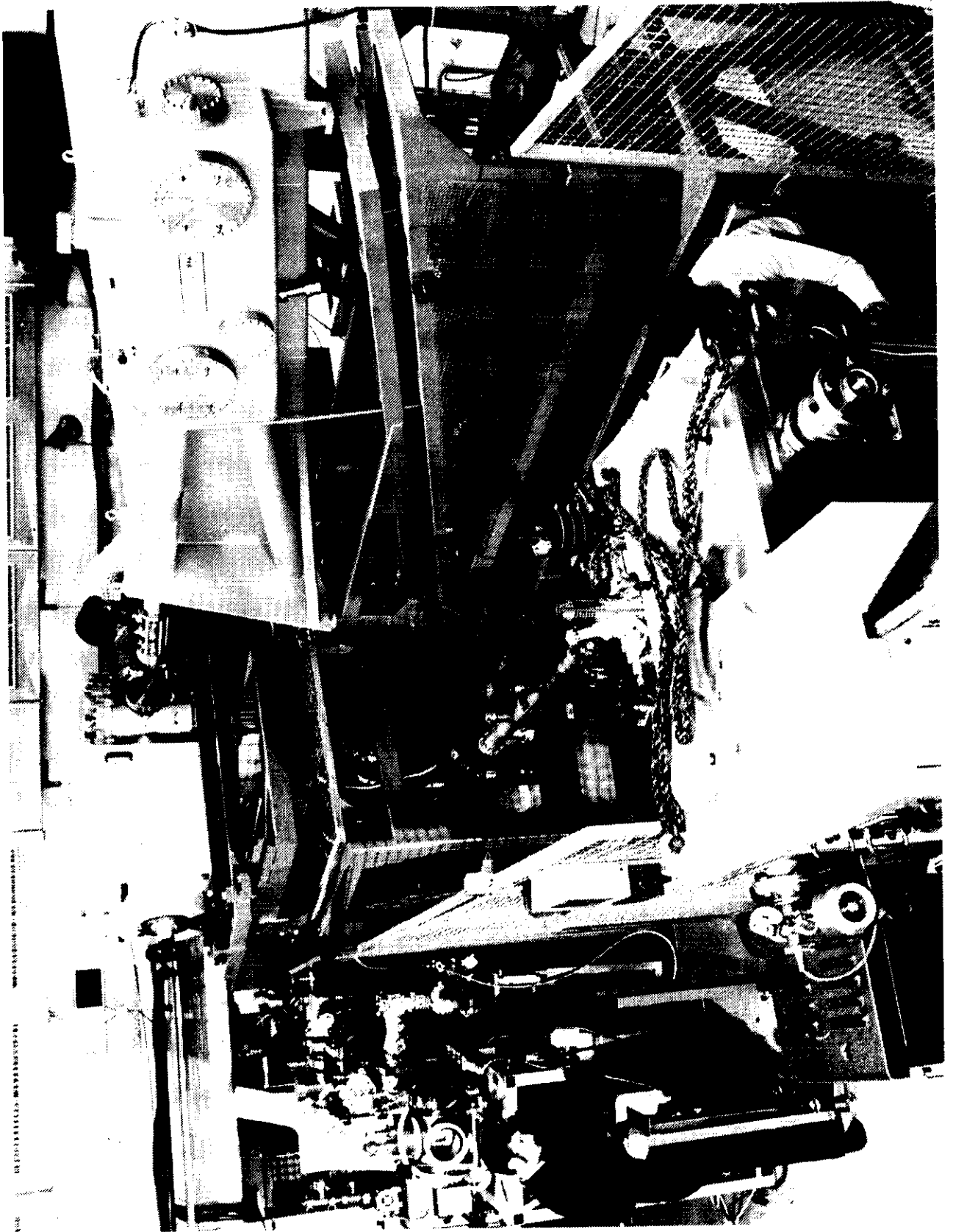


Fig. 3.2b)

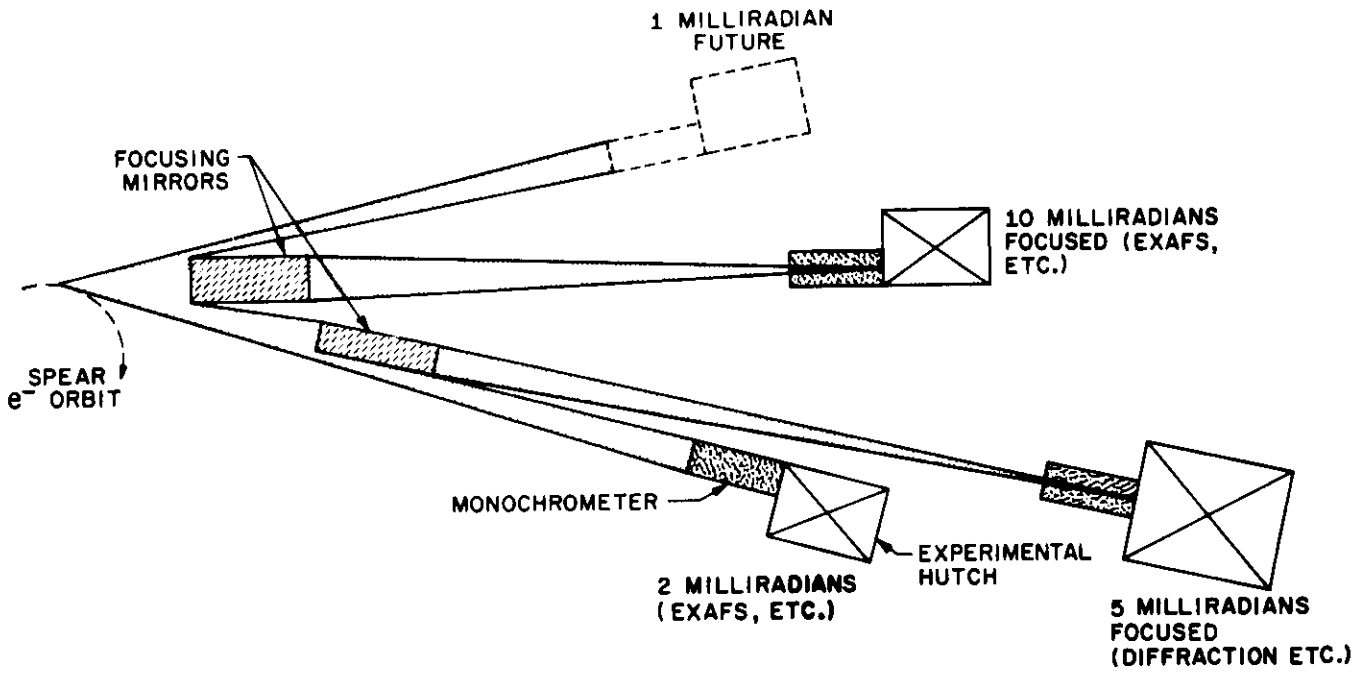


Fig. 3.4

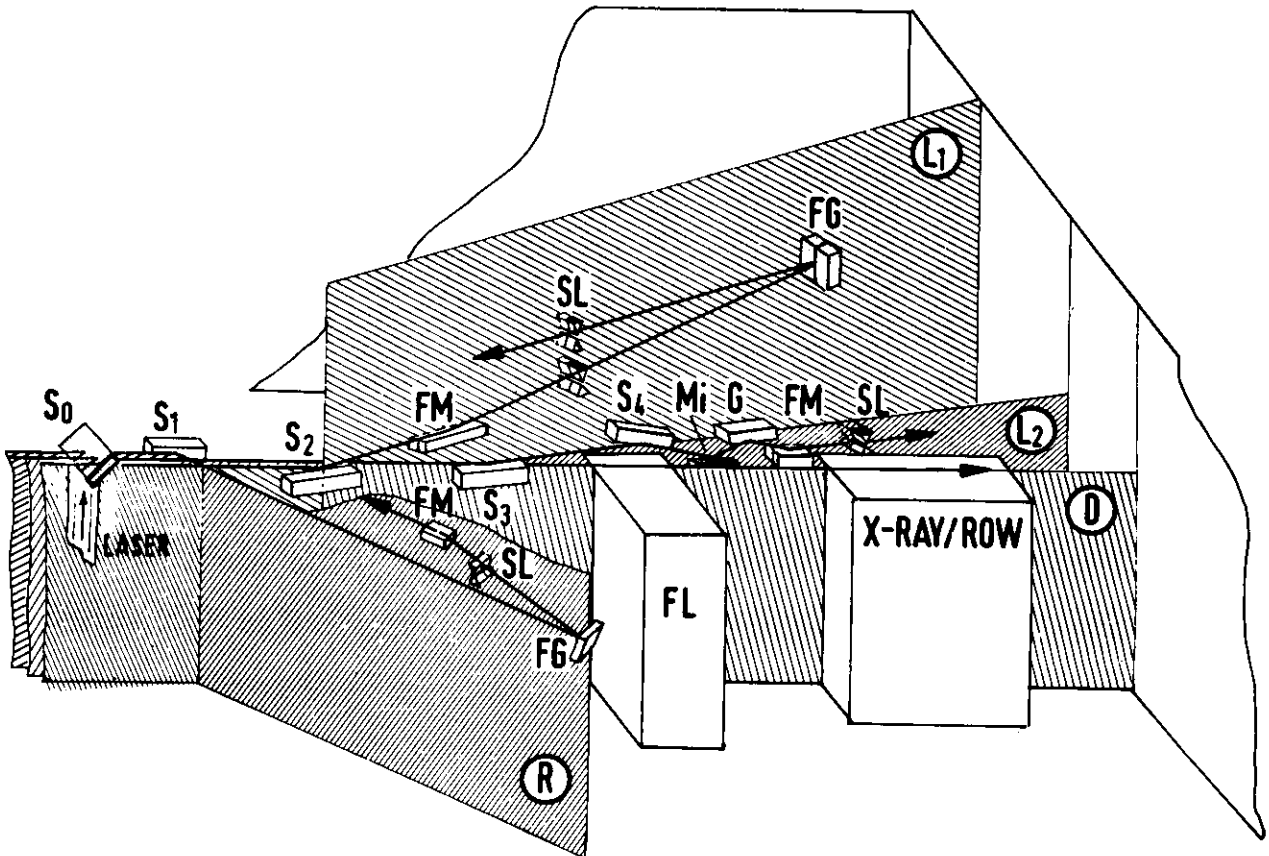


Fig. 3.3

- 148 -

- 147 -

27480

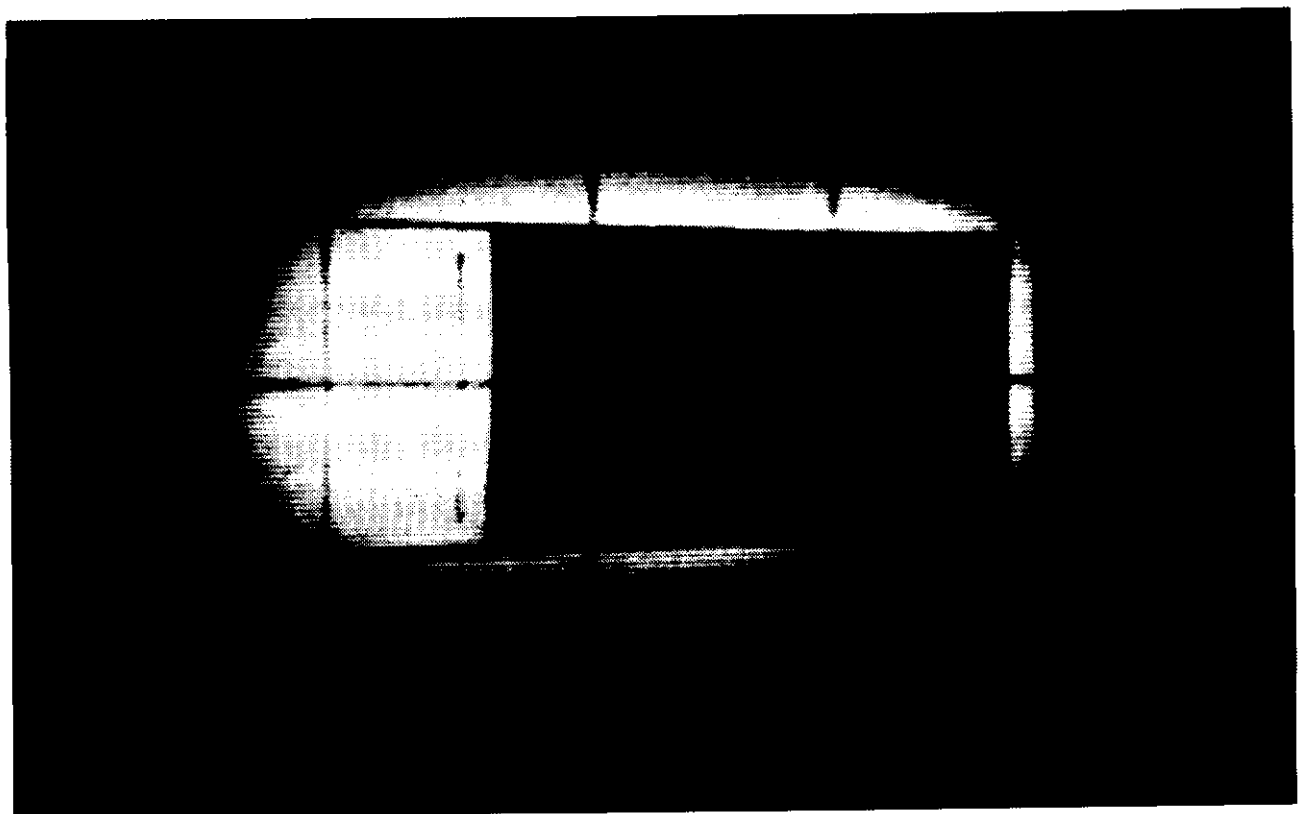
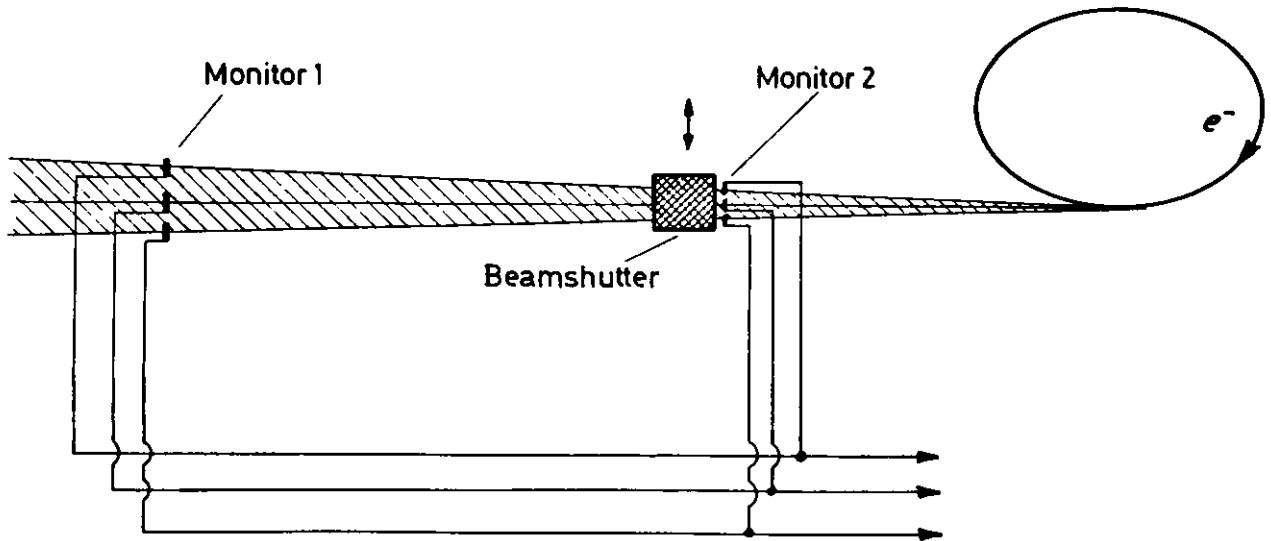


Fig. 3.5

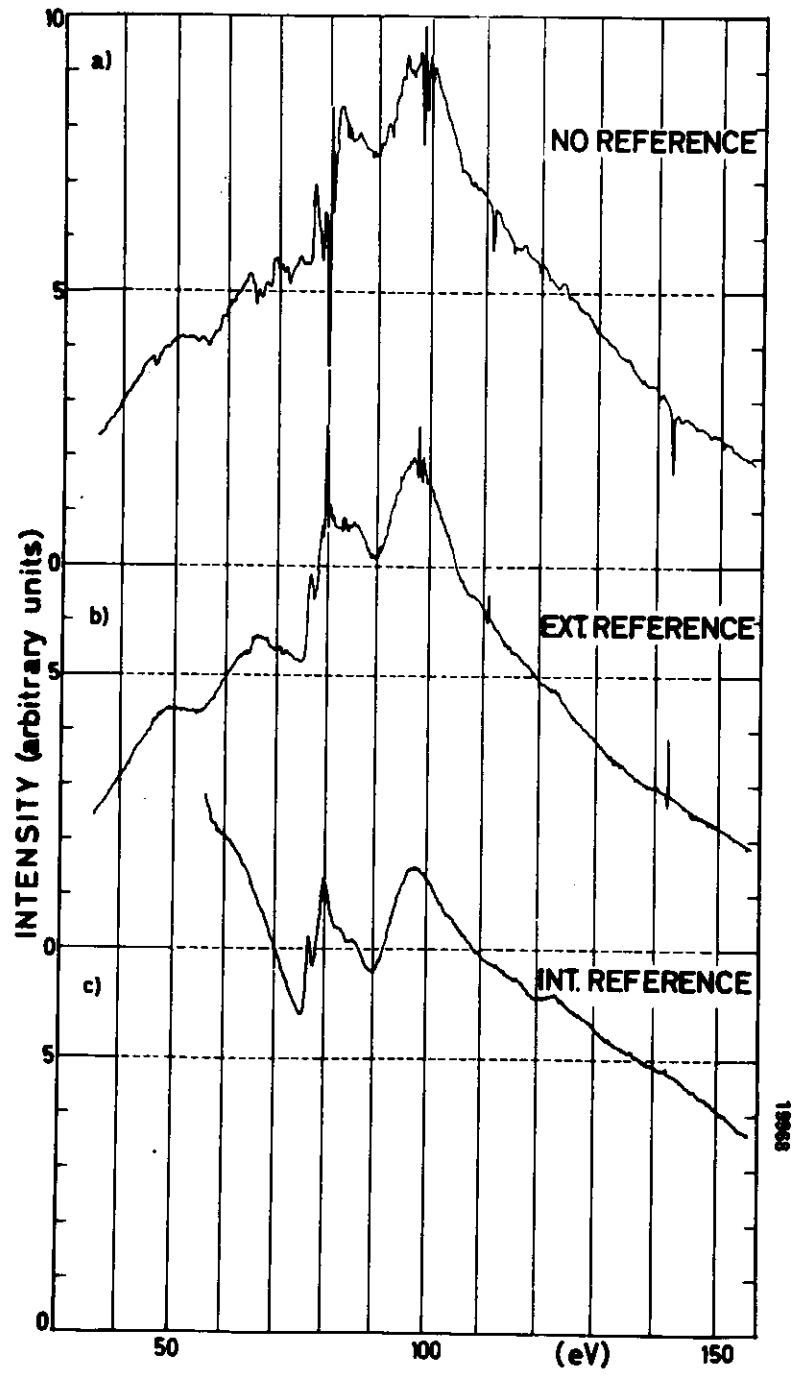


Fig. 3.6

27487

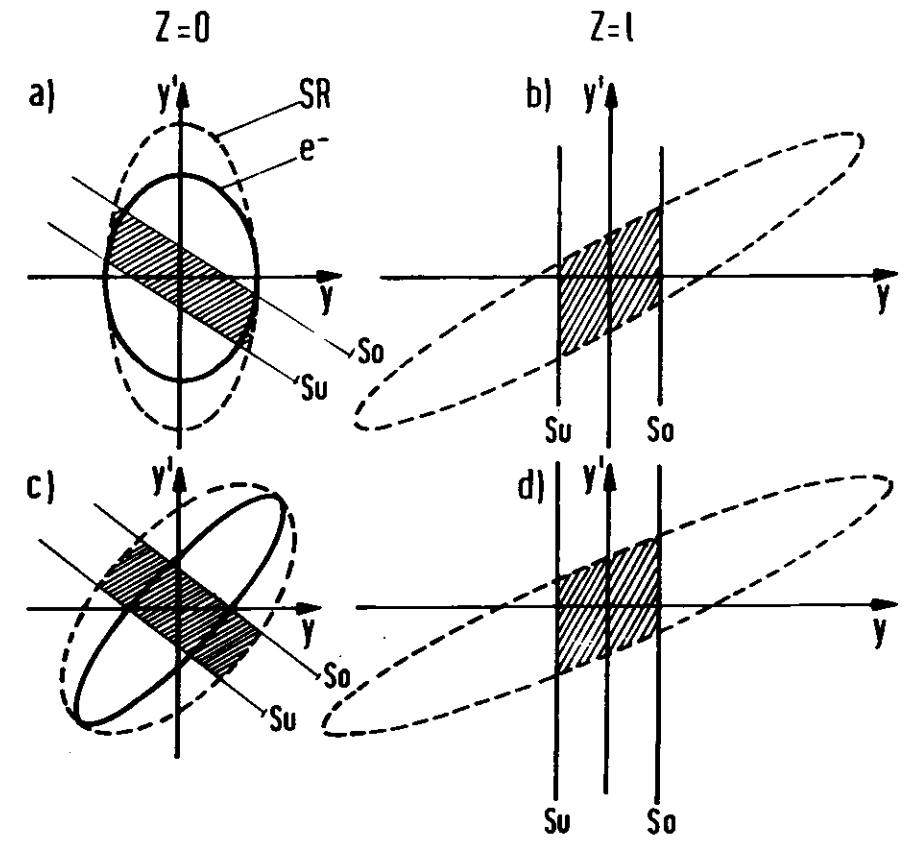


Fig. 3.7

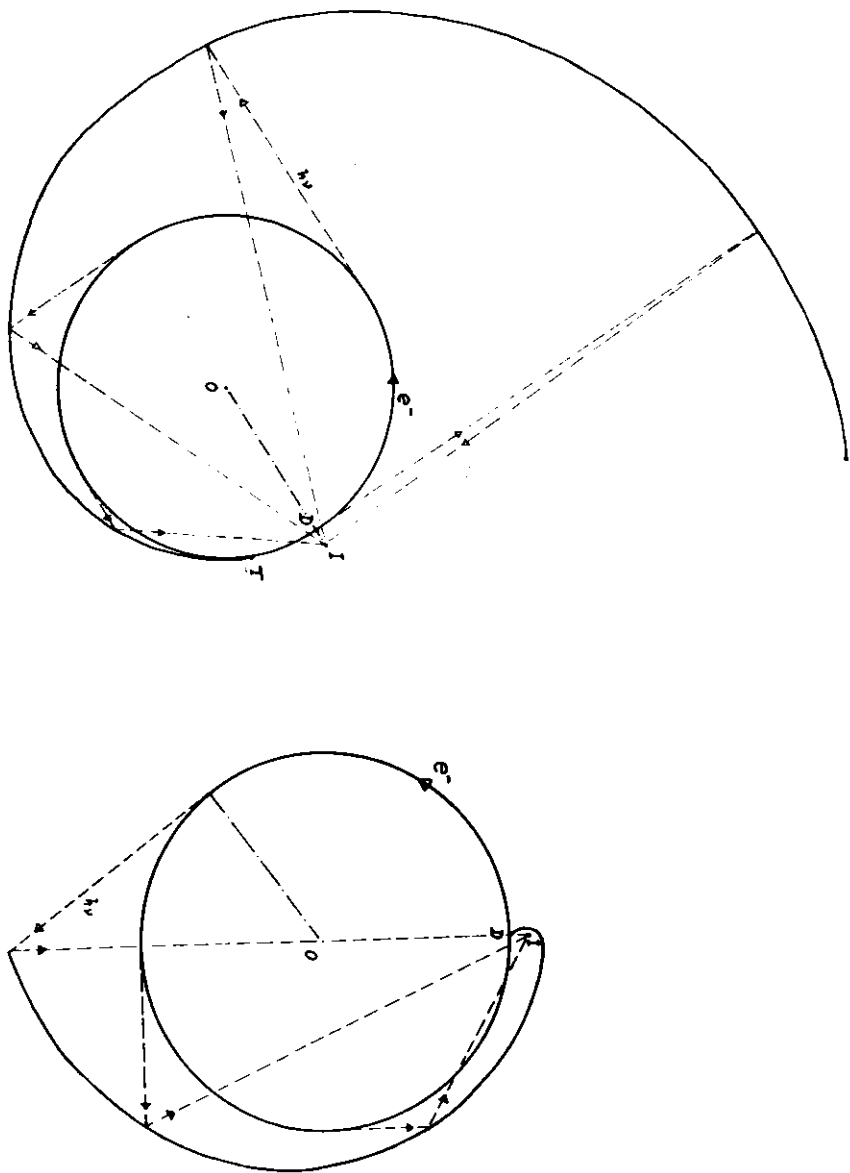


Fig. 3.8

27A23

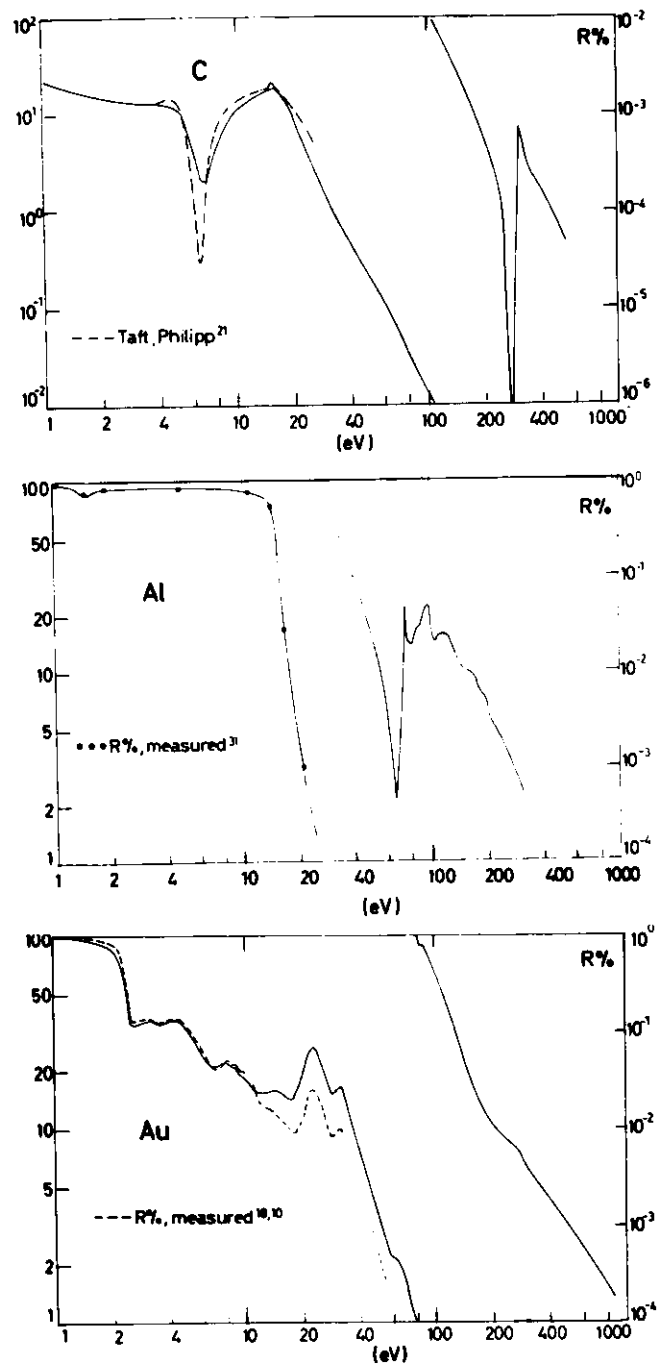


Fig. 3.9

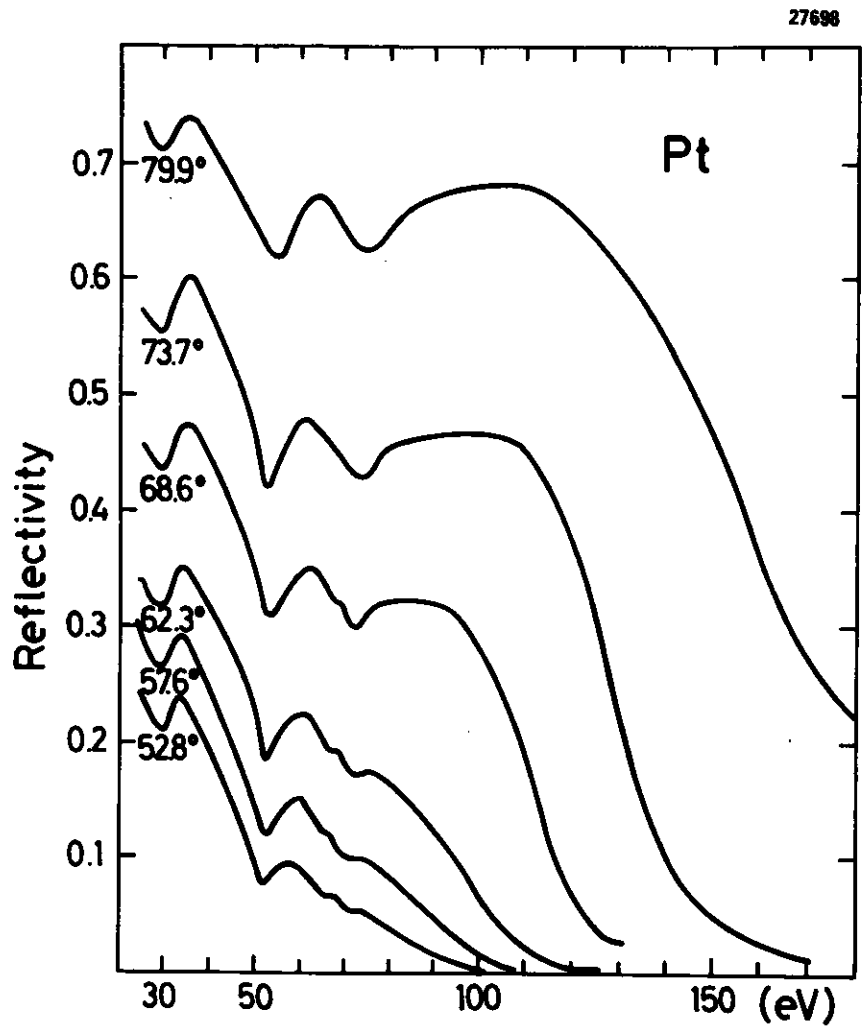


Fig. 3.10

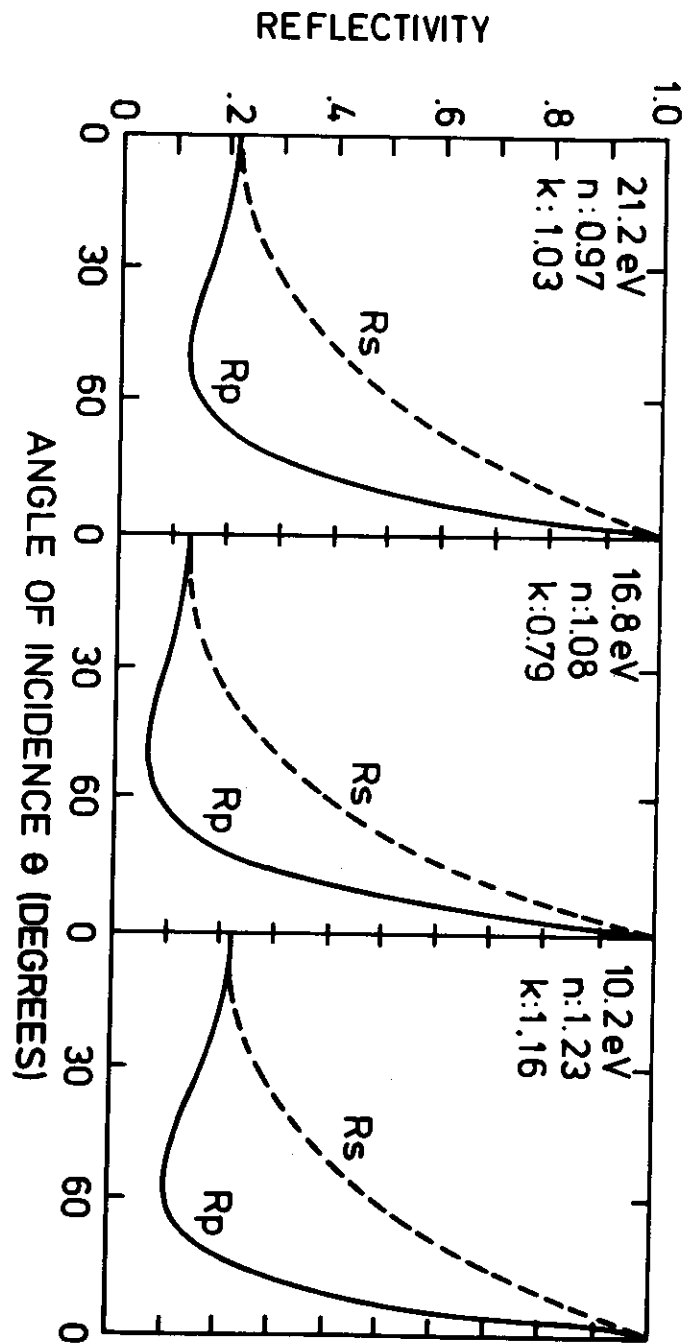


Fig. 3.11

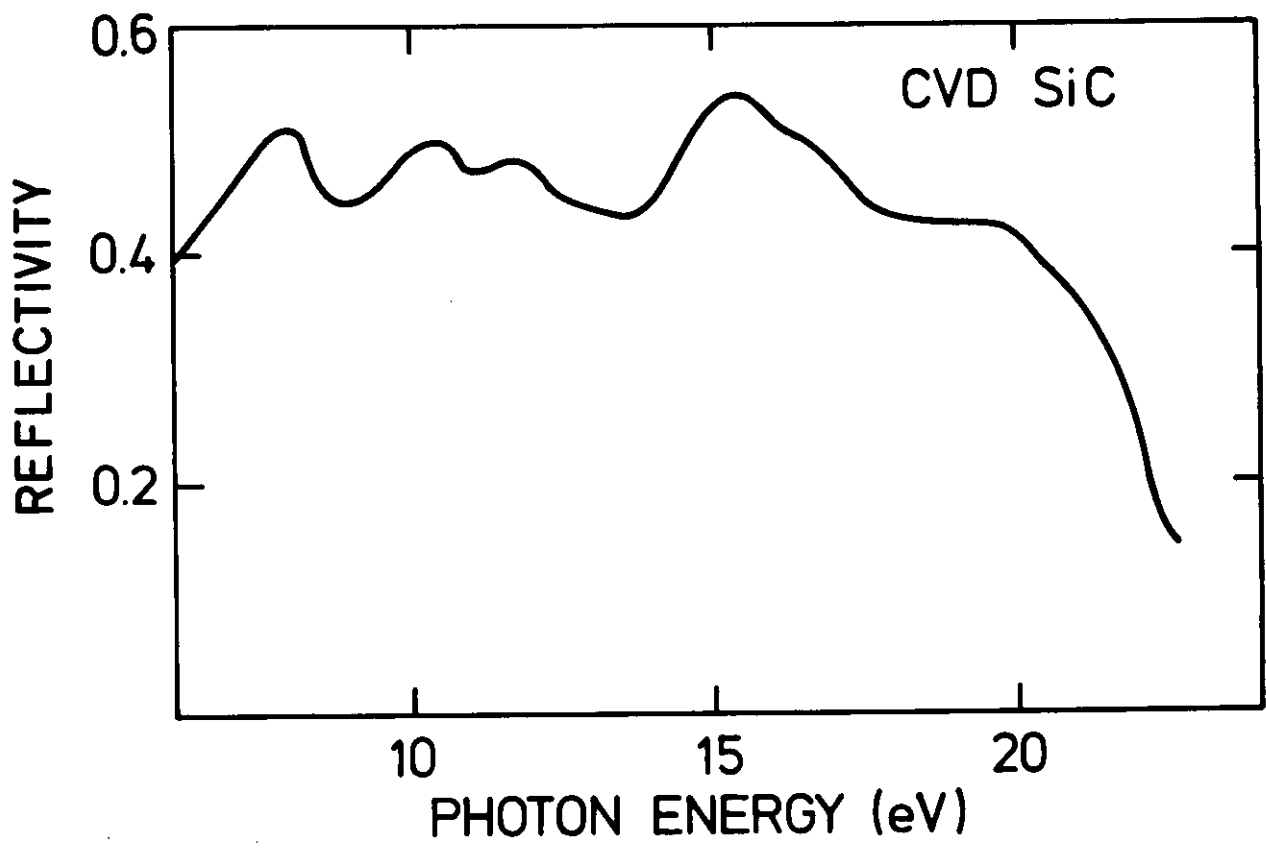


Fig. 3.13

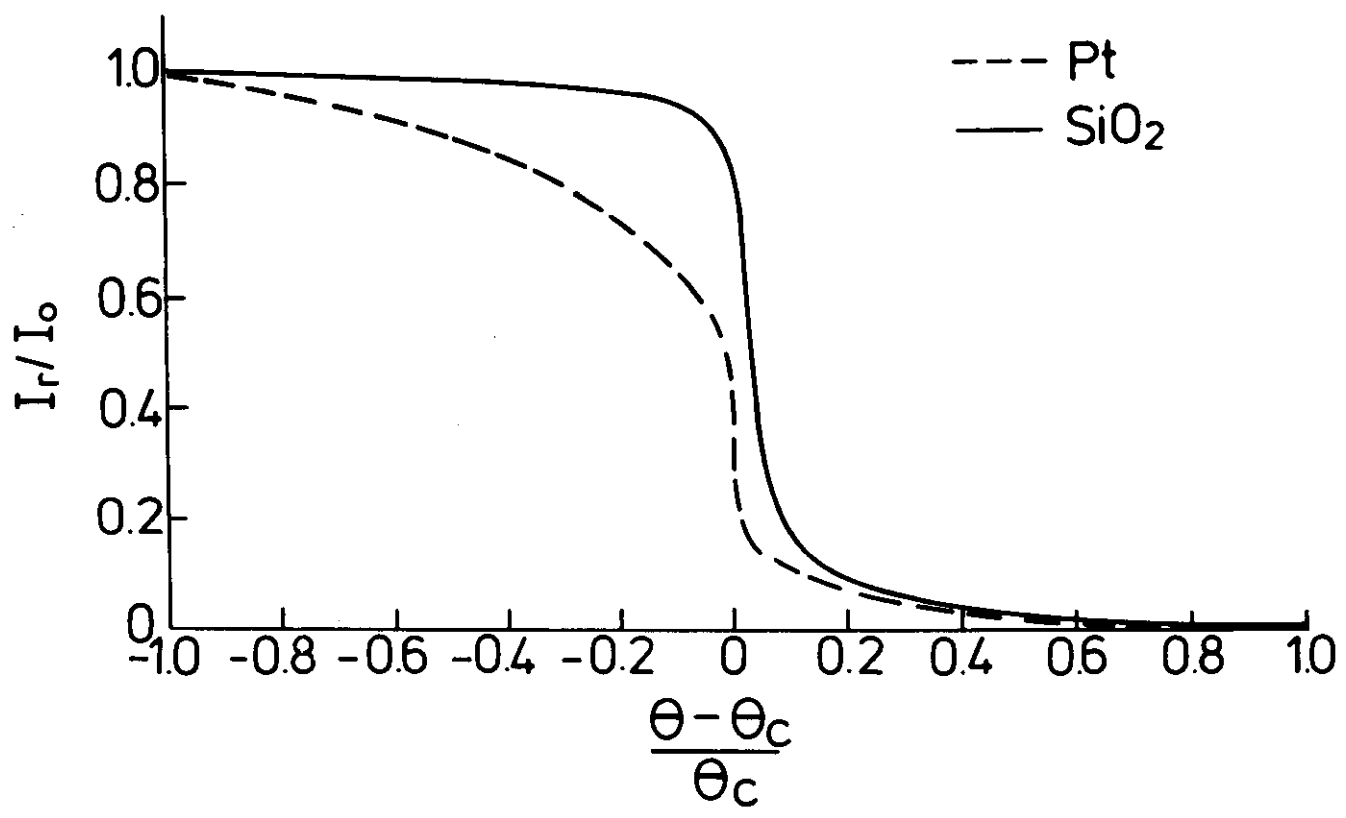


Fig. 3.12

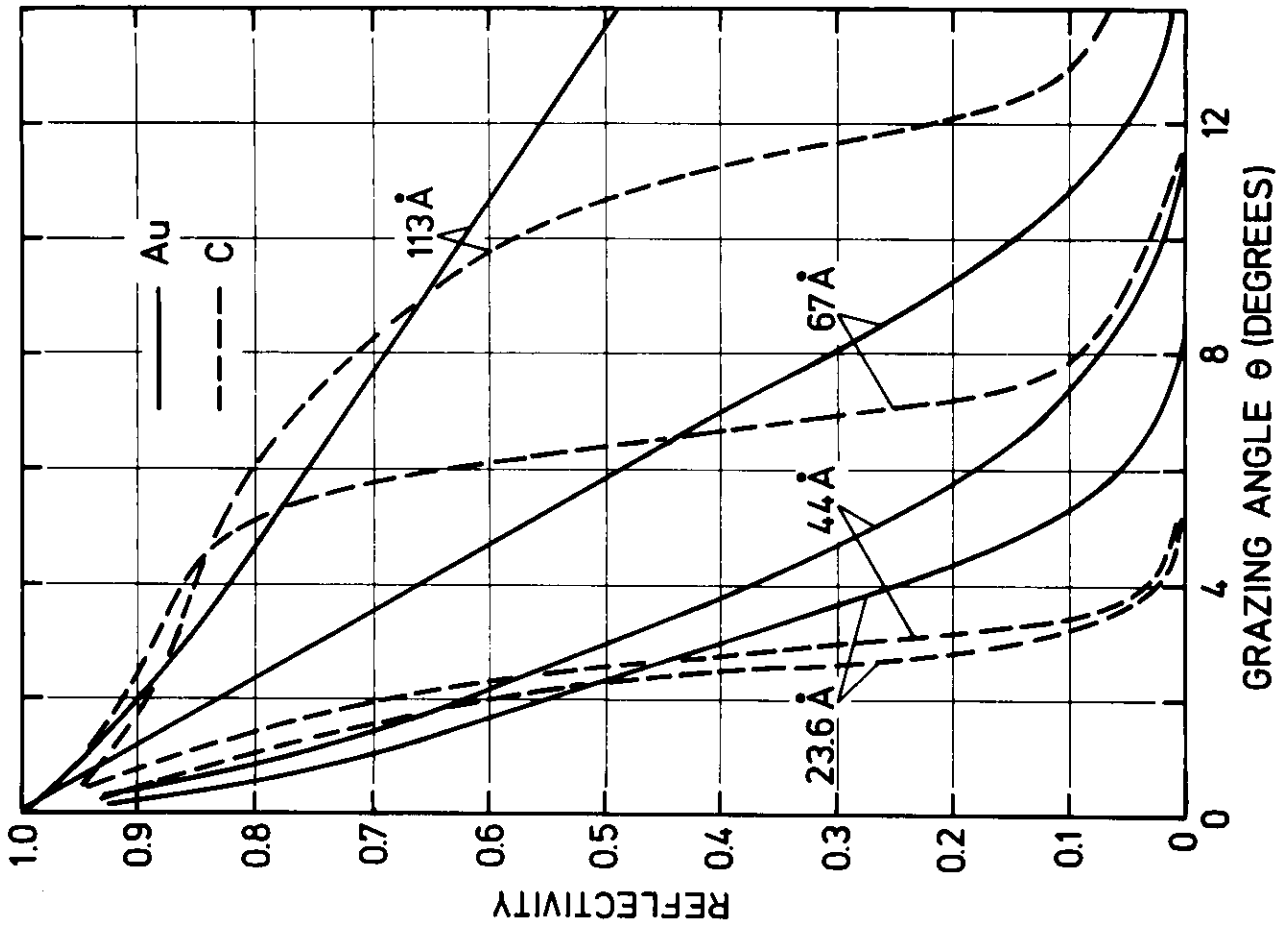


Fig. 3.15

24375

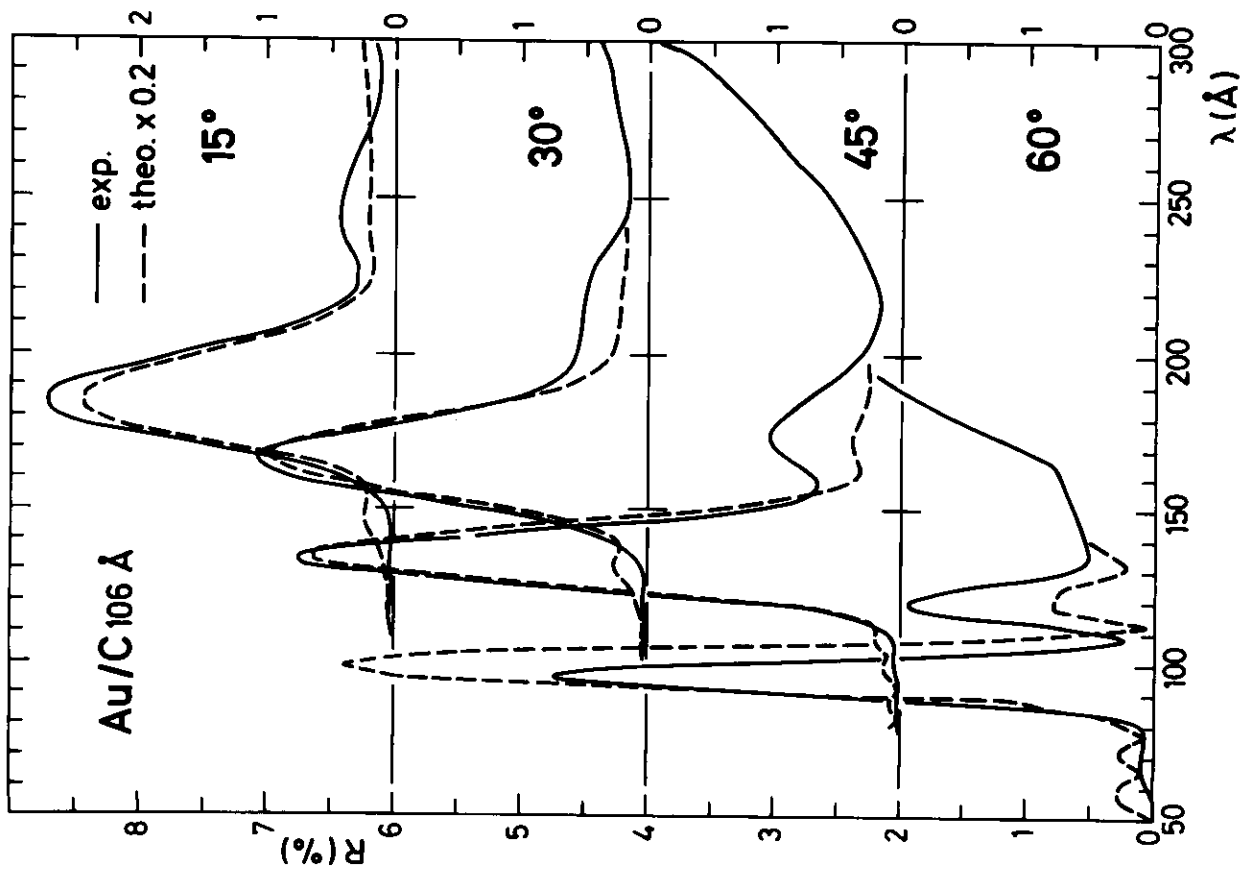


Fig. 3.14

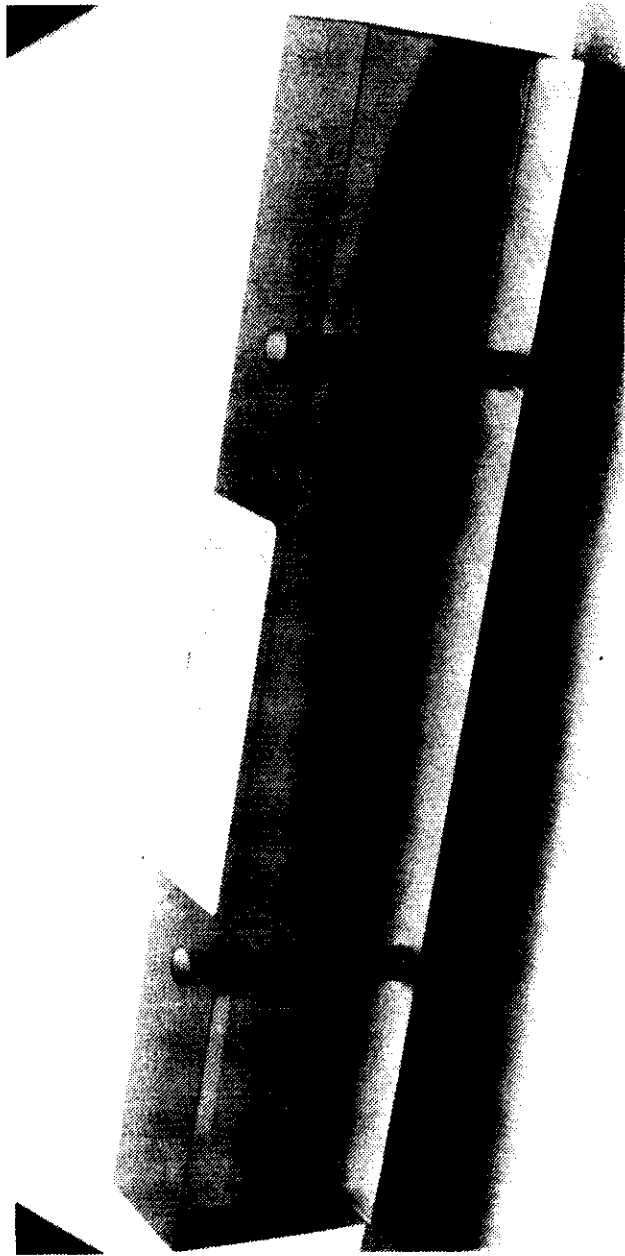


Fig. 3.16

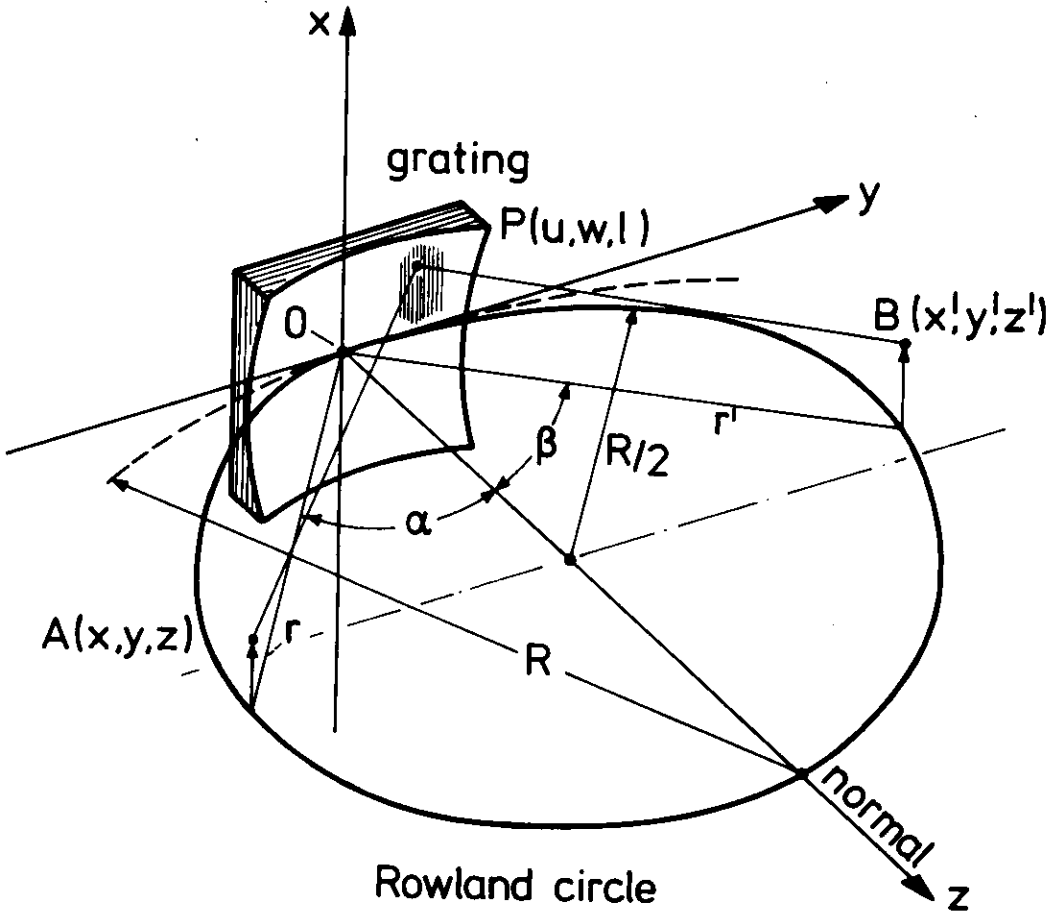


Fig. 3.18

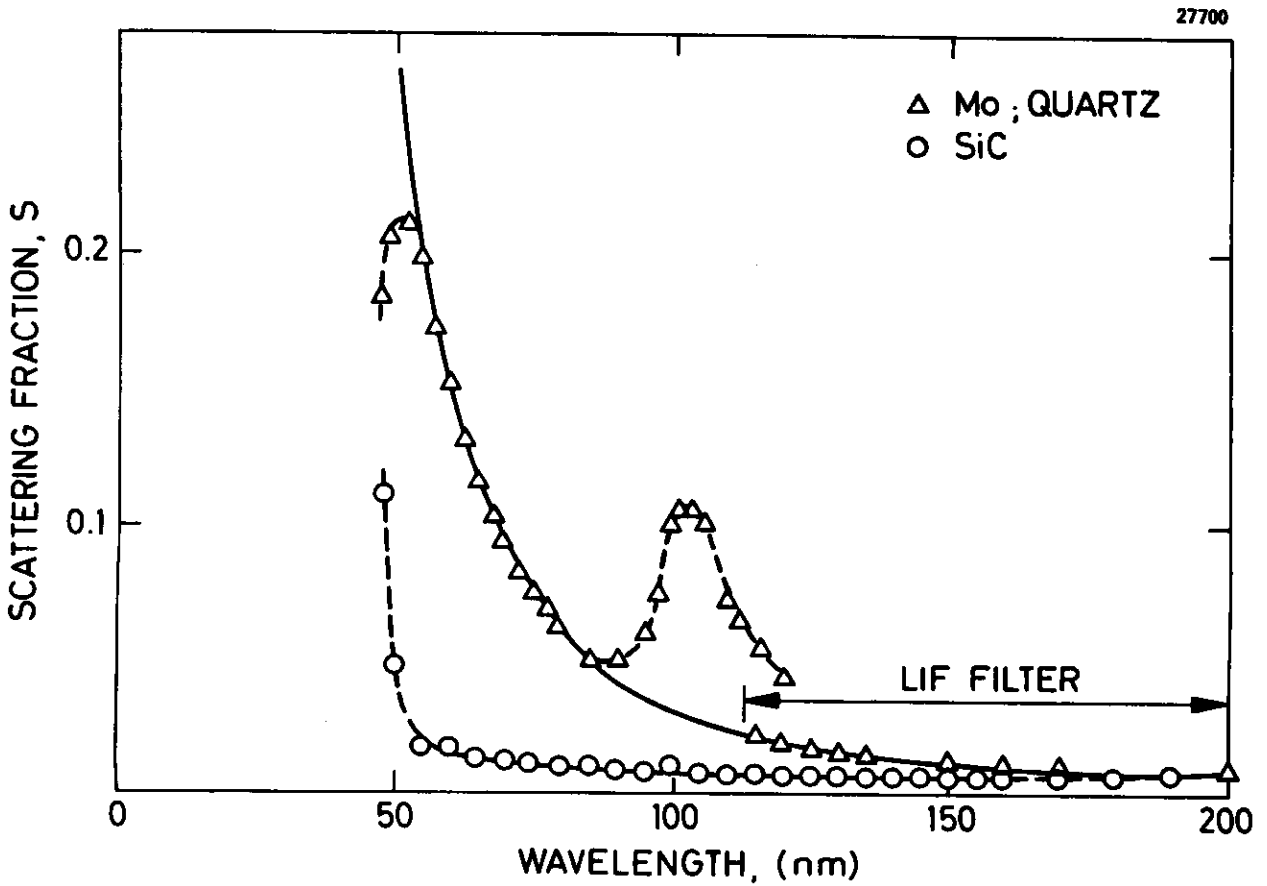


Fig. 3.17

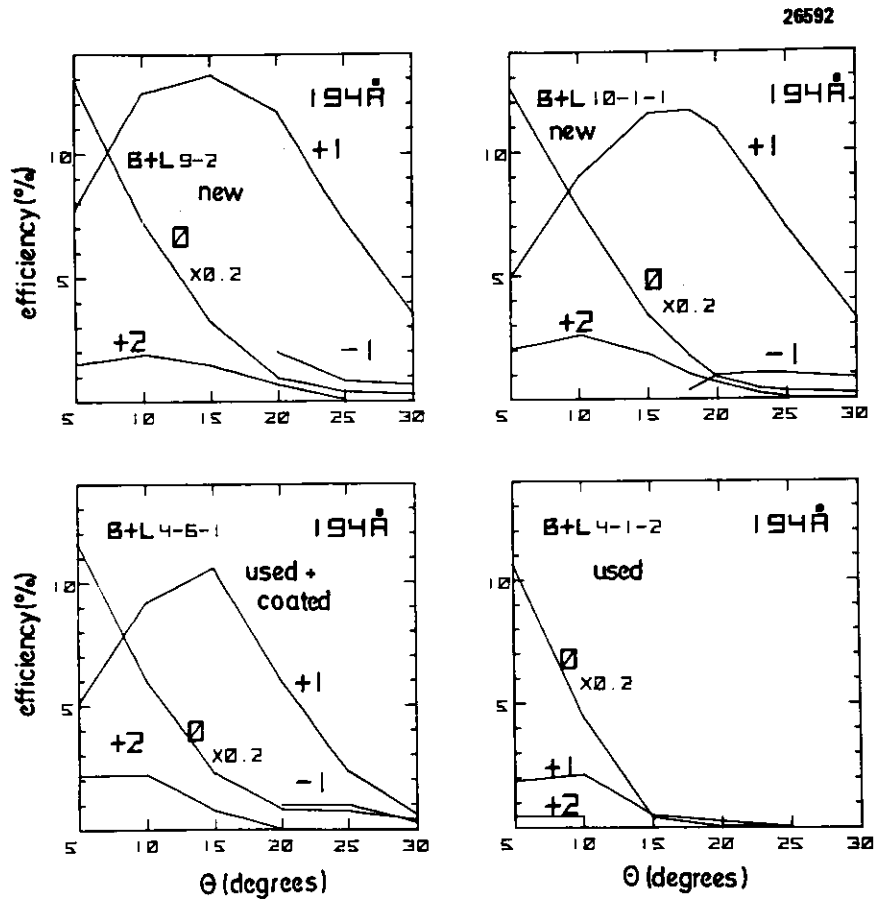


Fig. 3.19

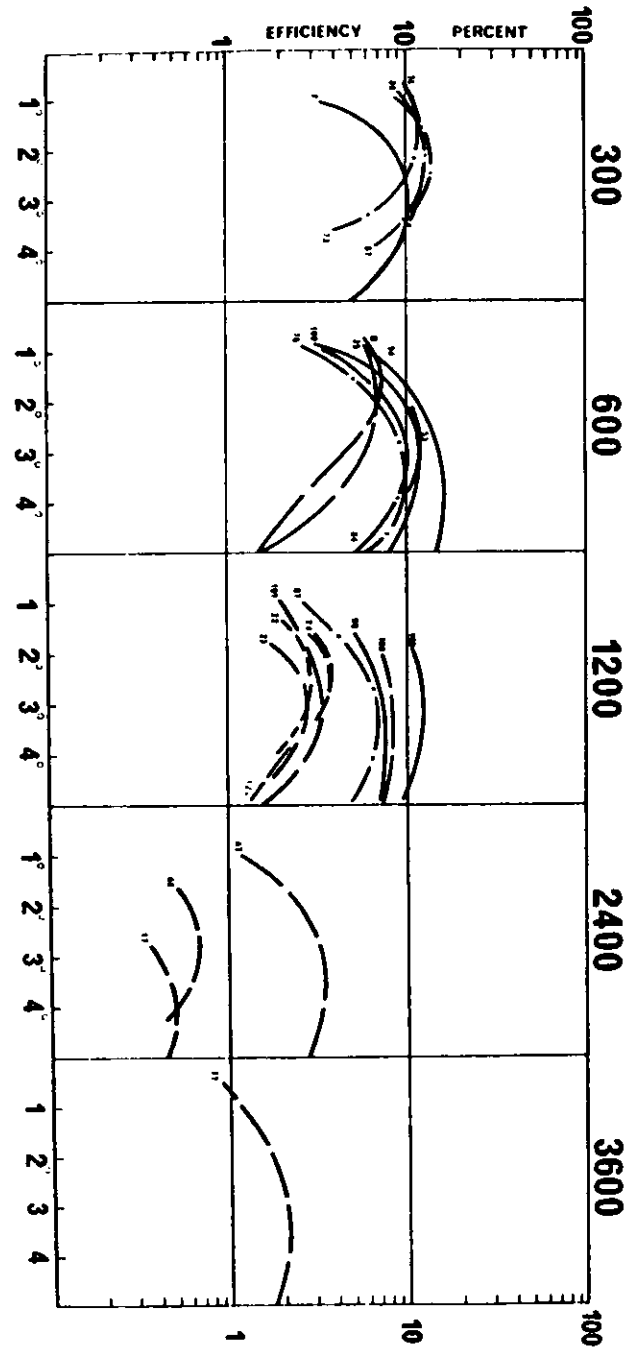


Fig. 3.20

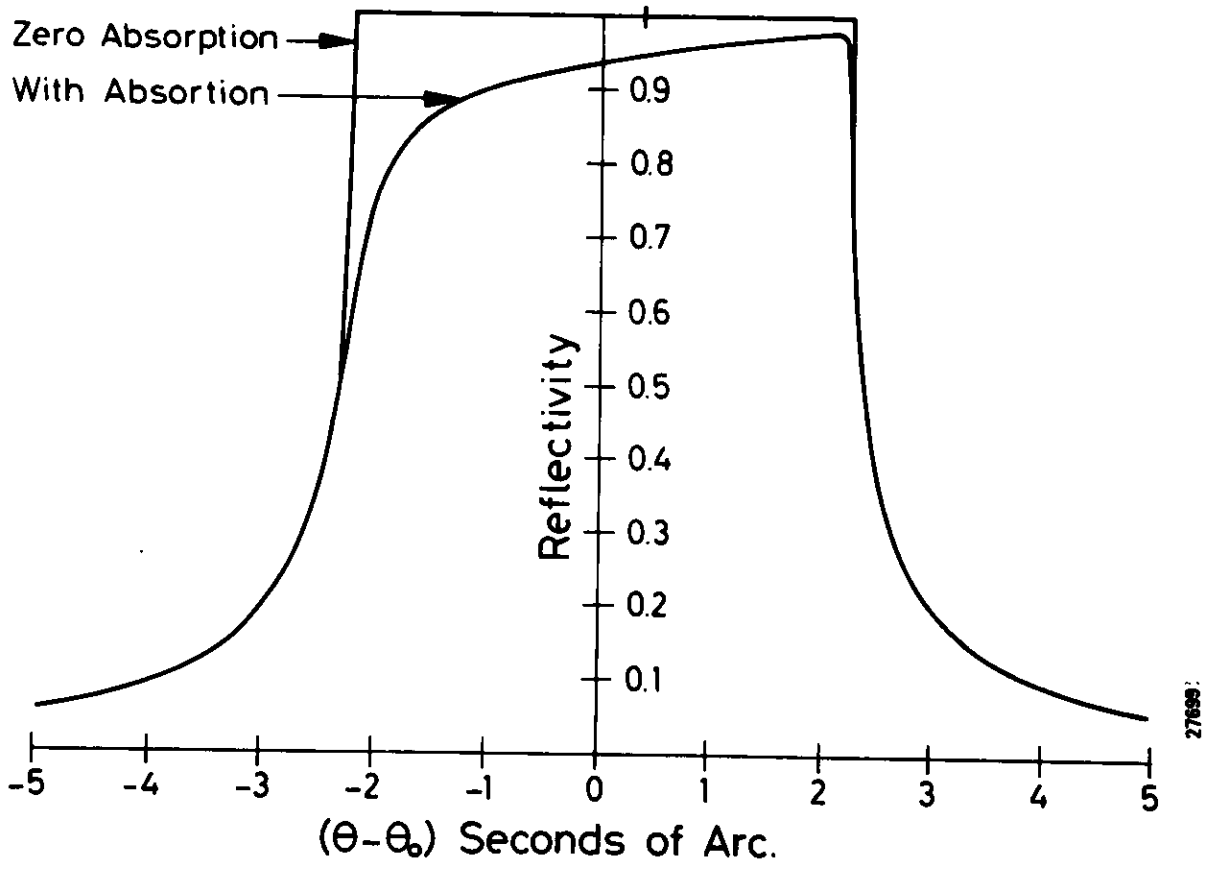


Fig. 3.22

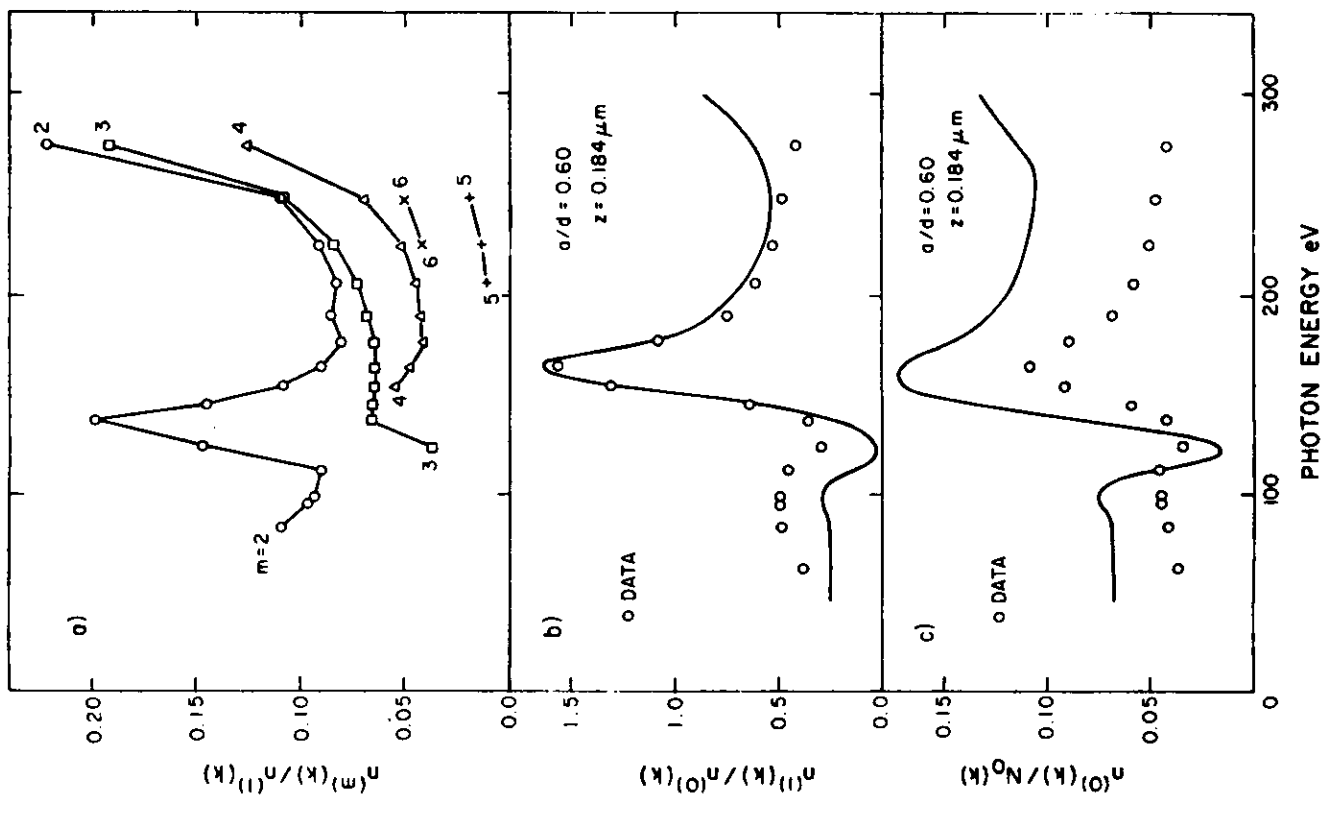


Fig. 3.21

27486

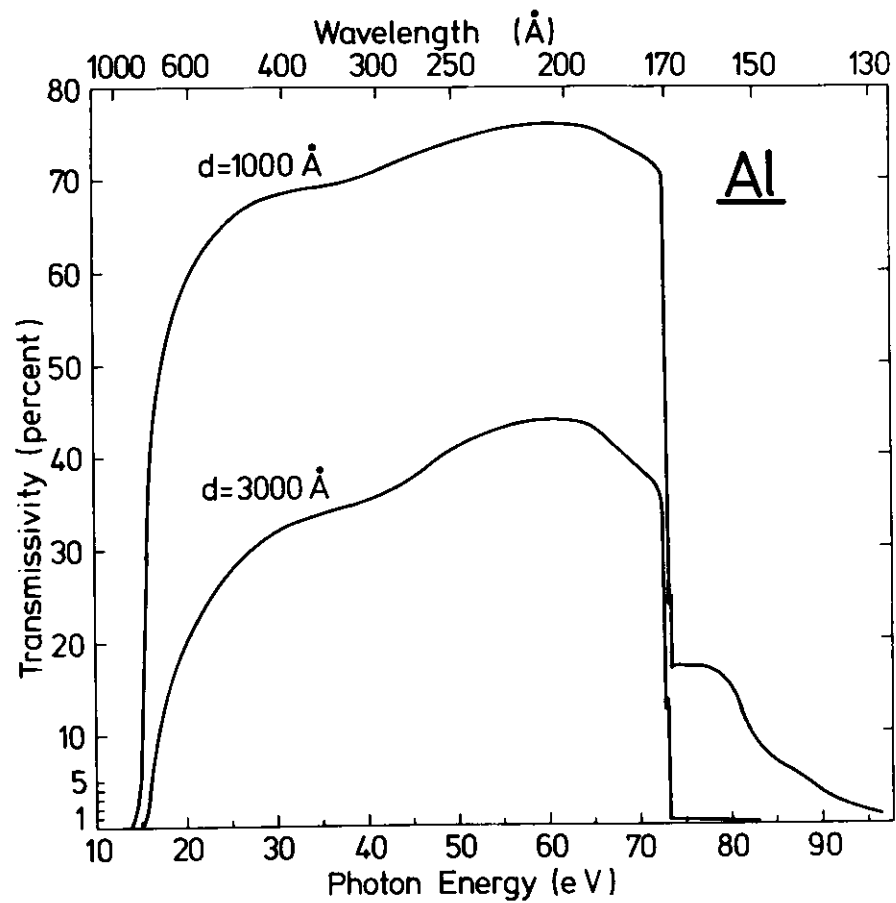
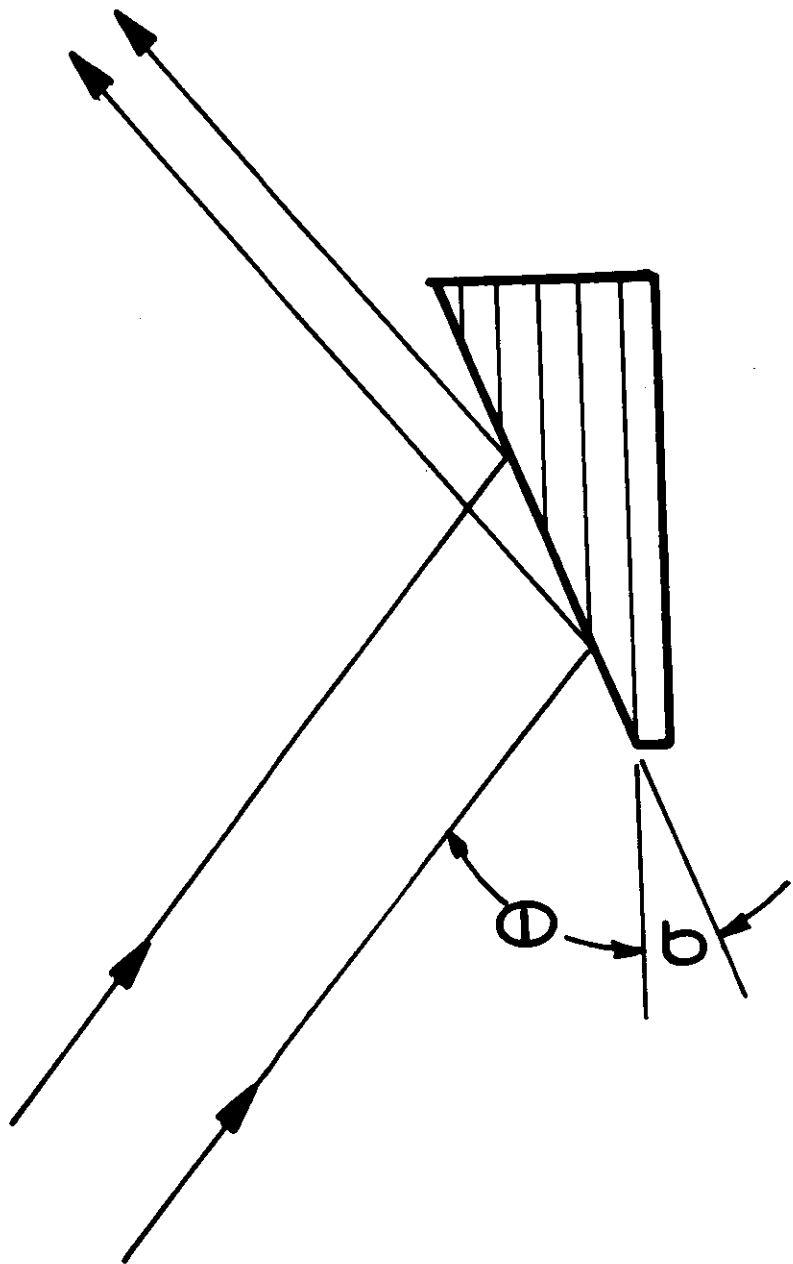


Fig. 3.24

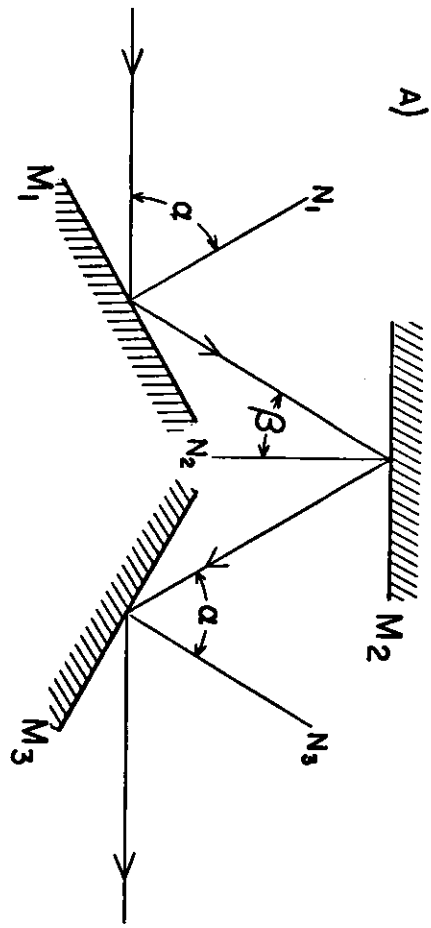


Fig. 3.25 a)

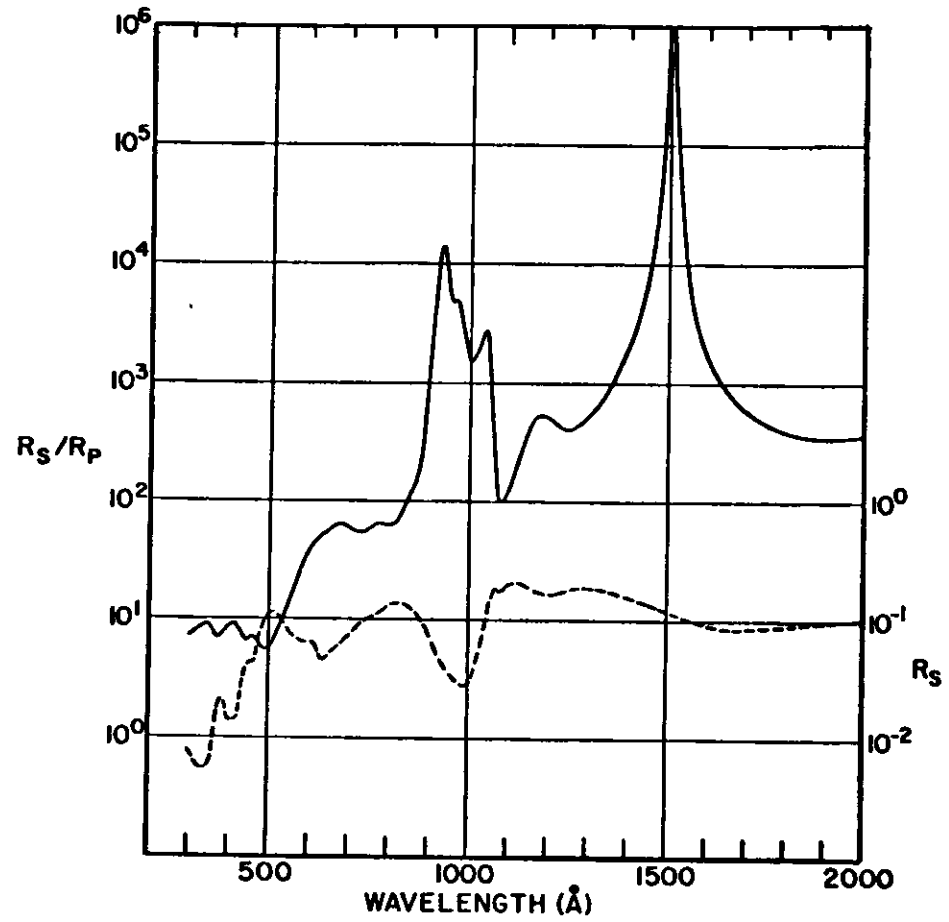
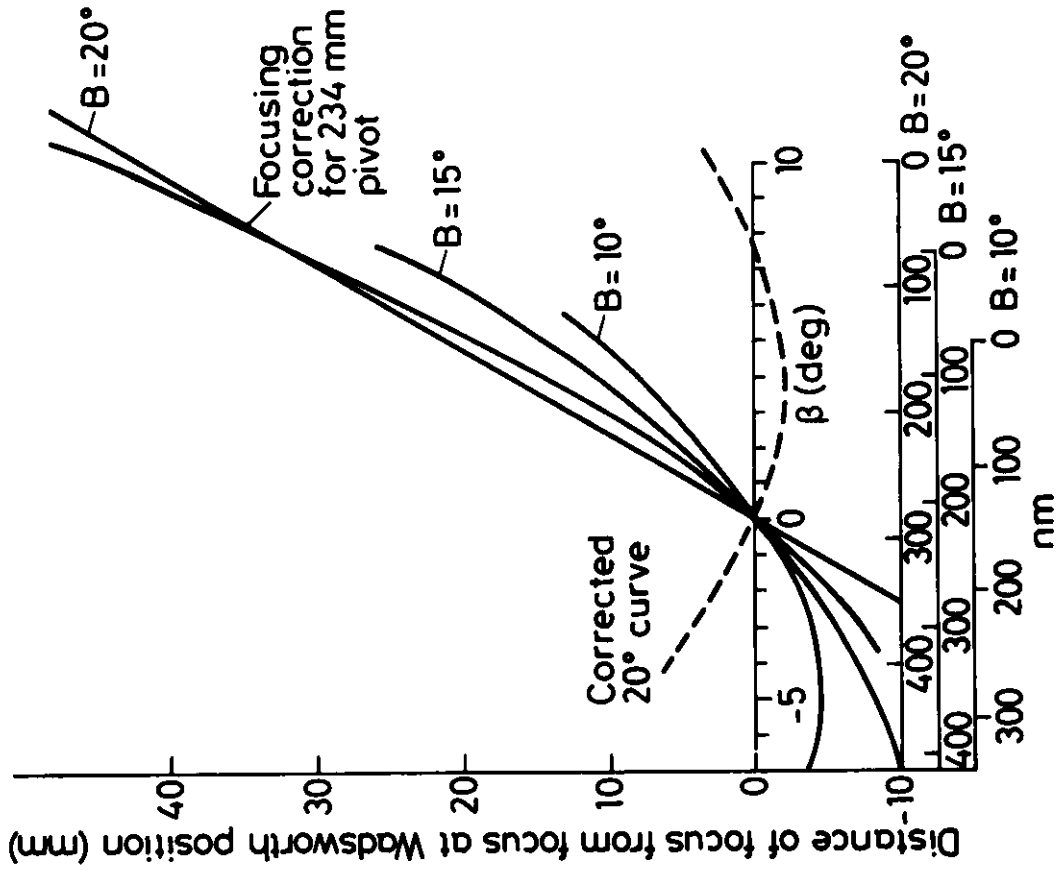


Fig. 3.25 b)

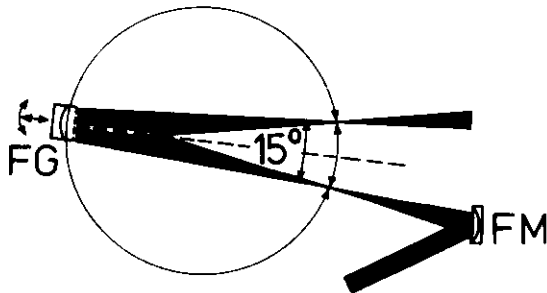
27701



27598

### Normal Incidence Monochromators

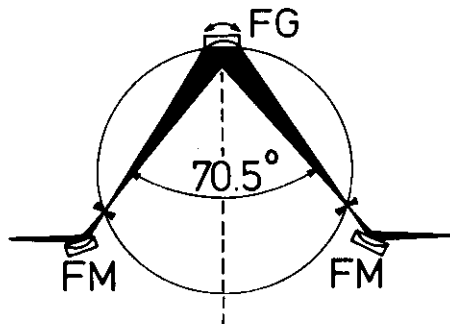
a) Mc Pherson Normal Incidence



c) Modified Wadsworth



b) Seya-Namioka



d) Higher Order Focusing

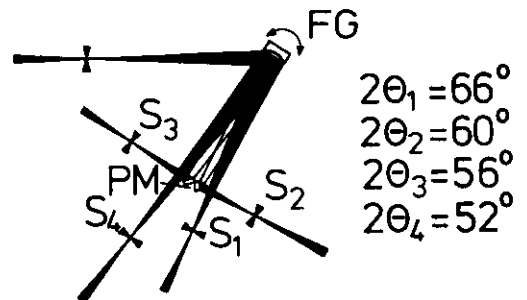


Fig. 3.27

Fig. 3.26

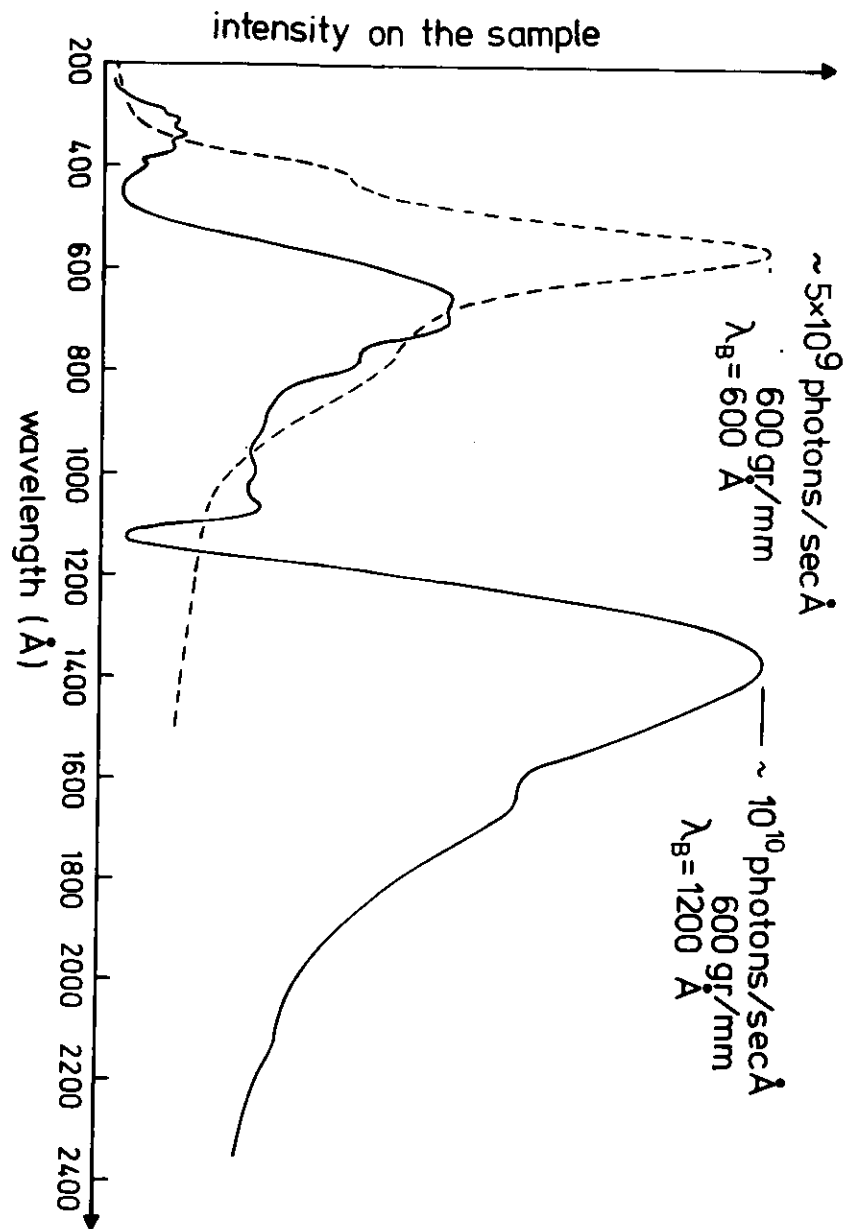


Fig. 3.28

### Plane Grating Monochromators

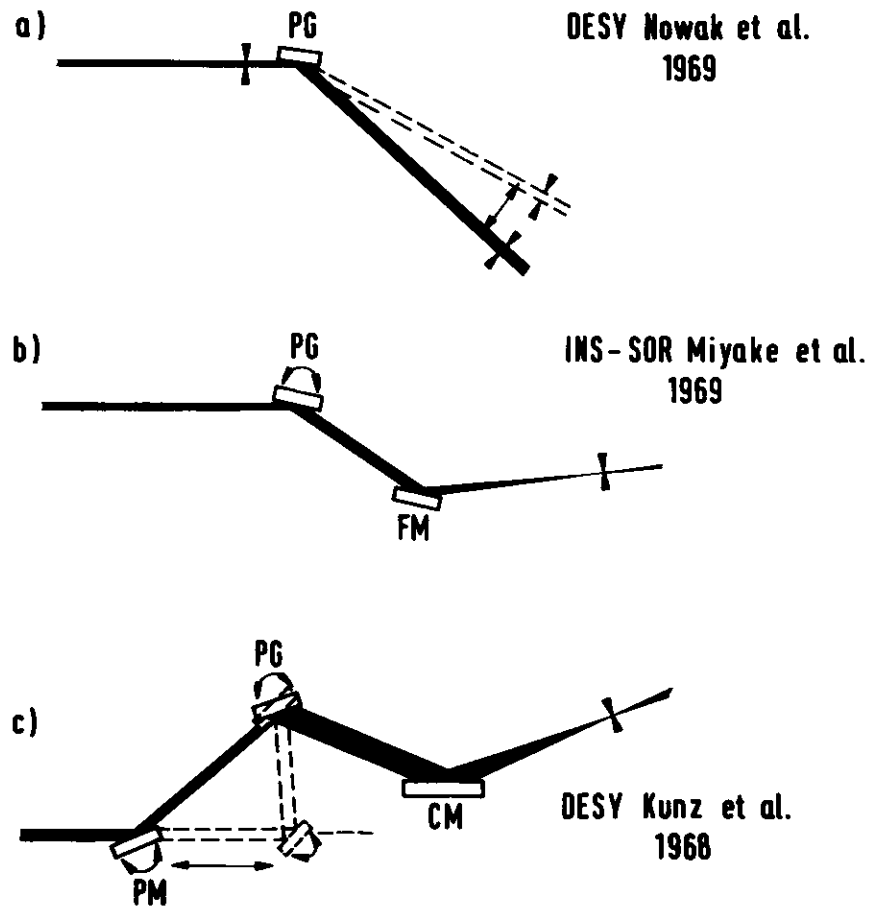


Fig. 3.29

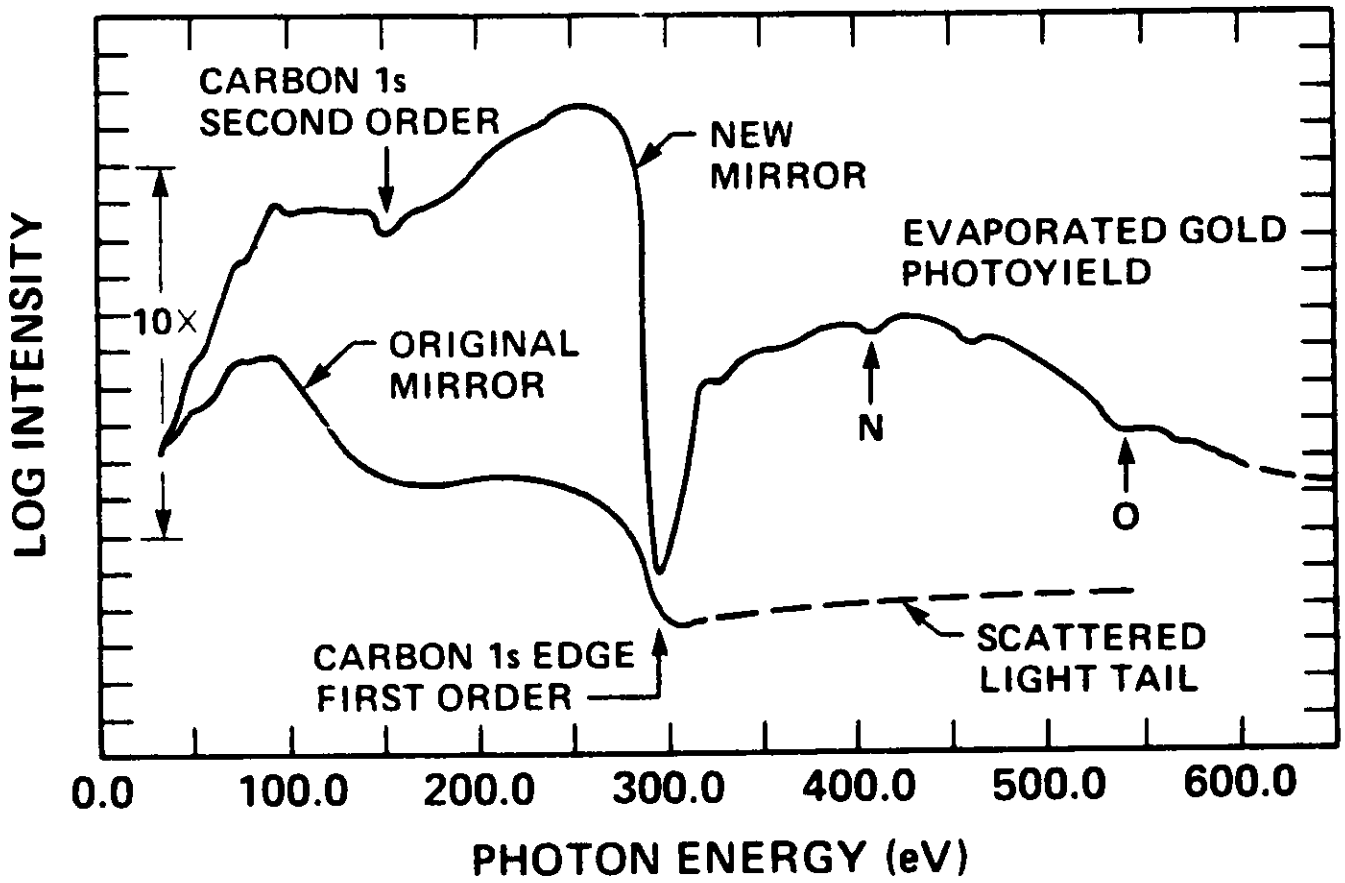


Fig. 3.31

27597

### Rowland Monochromators

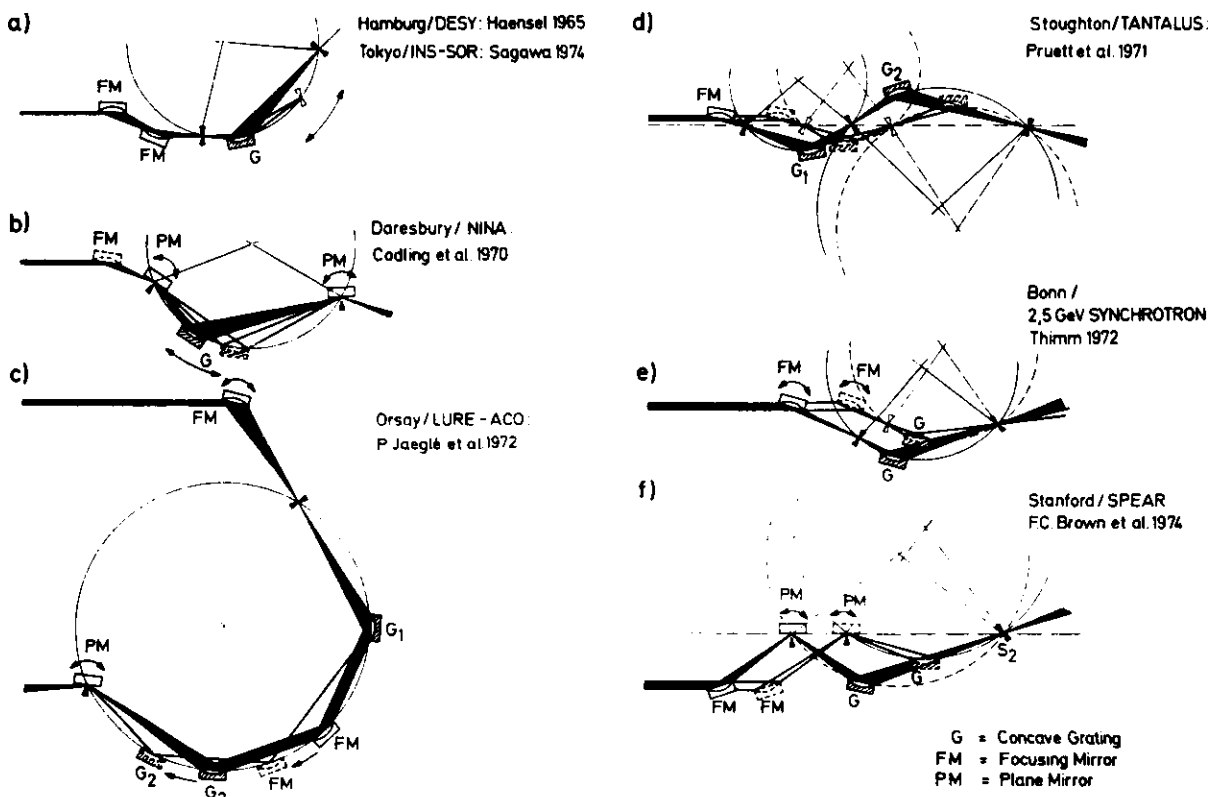


Fig. 3.30

# a) Toroidal Holographic Grating Monochromator

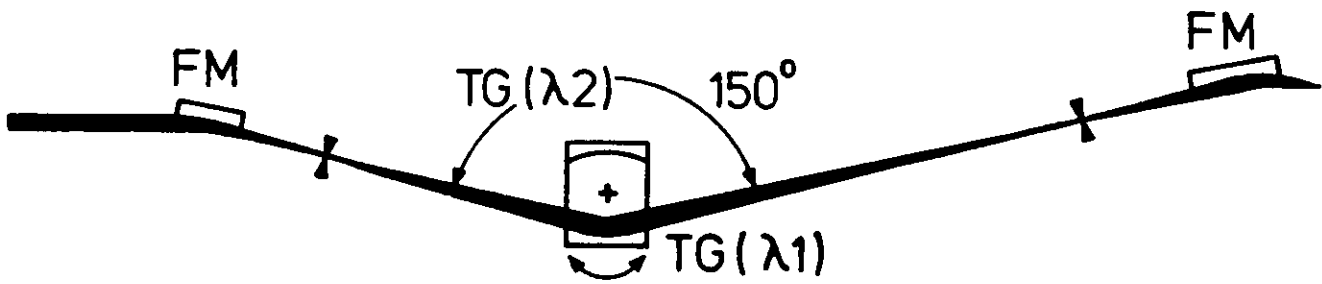
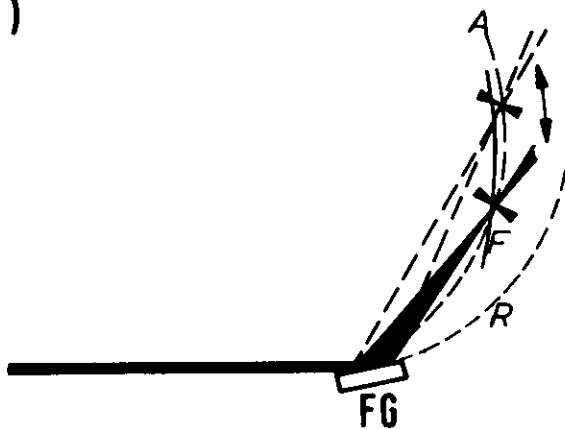


Fig. 3.33 a)

## Non Rowland Monochromators

a)



DESY 1967

b)



NBS  
Ederer et al. 1972

Fig. 3.32

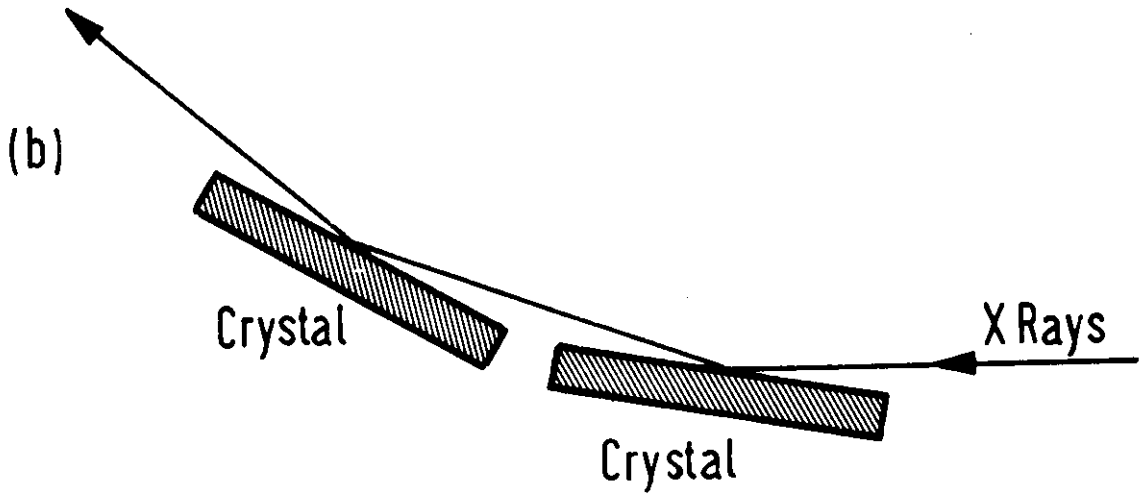
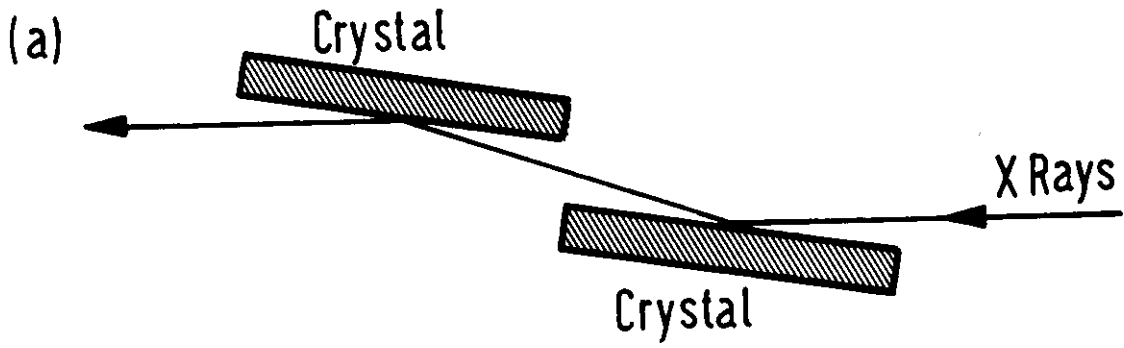


Fig. 3.34

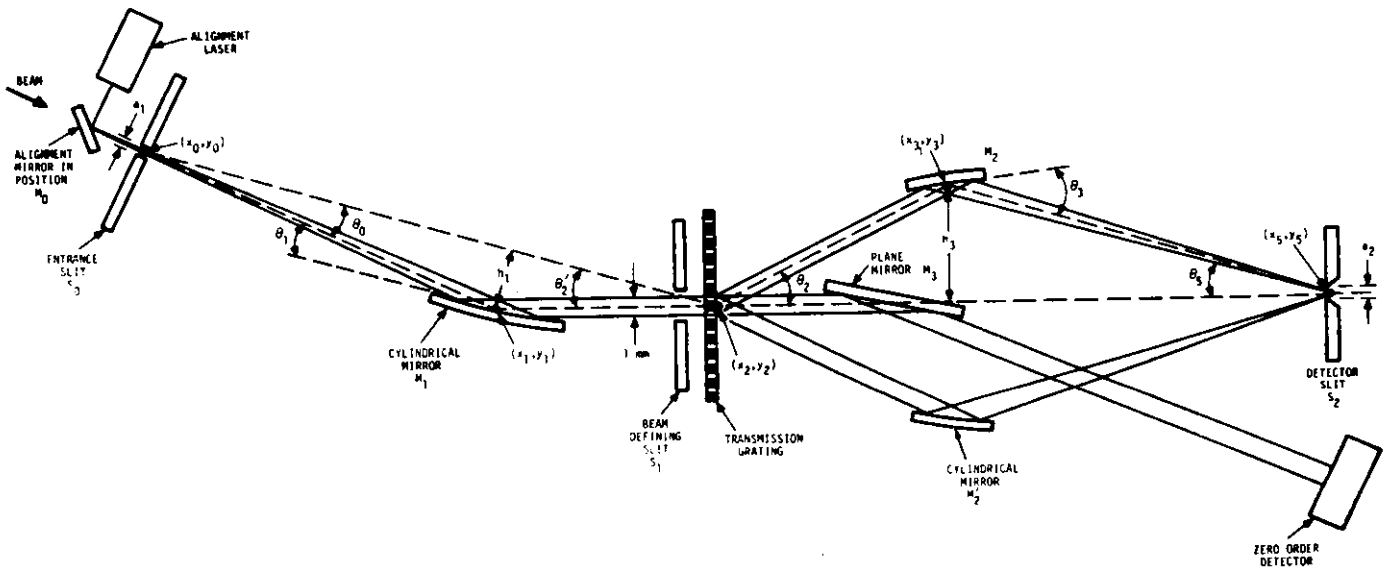
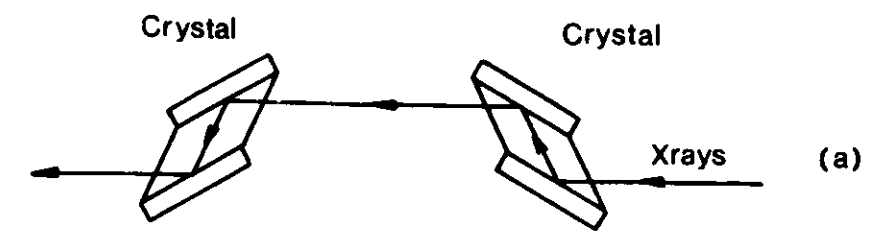
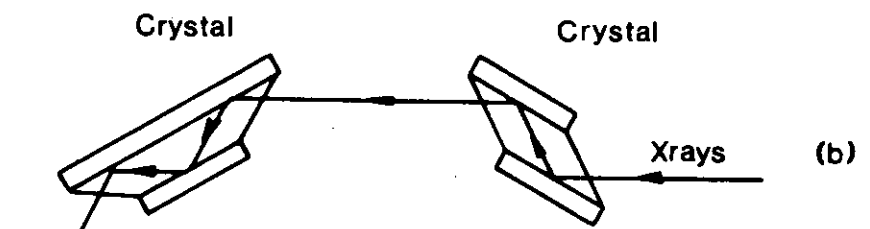


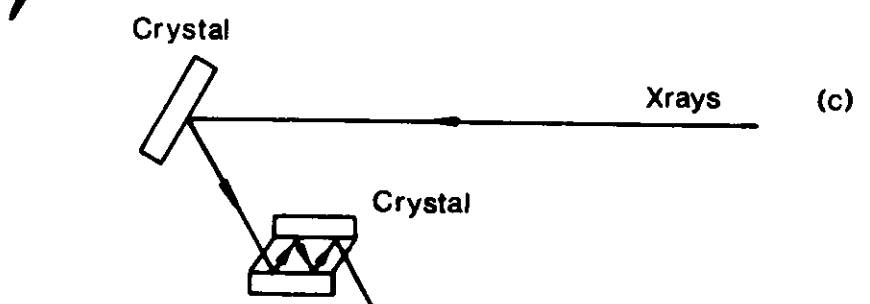
Fig. 3.33 b)



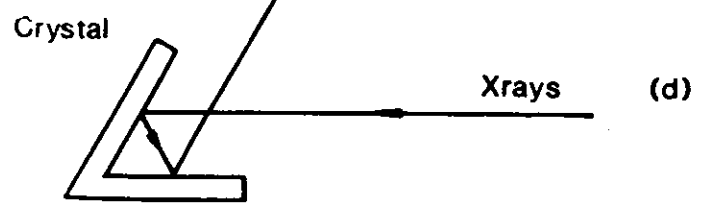
(a)



(b)



(c)



(d)

Fig. 3.35

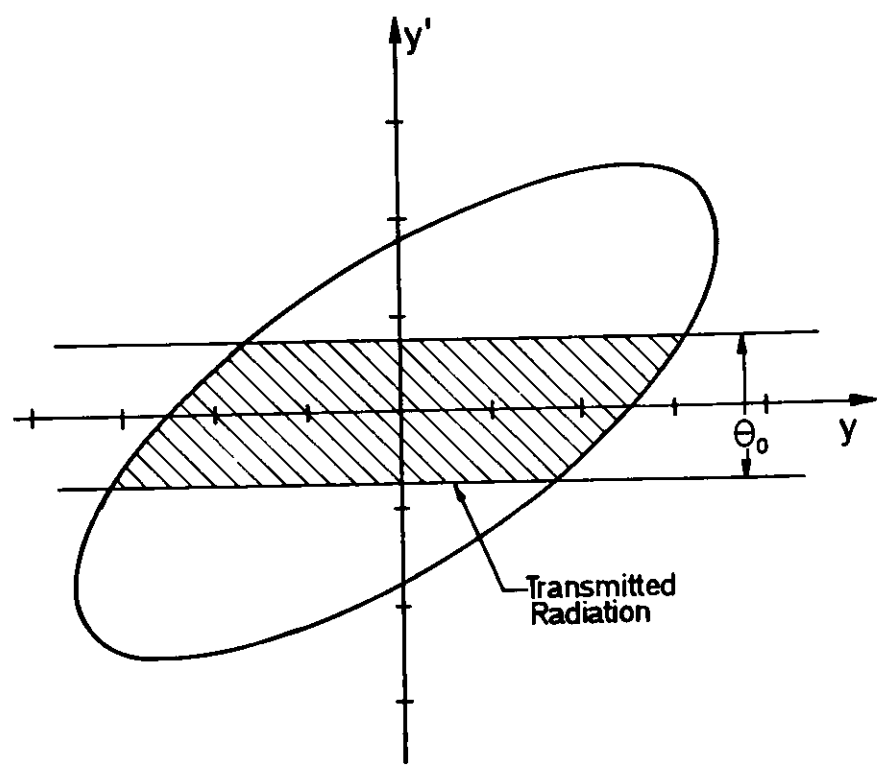


Fig. 3.36

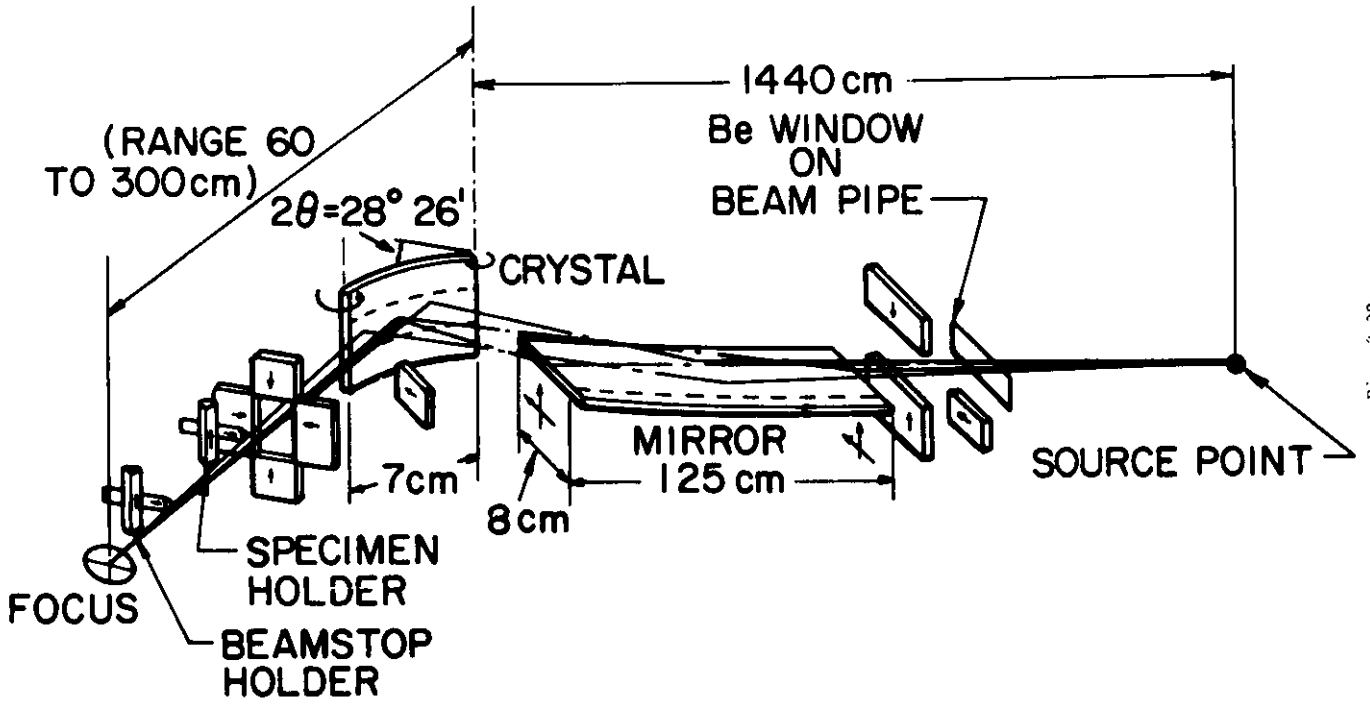


Fig. 3.38

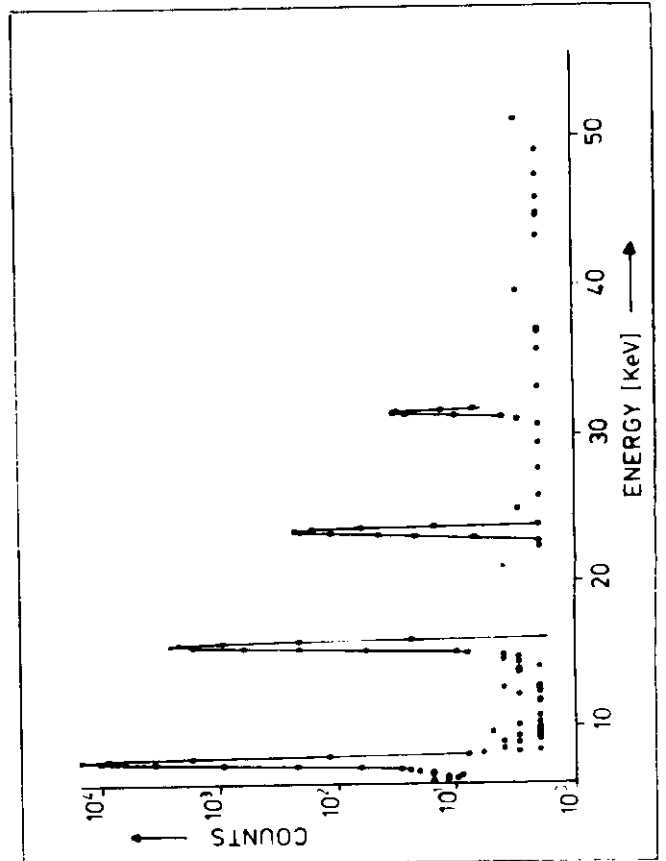
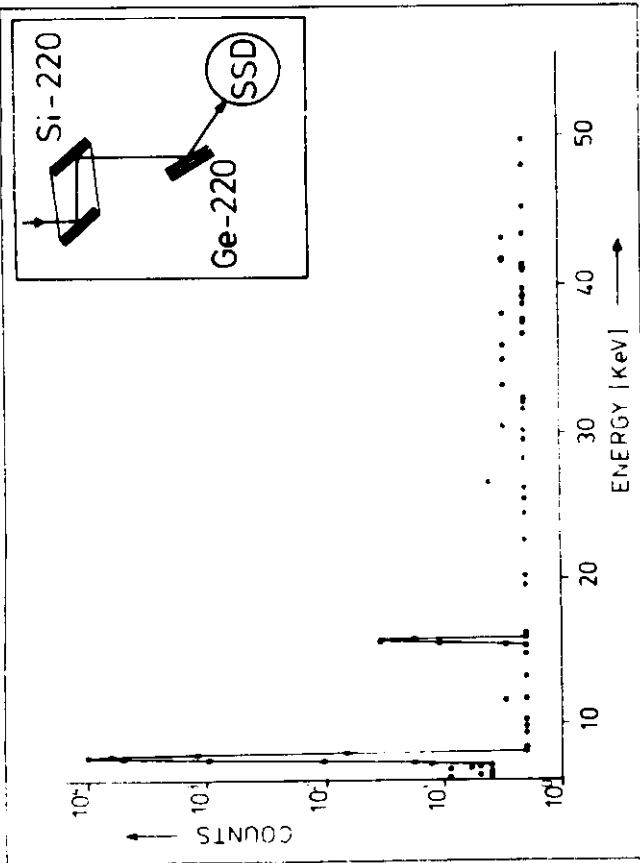


Fig. 3.37

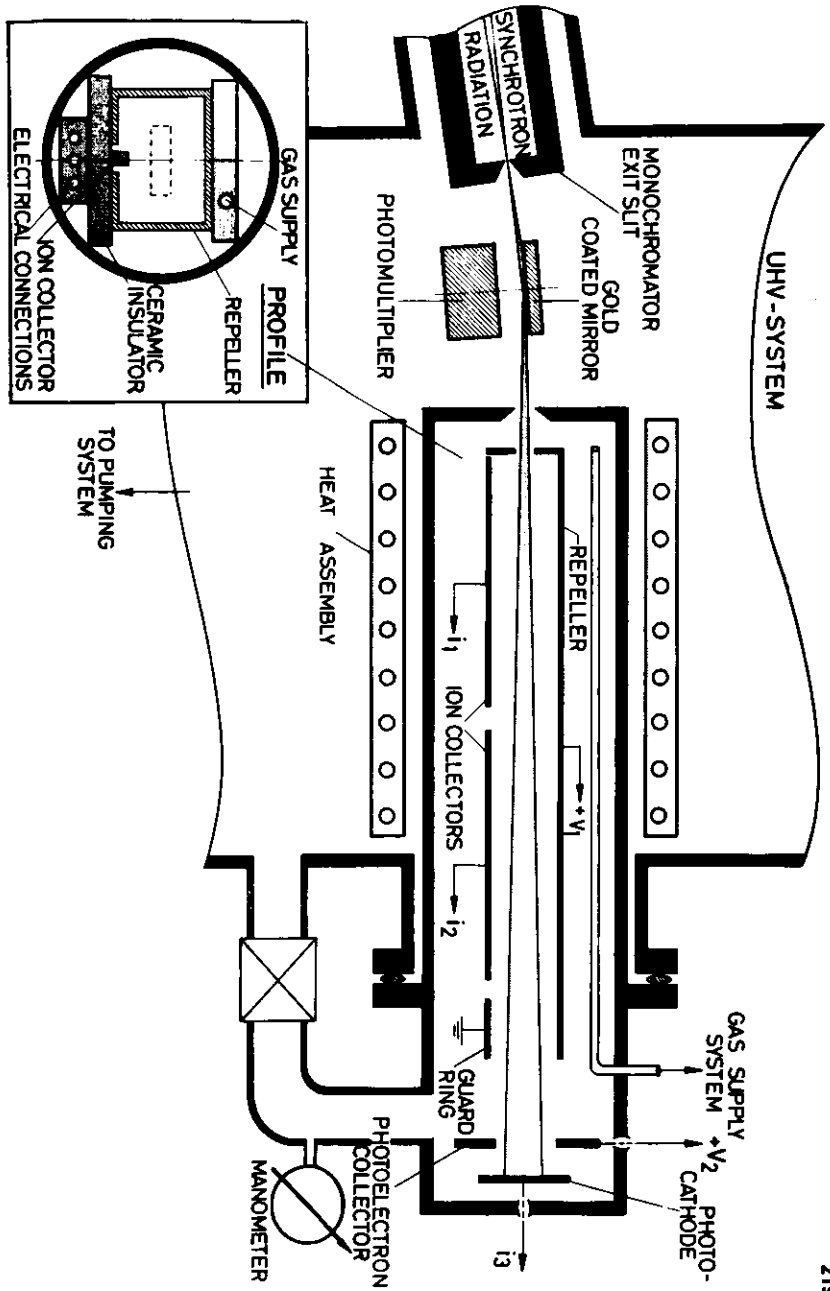


Fig. 3.39

21911

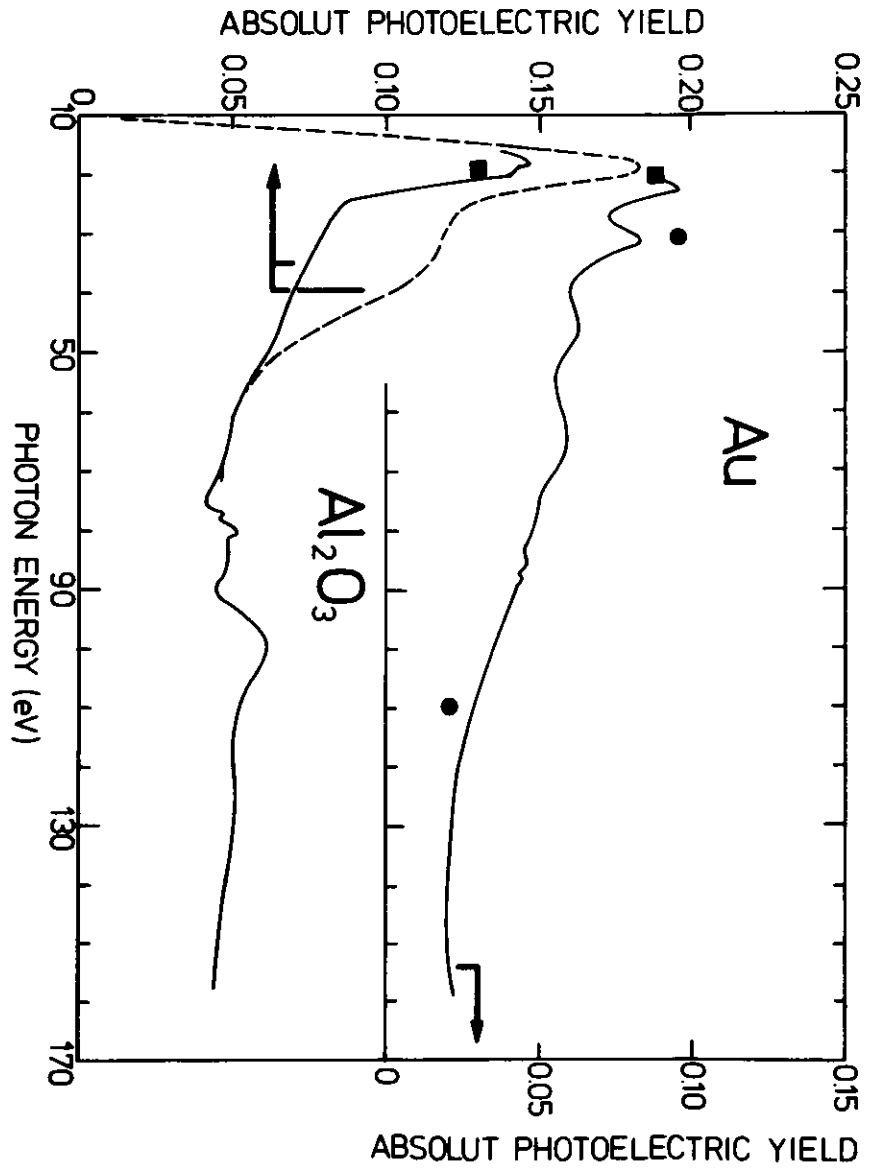


Fig. 3.40 a)

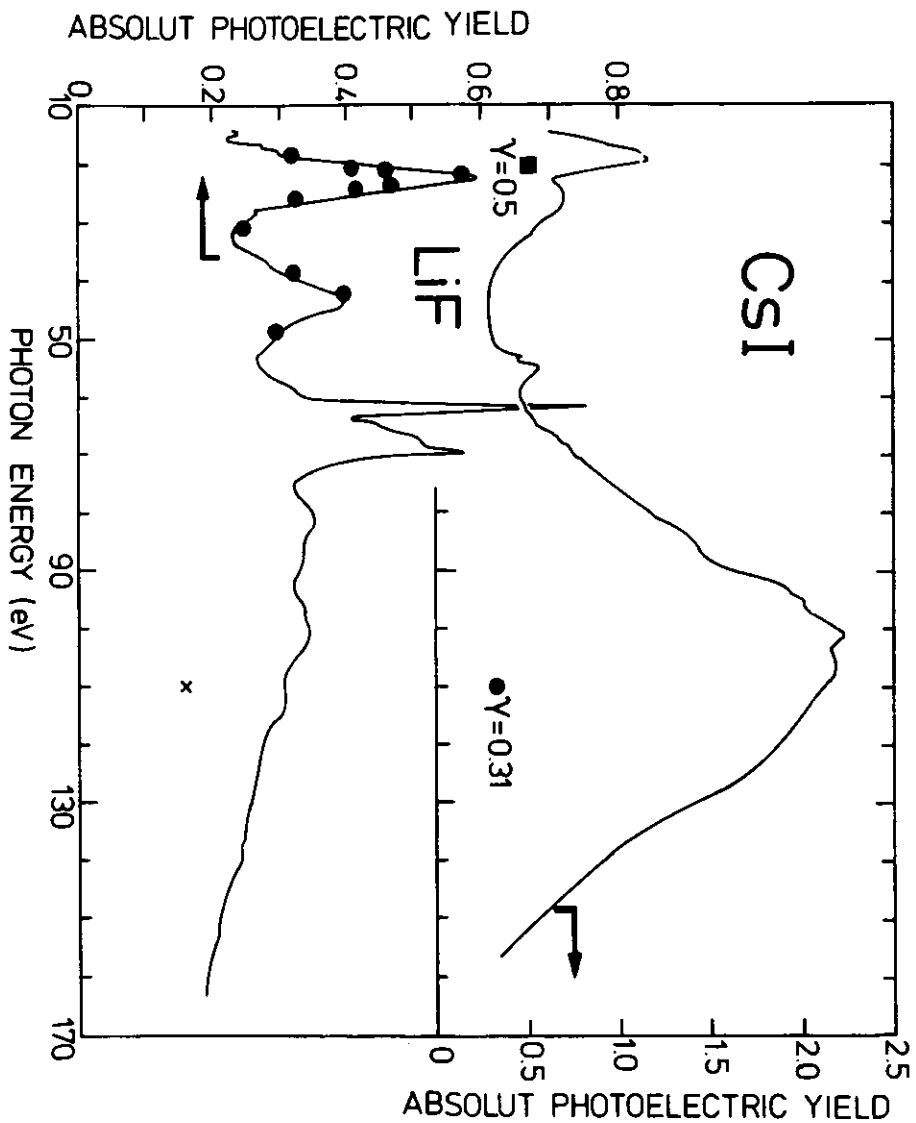


Fig. 3.40 b)

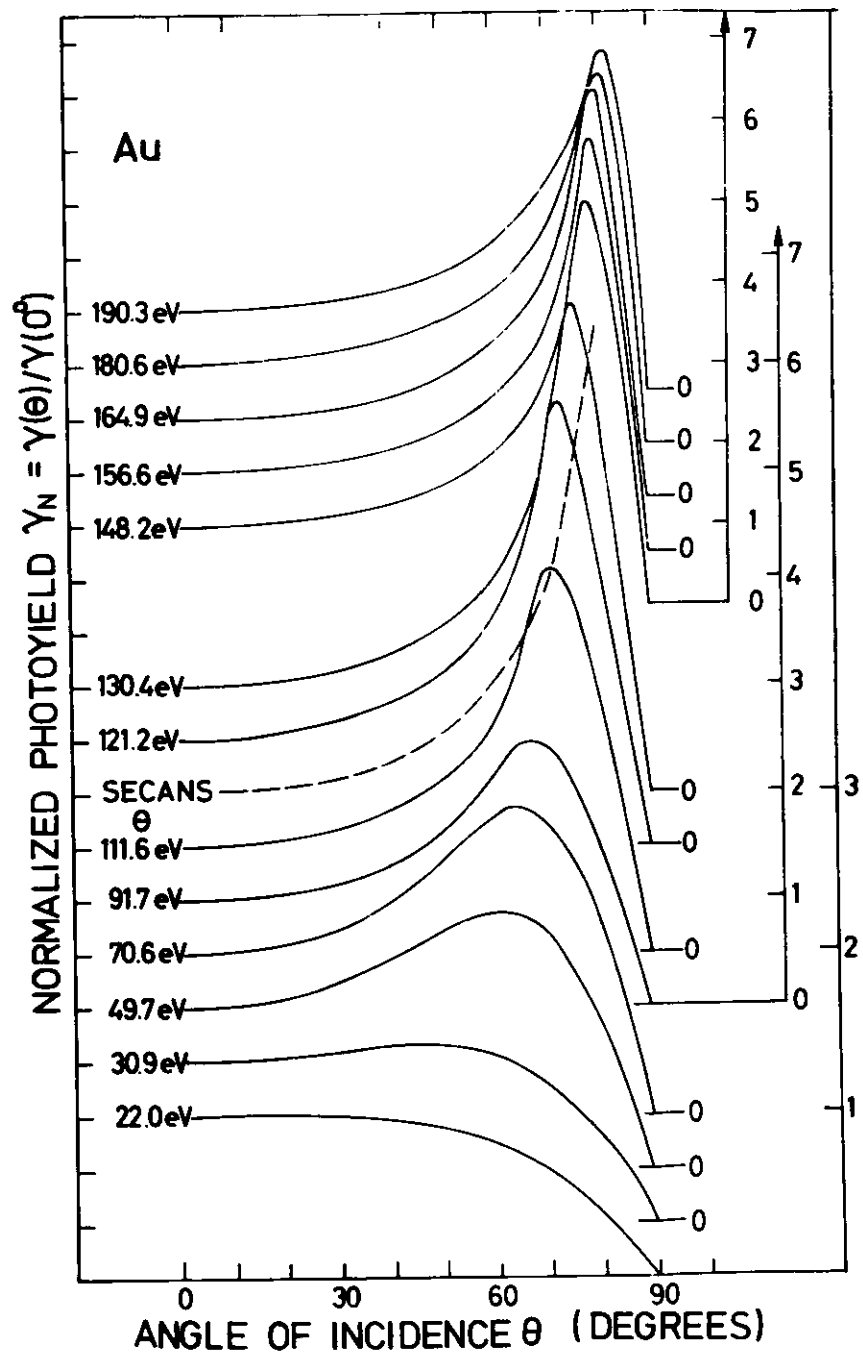


Fig. 3.41

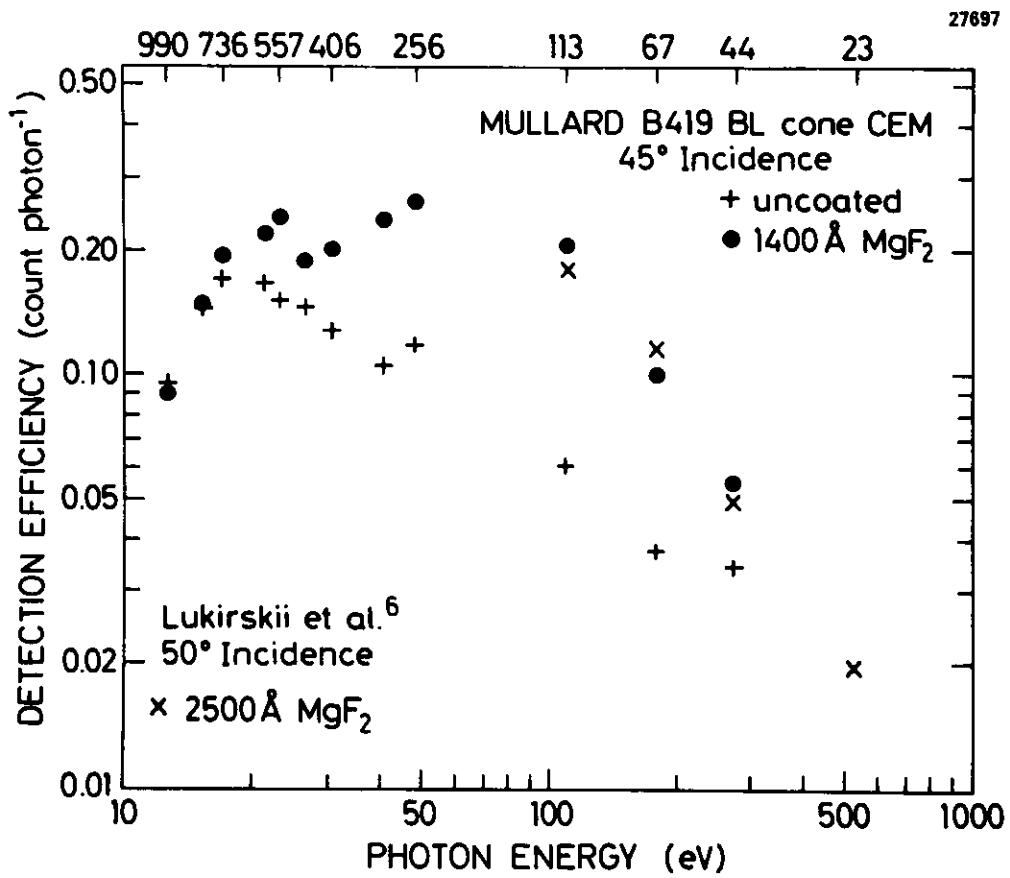


Fig. 3.42 b)

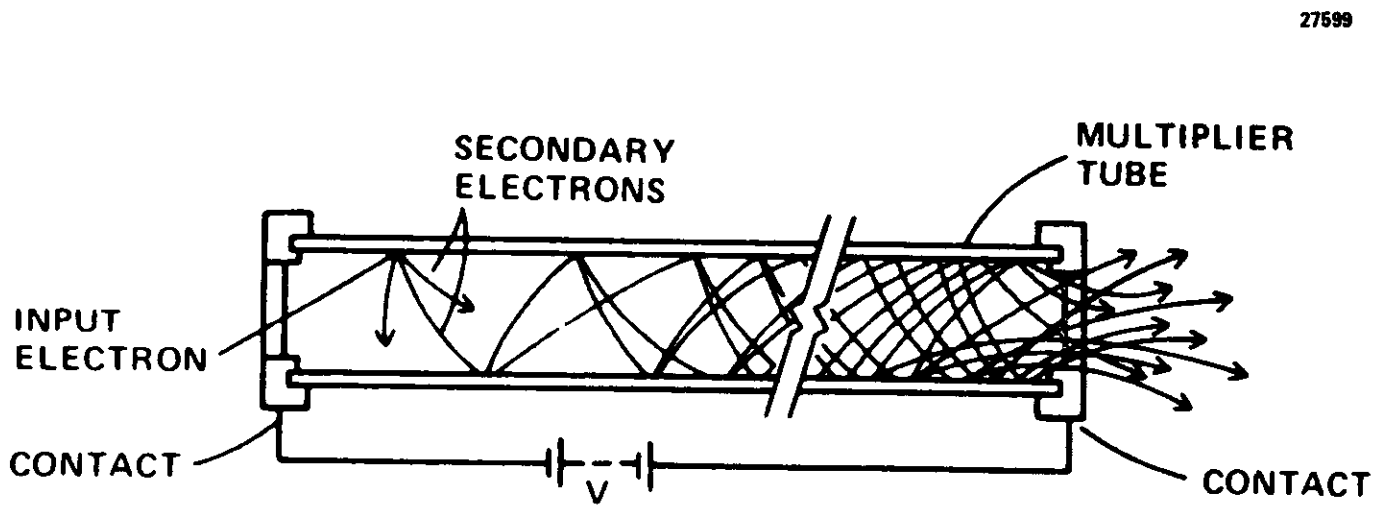
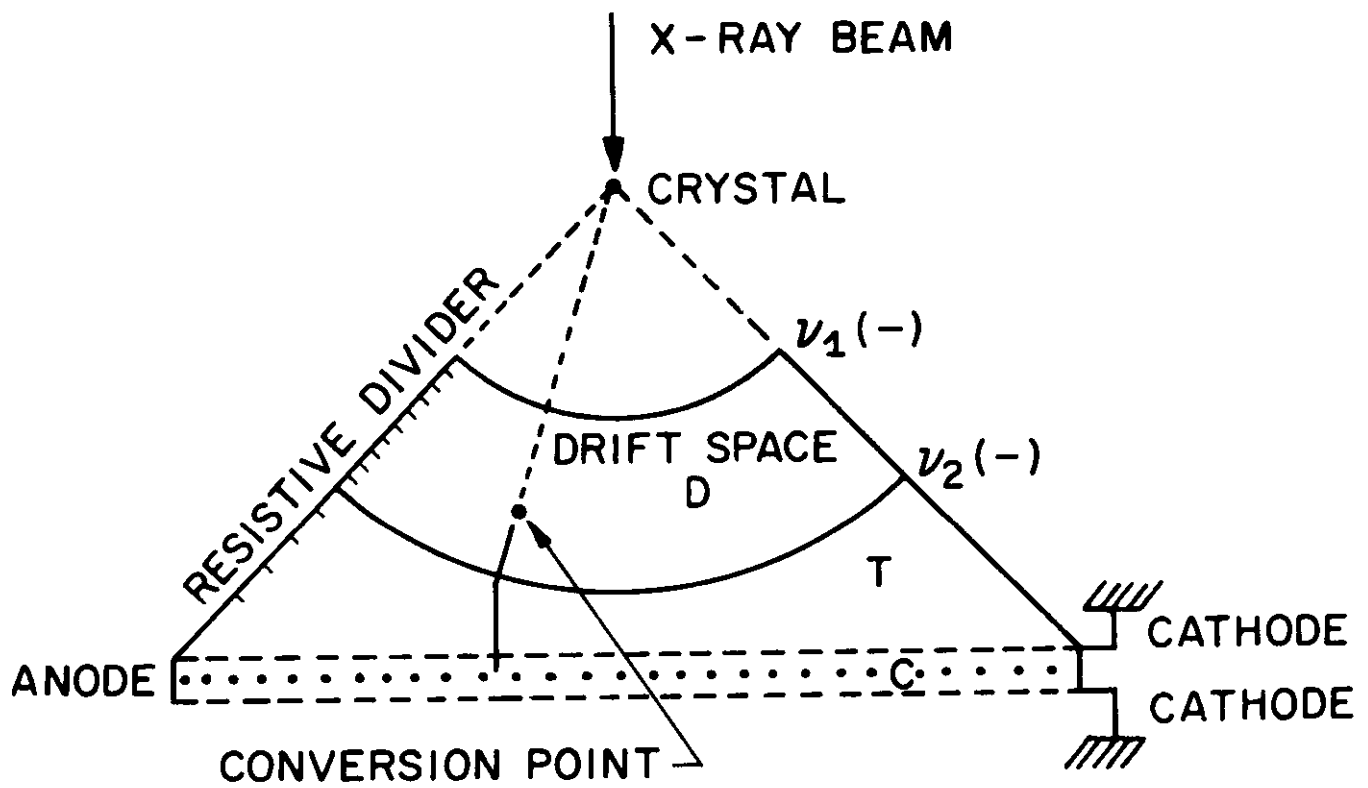
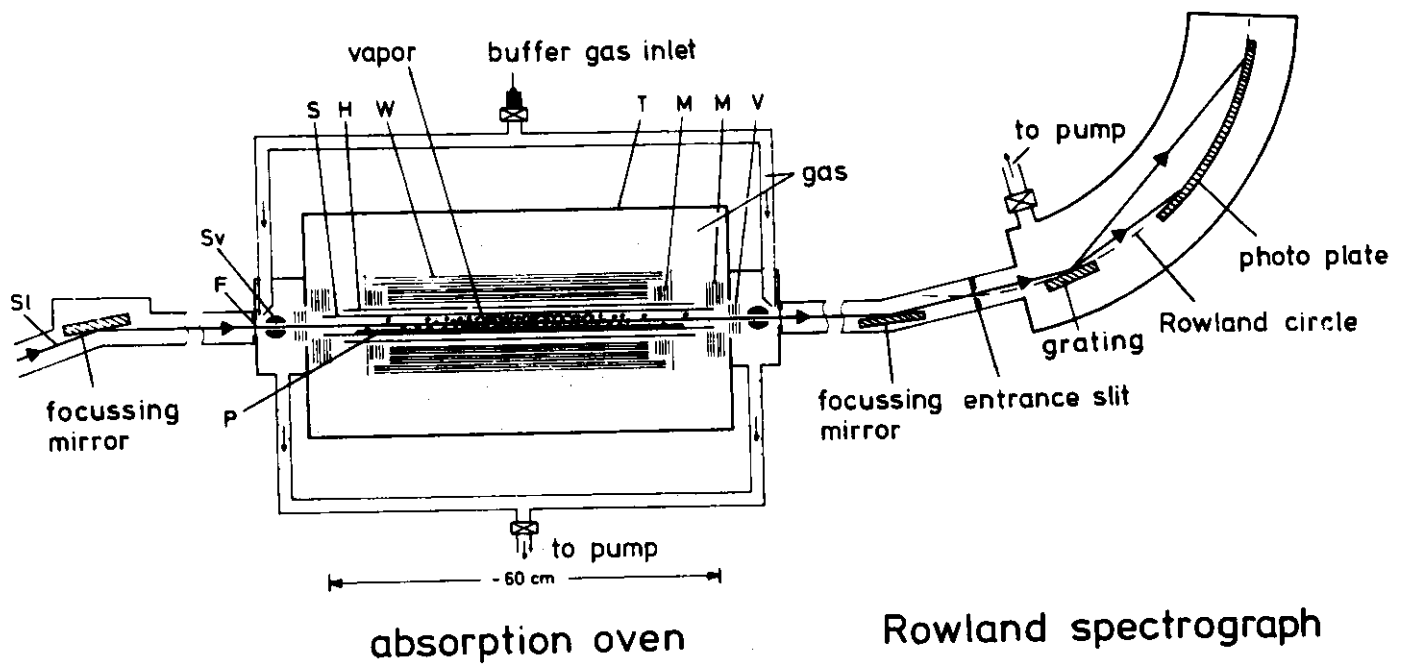


Fig. 3.42 a)



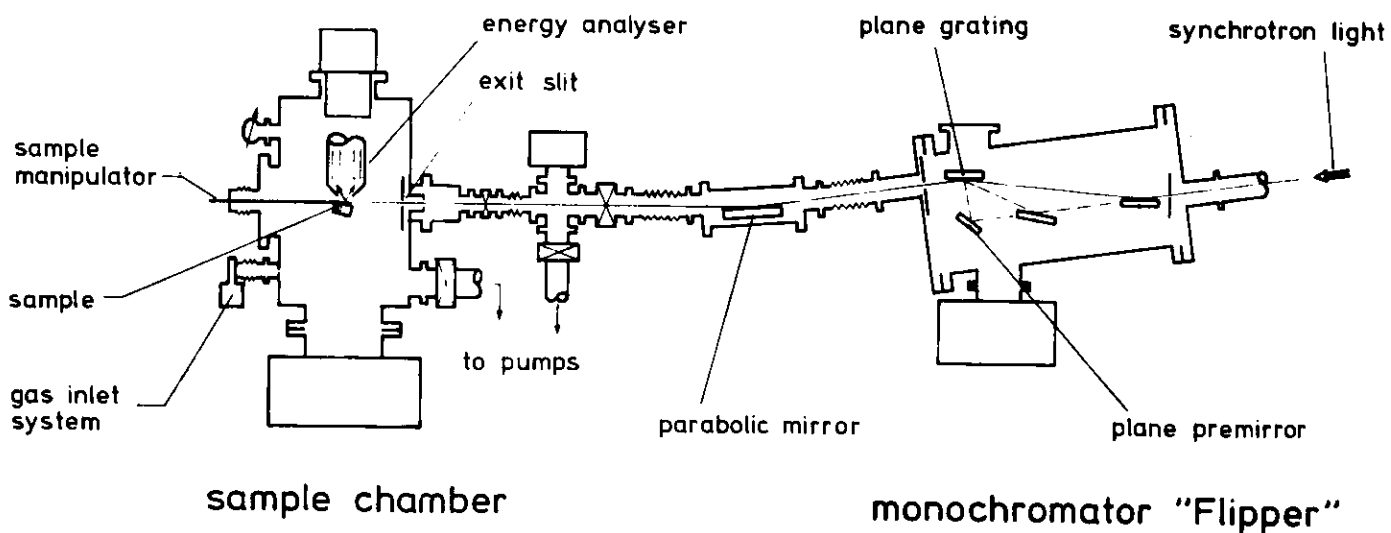


Fig. 3.46

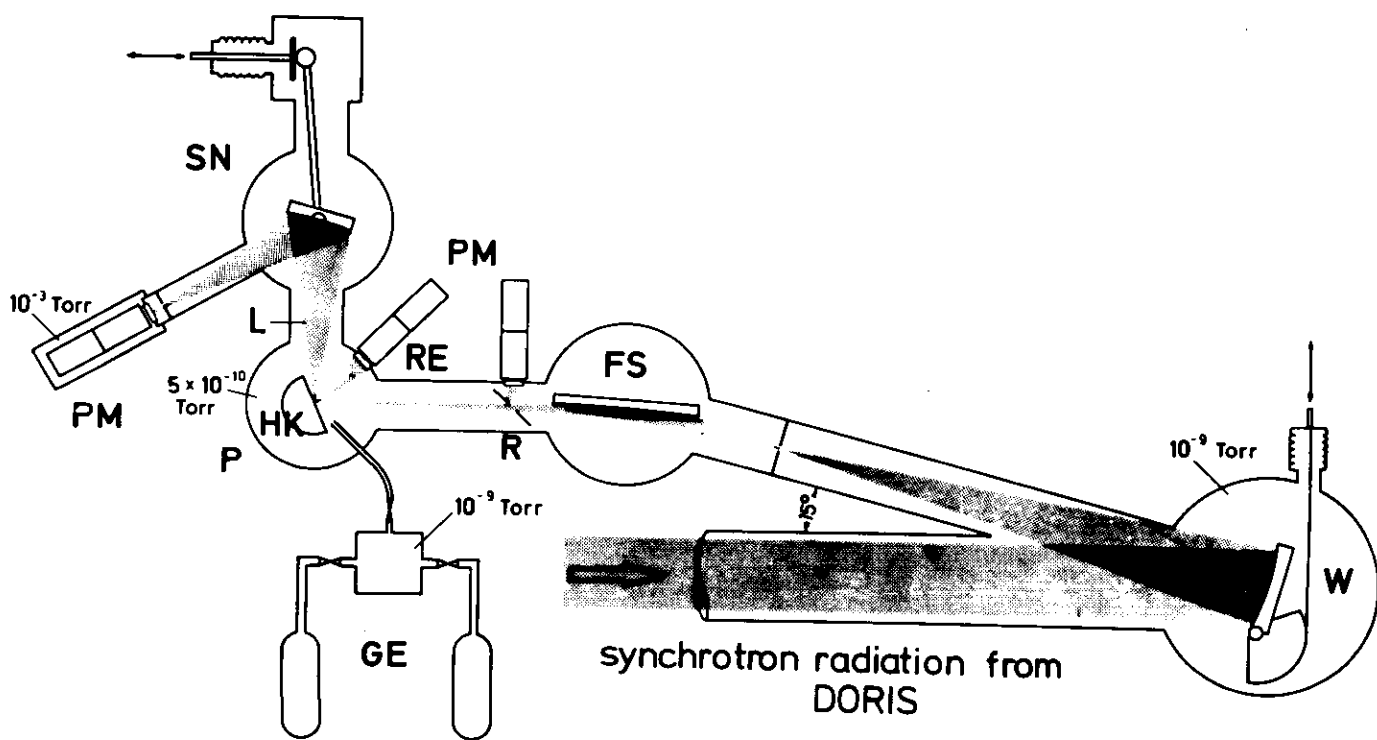
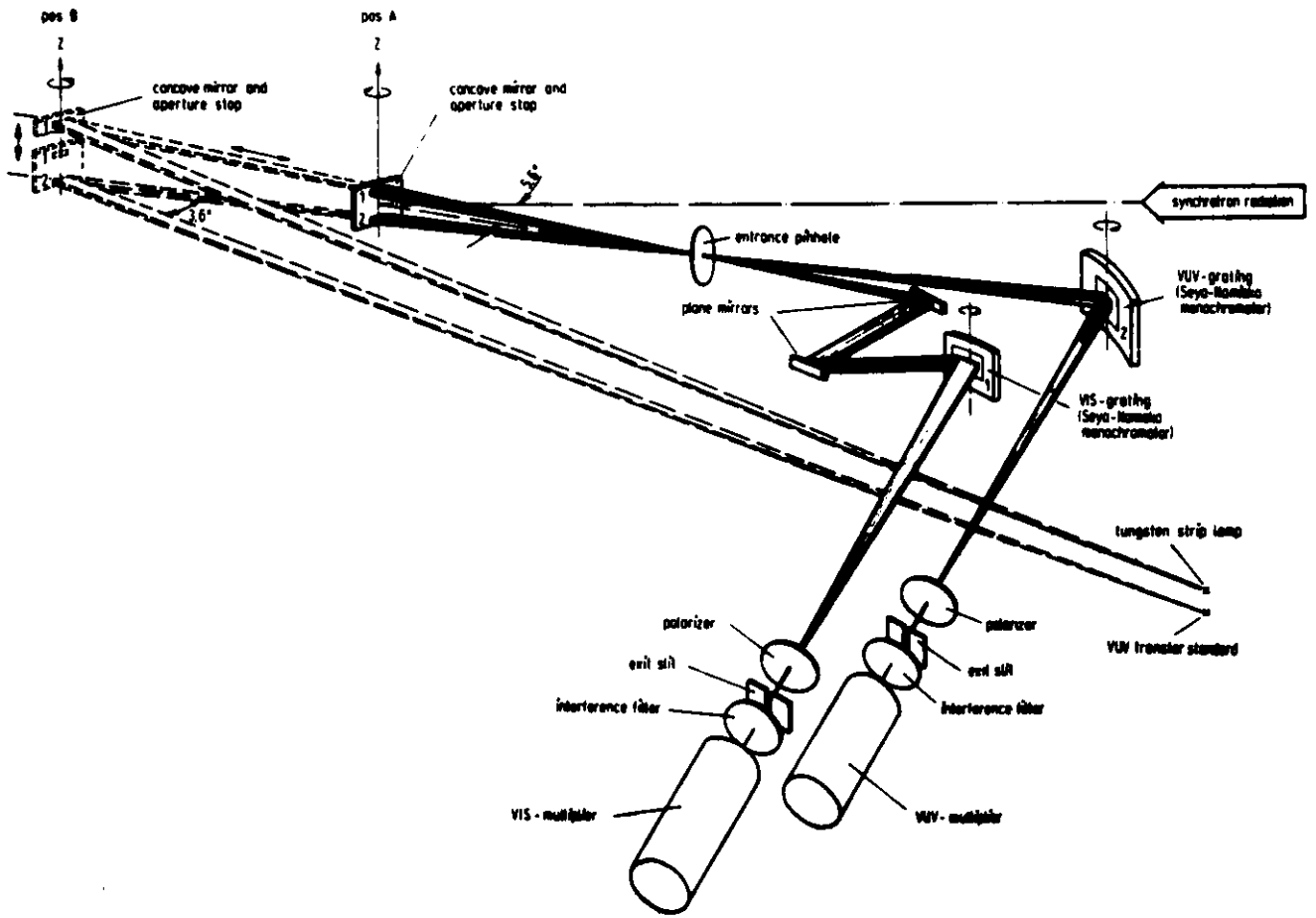
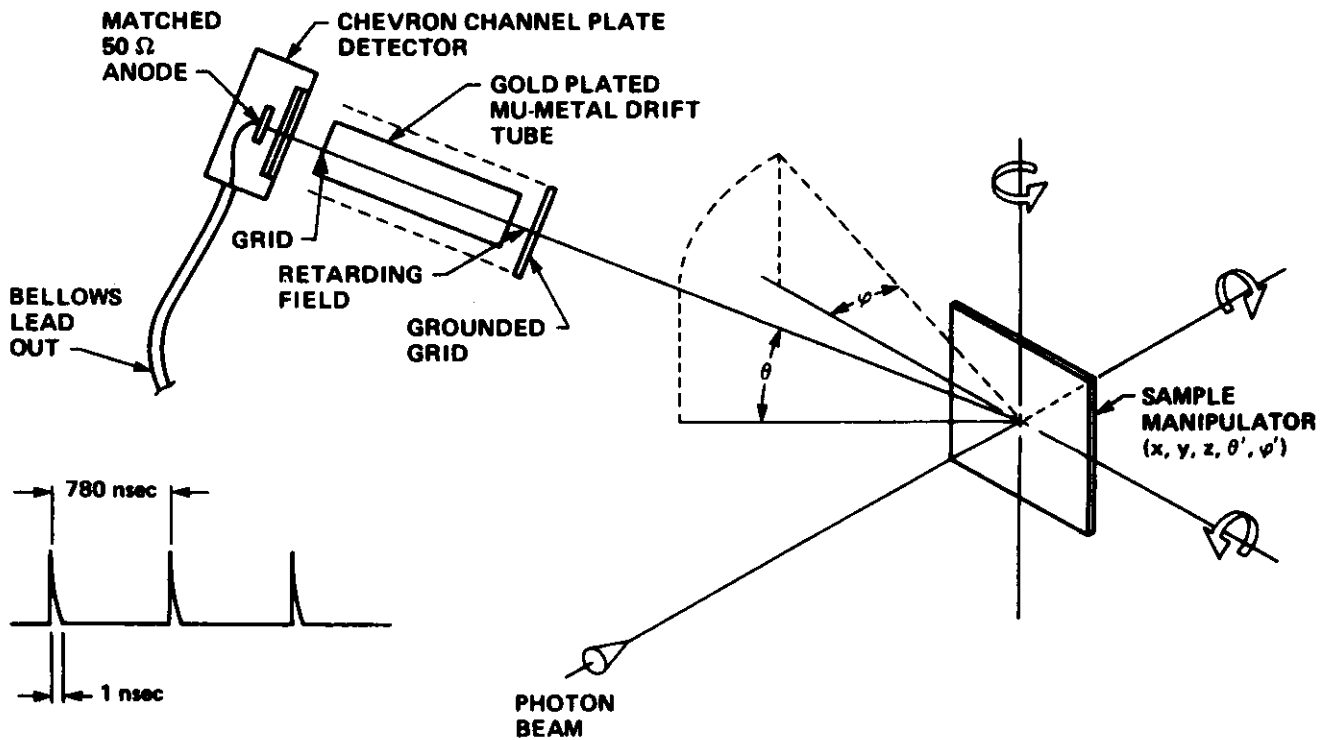


Fig. 3.45



### TIME OF FLIGHT ELECTRON ENERGY SPECTROMETER



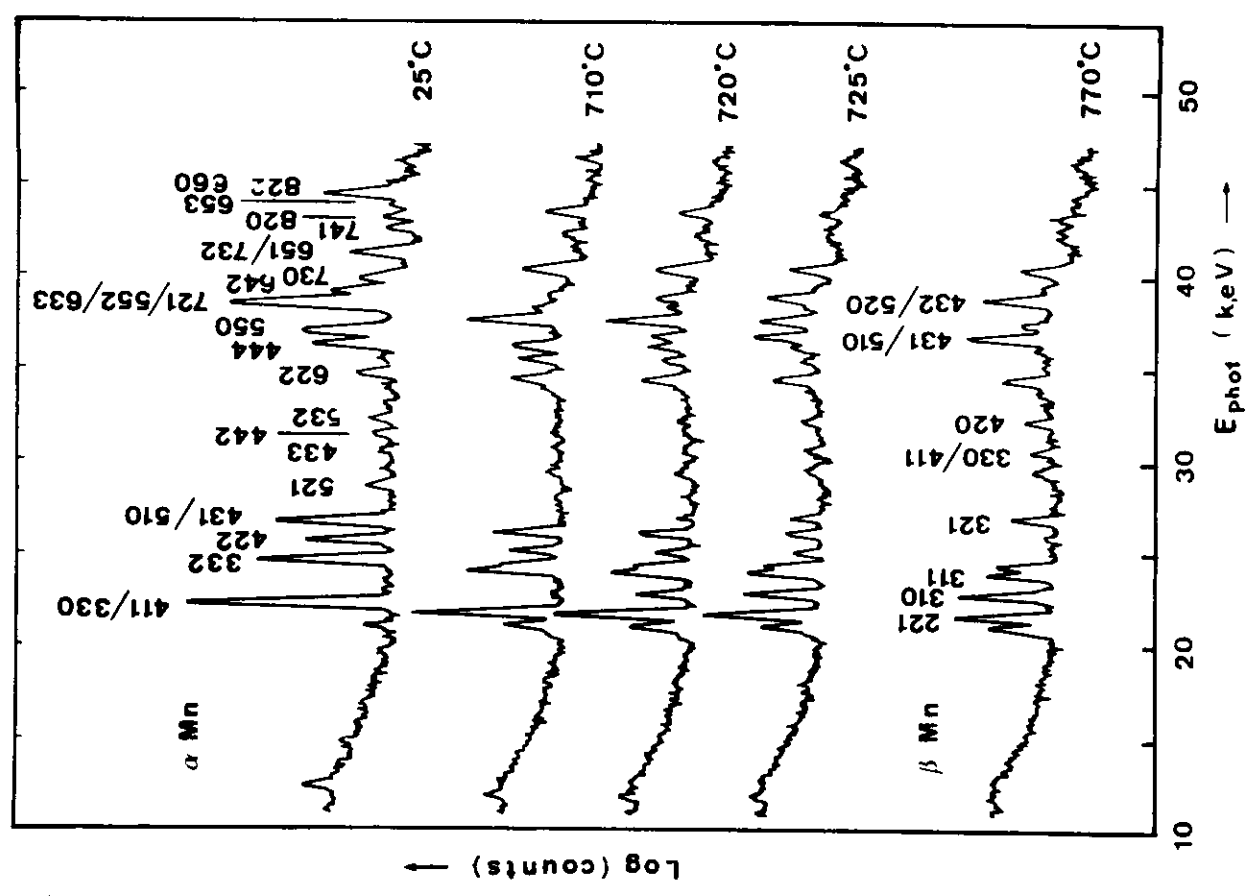


Fig. 3.50

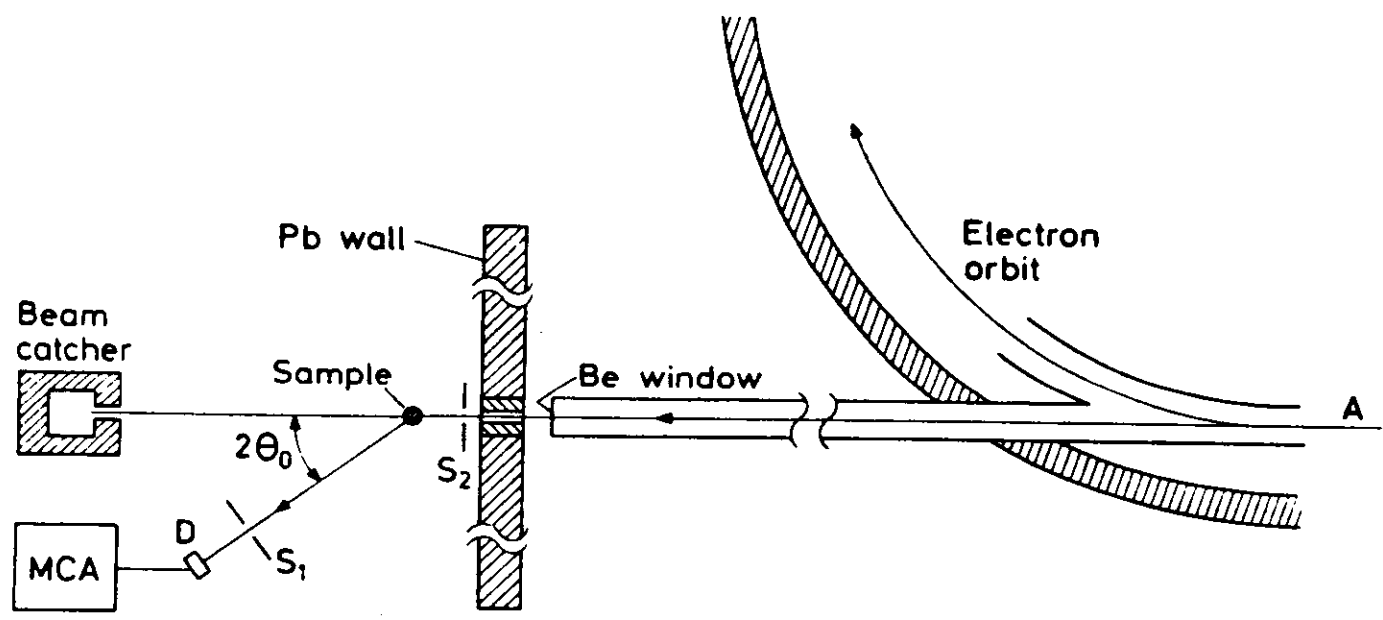


Fig. 3.49

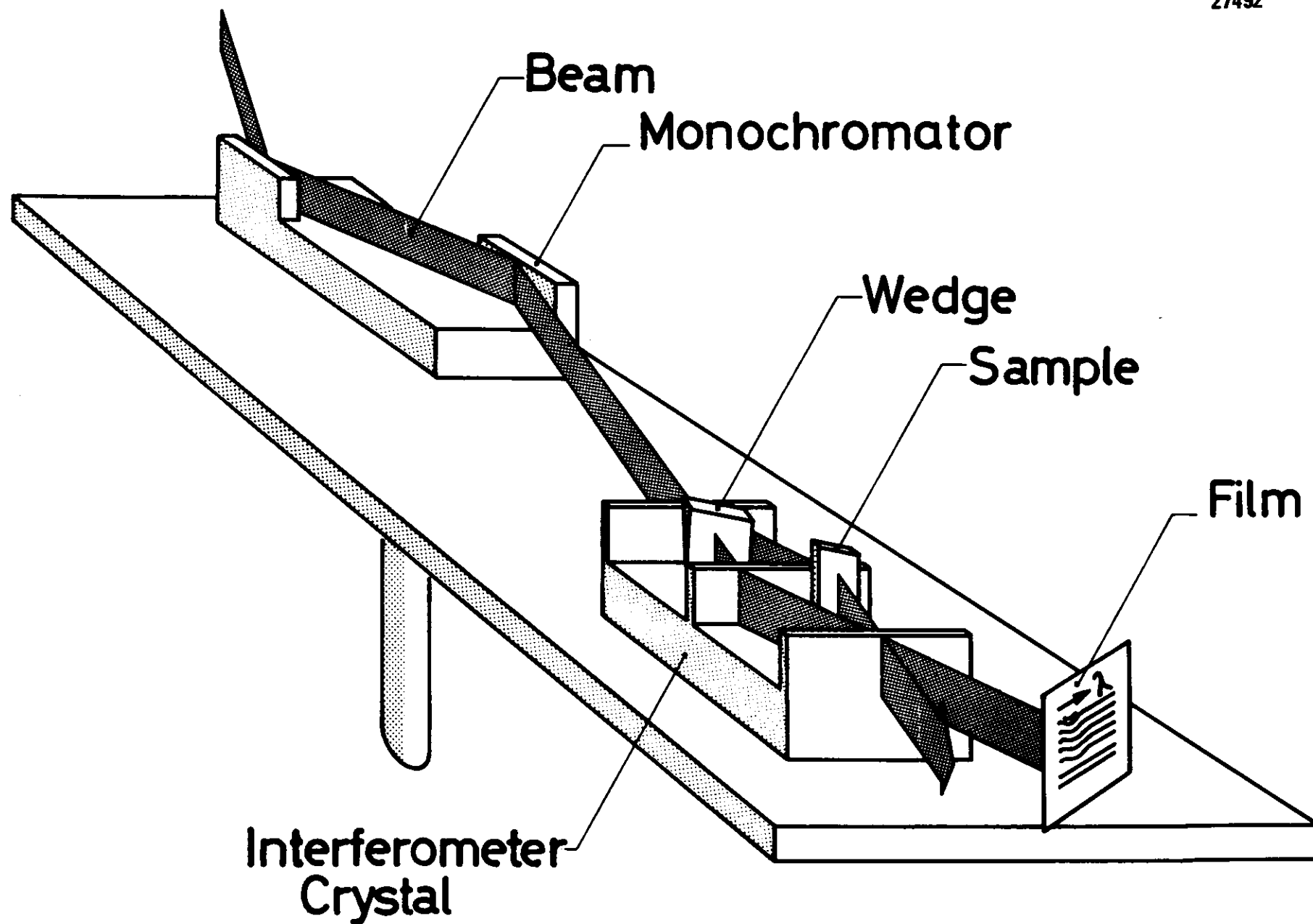


Fig. 3.51



Fig. 3.52

